GROWTH RELAXATION EFFECTS IN PULSED LASER DEPOSITION

By

LI CHEN

A dissertation submitted to the Graduate Faculty in Physics in partial fulfillment of the requirements for the degree of Doctor of Philosophy, The City University of New York.

2002

This manuscript has been read and accepted for the Graduate Faculty in Physics in satisfaction of the dissertation requirement for the degree of Doctor of Philosophy.

June 20, 2002

Date

Chairman of Examining Committee

August 27, 2002

Date

Executive Officer

Professor J.F.Cadieu

Professor Eugene Chudnovsky

Professor Ying-Chih Chen

Professor Mark Miksic

Professor Steven Schwarz

Supervisory Committee

THE CITY UNIVERSITY OF NEW YORK

ABSTRACT

GROWTH RELAXATION EFFECTS IN PULSED LASER DEPOSITION

By

Li Chen

Adviser: Professor F.J.Cadieu

The aim of this work is to investigate growth relaxation effects in PLD. Pulsed laser deposition (PLD) is an extremely versatile technique for preparing a wide range of thin films and multilayer structures. Due to the splashing, a stainless shadow strip has been used to block the direct transport of particulates to the substrate. Both shadowed and non-shadowed films have been investigated. Films were deposited onto various substrates, such as Al_2O_3, Si and glass substrates .The deposit in shadow region was particulate free.

For SmCo based films, the highest coercivity of 22.5 kOe was obtained for 248 nm laser wavelength and 11.3 kOe for 193 nm laser wavelength. The magnetic properties are a function of the laser pulse rate. The films show the presence of (111) in lower laser energy, while the higher energy deposition the films show the (110) and (200) structure. At optimized conditions, remnant to saturation ratio can be as high as 0.9, much higher

than the expected value $2/\pi$. It is believed that the fine grains have exchange coupling effect.

It has been shown that it has been possible to make strongly in plane textured magnetic properties with the dual deposition technique of PLD deposition in conjunction with sputtering with different matrix elements such as Al, Ti, Co, Si, Fe and Fe-Co. Highly corrosion resistant SmCo films were synthesized by PLD $SmCo_5$ deposition while simultaneously sputtering Al.

It also has been shown that $La_{0.7}Sr_{0.3}MnO_3$ polycrystalline films that exhibit the resistance maximum as a function of deposition parameters, T_p was up to 360 K and with stable smooth MR effects up to 320 K. The properties of LSMO are sensitive to the substrate type. The inexpensive polycrystalline alumina substrate is one of the suitable substrate for growing LSMO films. LSMO films exhibiting room temperature T_p values were patterned into thin strips by dry etch methods to yield appreciable low field MR for stable room temperature operation.

A stable memory element was constructed by placing a small interacting bias magnet strip parallel to and slightly above the film strip. Two appreciably different voltage states were observed for the zero applied field values following positive versus negative applied magnetic field excursions.

ACKNOWLEDGMENTS

I wish to express my deepest gratitude to my supervisor Prof. F.J.Cadieu for his generous support, patient guidance and timely advice. Sincere thanks to Dr.Qian for introducing me to here and helping me a lot in scientific research since I was graduate student in P.R.China.

I would like to thank Dr.Raj.Rani for her patience in answering my endless list of questions and help through the research work. It is my pleasure to extend my thanks to Dr.Biao Li and Mr.T.Theodoropoulos for their help and cooperation in the lab.

I am thankful to Professor Eugene Chudnovsky, Professor Ying-Chih Chen, Professor Mark Miksic, and Professor Steven Schwarz, members of Supervisory Committee, for their suggestion.

It is my pleasure to extend my thanks to all the members of the faculty and staff, and colleagues at Physics Department of Queens College.

Finally, the sincere gratitude must be extended to my wife, Yi Yao, for supporting and assisting me through five years of painstaking studying and writing the thesis.

My thesis and research is supported by U.S.Army Research Office Grants: No.DAAH04-94-0079 and No.DAAG55-98-1-0172, NSF-ARI Grant No.STI-9512308, partial support from NYS Graduate Research Initiative and partial support from Office of Naval Research under contract ONR-N00014-96-1-0767.

TABLE OF CONTENTS

LIST OF FIGURES

LIST OF TABLES

Chapter 1 INTRODUCTION AND BACKGROUND

1.1 Introduction

In recent years, magnetic film synthesis has become a very active research area due to its potential usage. For example, microwave components that utilize magnetic fields consist of an electric circuit surrounded by bulk piece of permanent magnets. Researchers are trying to replace these bulk pieces of permanent magnetic material by thin films. Magnetoresistive heads are another area in which permanent magnet films can play a significant role since magnetic field biasing is required to obtain magnetoresistive sensitivity. Small-scale magnetic sensors, actuators, and motors are other areas that can benefit from the development of film permanent magnets. Recently we reported several advances for permanent magnet as well as other magnetic films made by pulsed laser deposition, PLD. For the first time high coercivity permanent magnet SmCo based films were made by PLD.[1,2] To achieve these successes, it was necessary to introduce a new deposition variable for PLD involving the laser pulse repetition rate. In other studies, La-manganite films were made by PLD that exhibited an extreme variability in the temperature dependence of the resistivity[3,4] . Before continuing with details of these studies, some background information about these systems needs to be considered.

For any magnetic system to qualify as a good permanent magnet system, a high Curie temperature, high anisotropy, high saturation magnetization as well as high remnant magnetization need to be exhibited. Transition metals, TM, such as Fe and Co,

carry large magnetic moments, and high Curie temperature. Magnetism of the transition metals is due to the unfilled 3d bands and is caused by direct exchange splitting of the 3d electrons. Mean while, rare-earth elements, RE, show strong anisotropy but low ordering temperatures as their magnetization arises from the indirect exchange splitting of the largely localized 4f shell electrons. As a result, rare earth-transition metal inter-metallic compounds benefit from the high magnetic moments of the TMs and the high anisotropy of the REs, making them suitable for permanent magnet applications. SmCo based compounds satisfy the above said criteria. Among them, transition metal rich $SmCo_5$ and Sm_2Co_{17} compounds are widely used for their superior permanent magnet properties. These materials can be synthesized both in bulk and thin film form depending on their usage.

Film synthesis of these magnetic materials has been carried out by several different ways such as RF glow discharge sputtering, Pulsed Laser Deposition technique, Chemical Vapor Deposition technique, Molecular Beam Epitaxy (MBE), and evaporation. Each method has its own merits and demerits. However, sputtering has been proved to be very beneficial for obtaining uniform composition films from multi-element target. When materials are sputtered from target, a beam of relatively high-energy neutral atoms as well as secondary electrons are ejected from the target by momentum transfer processes. Sputter ejected constituents, predominantly neutral atoms, are then collected onto a substrate placed at a distance of about 3-10 centimeters away from the target.

Sputter process control has allowed the synthesis of highly textured permanent magnet films onto polycrystalline substrates. It is necessary to grow preferentially crystallographically aligned films, to make use of the high crystal anisotropy energy of the higher energy product permanent magnet systems. Such films are said to be textured or anisotropic as opposed to the randomly aligned crystallites of isotropic films. Control parameters such as substrate temperature, sputtering gas pressure and deposition rate each can play interconnected roles in determining whether a particular growth texture is favored over another. These sputtering parameters were carefully controlled to obtain nearly single-phase $CaCu_5$ type films from Sm-Co based combination targets. It was possible to shift the texture growth mode of the $CaCu_5$ phase films to be (200) by increasing the film deposition rate and by lowering the film deposition pressure [5,6]. Crucial to this growth process is the concept of surface mobility of the deposited atoms during the film growth process.

For a collection of uniaxial magnetic grains with the c-axes randomly layed about the film plane, the expected remnant to saturation ratio is $2/\pi$. For small grains that are very closely spaced, the grains no longer act independently and such grains are then said to be exchange coupled. For such exchange coupled systems, the remnant to saturation ratio can exceed that expected for independently acting magnetic grains. The high coercivity SmCo based films we recently reported by PLD synthesis were of this type and exhibited remnant to saturation ratios averaging about 0.9 [1,2].

PLD is probably the simplest among all the thin film growth techniques. A high-power laser is used as an external energy source to vaporize materials and to deposit thin films. A set of optical components is used to focus and raster the laser beams over the target surface. Film growth can be carried out in a reactive environment containing any kind of gas with or without plasma excitation. When the laser radiation is absorbed by a solid surface, electromagnetic energy is converted first into electronic excitation and then into thermal, chemical and even mechanical energy to cause evaporation, ablation, excitation, plasma formation, and exfoliation. Evaporants form a "plume" consisting of a mixture of energetic species including atoms, molecules, electrons, ions, clusters, micron sized solid particulates, and molten globules. This process attributes to many advantages as well as disadvantages. The advantages are flexibility, fast response, and energetic evaporants. The disadvantages are the presence of micron sized particulates in a splash, and the narrow forward angular distribution. The presence of particulates makes it extremely difficult to control the homogeneity and elemental composition in the film. Many different materials have been made in recent 20 years [7]. But for the materials of interest here, especially for the rare-earth containing systems, there have still been only limited successes reported. A major problem is particulate splashing which limits the control of film properties for the case of high volatility Sm-based compounds. Due to this reason, there have been only a few reports RE-TM based systems as grown by PLD and those are mostly confined to our work on high coercivity SmCo based systems and to some $Nd_2Fe_{14}B$ films with inferior magnetic properties.[8]

1.2 Pulsed Laser Deposition

1.2.1 Introduction

PLD remained little known until late 1980s. One reason is the competition from other thin-film growth techniques, most notable sputtering and molecular beam epitaxy (MBE). Sputtering has been routinely used commercially for depositing thin films of metals, dielectrics, and oxides. MBE was initially focused on the growth of III-V compound semiconductor epitaxial layers. It underwent more than one decade of research and development before being transferred from laboratory to production line for growing custom-designed semiconductor structures for making advanced electronic and optoelectronic device.

PLD is an extremely versatile technique for preparing a wide range of thin films and multilayer structures. One of its great advantages, and certainly one of the reasons for its ready acceptance among materials scientists, is the attractive start-up cost of PLD research. The cost advantage is especially striking when one considers that PLD systems can produce films with quality comparable to molecular beam epitaxy (MBE) systems that cost 10 times as much, and more! A second advantage of PLD is that the laser is independent from the deposition system. Thus, complex multilayer films are straightforward to produce within a single system by moving various targets into and out of the beam focal point. And, by using mirrors to change the beam path, several

deposition systems can be clustered around a single laser to create an entire deposition laboratory.

1.2.2 Equipment [7,9]

Conceptually and experimentally, PLD is extremely simple, probably the simplest among all thin film growth techniques. Figure1.1 shows a schematic diagram of an experimental setup. It consists of a target holder and a substrate energy source to vaporize materials and to deposit thin films. A set of optical components is used to focus and raster the laser beam over the target surface.

In general, the useful range of laser wavelengths for thin-film growth by PLD lies between 200nm and 400 nm. Most materials used for deposition work exhibit strong absorption in this spectral region. The excimer is a gas laser system. Excimer lasers emit their radiation directly in the UV. High outputs delivering in excess of 1J/pulse can be achieved. These systems can also achieve pulse repetition rates up to several hundred hertz with energies near 500 mJ/pulse.

Table 1.1[7] gives a list of excimer wavelengths that have been developed into commercial laser systems. The corresponding active excimer molecule is indicated as well. Of the excimers listed, KrF and XeCl have been extensively pumped excimer lasers and is the popular choice among the PLD community

The lenses are very important optical elements used in PLD. The main function of these lenses is to collect radiation from a point on the source (laser) and focus to a corresponding point on the target to achieve the required energy density for ablation.

Both spherical and cylindrical lenses can be used in PLD. The spherical lenses images a point source as a point while the cylindrical lenses images a point source as a line.

The mirrors used for PLD are dielectric multilayer mirrors and are designed for a specific wavelength. Most mirrors are for 45° incidence, with the laser bean incident on the coating side. The dielectric multi-layer coatings are optimized for a single wavelength or a very narrow spectral range.

A target carousel containing six targets can be employed for a single film deposition. Combined with programmable mirror, the target positioning and the laser triggering then can be programmed into a routine. Multi-layer structures can be formed with ease.

1.2.3 Limiting the particulates

There are two major drawbacks of PLD: one is the lack of uniformity over a large substrate area is due to narrow angular distribution of the plume, the other is so-called splashing. The splashing, which cause many particulates, is particularly problematic for electronic device quality semiconductor films and optical films where the particulates can

induce the formation of defects and some other problems. There are several origins for splashing. Subsurface boiling, expulsion of the liquid layer by the shock wave recoil pressure, exfoliation are most common causes.

. The nature of the particulates, including the generation rate, the energy or velocity, the size, the chemistry, and the microstructure, depends upon the process conditions and the type to the material. The specific tolerance of particulate density and size depends on the specific use of the materials. By proper choice of process parameters, the particulate size and density can be minimized. When particulate-free films are required, further reduction of particulates can be accomplished by various techniques. There are a number of mechanical approaches, such as velocity filter, plume manipulation, target surface improvement, off-axis deposition, as well as substrate bias. In this work, we introduced a narrow strip to block direct deposition, so there are shadow and non-shadow region on one sample[1,2,3,4]. The shadow is particulate-free, while the non-shadow region is not.

The majority of the mechanical approaches are based on the fact that the particulates travel much slower than the atomic and molecular species. As described in the book[7], typical particulate velocities are in the range of $2x10^3$-$5x10^4$ cm/s, which is at least an order of magnitude smaller than those of the atomic and molecular species. Velocity filters can therefore be used to select the fast the moving atomic and molecular species[10].

Using the deposition geometry also can produce the particulate-free film. Kennedy[1.11] presented an "off-axis" laser-ablation geometry to overcome the particulate problem. The

advantage of indirect or off-axis deposition, as originally applied to sputtering, is due to the fact that while the particulates are constrained to travel along their initial trajectory directions, the light species undergo significant scattering; consequently their paths are randomized by the plume and ambient gas interactions. The deposition rate is reduced by only a factor of 3 when compared with direct deposition. An additional benefit of this technique includes the coating of irregularly shaped surfaces, since it is not a line-of-sight deposition process.

Lubben[10] et al. have shown that the application of a negative bias significantly decreases the density of Ge particulates embedded in the resulting film. The particulate density for the −150V biased sample was about five times less than in the unbiased case. One explanation, provided by Lubben et at., for the bias effect is that the particulates have a negative charge and are repelled by the biased substrate. The charge is most likely accumulated while the particulate coexists with the laser-induced plasma, charging up to the plasma potential.

There are several large area PLD approaches. Most of them require either rotating the target or rotating substrate or rotating both target and substrate.[12,13] Using a programmable reflecting mirror to sweep the beam also can be an alternative choice[14,15].

Pulsed laser deposition (PLD) is emerging as one of the premier thin film deposition technologies. It has successfully used for depositing high-temperature superconductors,

ferroelectrics, electro-optic materials, magnetic materials and half metal materials. Once these two major concerns have been resolved, PLD's popularity will increase.

Three modes of film growth in the initial stages have been described by Lewis and Anderson(1978)[16]. Island (Volmer-Weber) growth results in the formation and growth of isolated islands. This occurs when the cohesive energy of the film atoms is greater than the cohesive binding between the film and substrate atoms. This mode can result in an epitaxial film that has a rough surface, or a polycrystalline film containing voids. Layer-by-layer (Frank-Van der Merwe) growth consists of deposition of one monolayer at t time and results in a very smooth epitaxial film. It occurs when the cohesive energy between the film and substrate atoms is greater than the cohesive energy of the film, but monotonically decreases as each new film layer is added. Mixed (Stranski-Krastanov) growth consists of island growth after the first monolayer forms successfully. It occurs when the monotonic decrease in binding energy with each successive layer is energetically overridden by some factor such as strain energy due to lattice mismatch and island formation becomes more favorable.

1.3 Permanent Magnetic Thin Film

1.3.1 Introduction

A permanent magnet is a passive device used for generating a magnetic field. The permanent magnet is classified to have coercivities about 10kA/m (125 Oe)[1.17]. No matter what the coercivity of the permanent magnet is it will be of little use if the remament magnetization is low. Therefore a high remanence combined with a high coercivity is essential. Another parameter that is often of interest of permanent magnet manufacturers and users is the maximum energy product, which is the maximum value of BH obtained in the second quadrant. So the search for new permanent magnet materials actually is to identify compositions characterized by high levels of saturation magnetization, $4\pi Ms$, high Curie temperatures, Tc, and strong uniaxial magnetocrystalline anisotropy fields, H_A.

There are several types of permanent magnetic materials available: the Alnico alloy, barium or strontium ferrite platinum-cobalt, samarium-cobalt, $Sm_2Fe_{17}N_x$, tetragonal $ThMn_{12}$-type materials and neodymium-iron-boron.

In recent decades, there are more and more demands for the magnetic materials in the form of thin film. So many materials have been studied in thin film form[18-24].

1.3.2. Thin film technology

Actually there are variety application fields for permanent magnetic thin film[25-29]: the application in integrated electromagnetic circuit information storage, either in magnetic or magneto-optical media, microwave device small-scale sensor, etc.

Permanent magnet thin films can be made by several different methods: RF glow discharge sputtering, Pulsed Laser Deposition technique (PLD), Chemical Vapor Deposition technique (CVD), Molecular Beam Epitaxy (MBE), etc. PLD and sputtering have a relatively narrow range to the average energy per atom, but only PLD has an instantaneous value of deposition rate that can exceed 10,000Å/s. only the CVD sputtering and PLD are capable of operating in pressures of reactive gases greater than 10 mtorr. PLD can operate in a pressure range from UHV to 1 torr, which is easily the widest pressure range of any of the methods. MBE may require ultra higher vacuum conditions.

Principally, all the methods can be classified into three categories, film subsequently crystallized from amorphous deposits[30-32], films directly crystallized onto heated substrates[1-4,22], and epitaxial growth films[33-35].

1.3.3. SmCo based thin films

Sm, Co binary system is known to have many stable compounds such as $SmCo_2$, $SmCo_3$, $SmCo_5$, $SmCo_{12}$ and $SmCo_{17}$, etc[36]. $SmCo_5$ was first reported in the late 1960's[1.2, 1.3]. $SmCo_5$, with the $CaCu_5$ crystal structure, has a large magnetocrystalline anisotropy(28 T, $5.5x10^7$ ergs/cm^3), arising from the single-ion anisotropy of Sm^{+3} ions; a relatively large saturation magnetization magnetic ordering temperature (1000K), due to strong exchange interactions between the Co 3d electrons. Replacement of some of the cobalt by iron and increasing the amount of transition metal in order to increase the saturation magnetization led to the development of $Sm_2(Co,Cu,Fe,Zr)_{17}$ magnets. $SmCo_{17}$ has a high saturation moment and high Curie temperature as compared to $SmCo_5$ but low magnetocrystalline anisotropy.

$SmCo_5$ can be synthesized both in bulk and thin film form depending on their usage, for $SmCo_5$ widely reported are sputtering, Molecular beam epitaxy (MBE) and most recently Pulsed laser deposition (PLD).

Using RF sputtering technology, it has been reported that the $SmCo_5$ can be either directly crystallized onto heated substrates or subsequently crystallized from amorphous deposits.

For permanent magnet material deposition, the main effort is focusing on controlling the texture of the films either by varying the growth condition[37] or using textured buffer

layers[38-41]. High-coercivity SmCo films grown by epitaxial growth onto Cr and W buffer layers have been reported[33,34]. Textured Cr buffer layers are used to maintain the Co-based film's anisotropy in plane via epitaxial growth, which, in turn promotes high in plane coercivities. Such films have the intrinsic coercive field about 4.1T at optimize thickness. For epitaxial growth, the growth rate is typically less than 1Å/s. Such low growth rates mainly require ultrahigh vacuum chambers.

It has been reported that high coercivity $SmCo_5$ films were obtained by subsequent crystallization of amorphous deposits[37]. Room temperature ${}_iH_c$ can be as high as 40 kOe. But this kind of films were isotropic in-plane, so only relatively low energy product were obtainable.

For the directly crystallized $SmCo_5$ film, one of the advantages is able to apply the in-plane magnetic field during the film growth. The high static energy products 12 MGOe have been reported using in-plane applied field during the sputtering[42]. But the field H_s applied during the sputter deposition only provides slight degree of in-film-plane alignment of the crystallite c-axes, not to a major extent[43]. It was studied that the $SmCo_5$ films in the $CaCu_5$ structure could be switched from a dominant (110) texture for a moderate amount of oxygen contamination during sputtering deposition, to a dominant (200) texture as the oxygen was removed from the sputtering system[44].

The controlling of texture also can be done by adjusting the various growth conditions[1, 2, 37]. For example, the preferential texturing of SmCo based films is a function of sputtering-gas pressure; the higher laser energy can make fully textured (200) and (110) dominated $SmCo_5$ films; at different thermal conditions, the $SmCo_5$ may show either dominated (200) structure or (110) structure; the different sputtering rate also contributed to the preferential texture (200) or (110). Changing of the sputtering gas pressure also can change the compositions of the film because the scattering between gas and sputtering species[45].

Section 1.4 MR effect of $La_{0.7}Sr_{0.3}MnO_3$

Discovered by Lord Kelvin in 1856 [46], Magnetoresistance (MR) is the name given to the relative change in a material's electrical resistance due to an applied magnetic field. MR is a very small effect- a tiny fraction of 1%. When much bigger MR effects of a few percent were seen in layered sandwiches of two or more different materials, the term "Giant MR" was introduced. Then, in the early 1990s, certain manganites were found to exhibit MR that could approach 100%, but usually only near the magnetic ordering temperature. The term "colossal MR" (CMR) was coined to denote the phenomenon.

$La_{0.7}Sr_{0.3}MnO_3$ has a large magnetoresistacne (MR) observed near the ferromagnetic ordering of Mn spins [47]. The bulk $La_{0.7}Sr_{0.3}MnO_3$ samples exhibit a ferromagnetic Curie point of 364 K[48,49]. Curie temperature, Tc, marks the transition from a high temperature paramagnetic insulator to a low temperature ferromagnetic metal. The basis for the theoretical understanding of these materials is the notion of double exchange, which considers the magnetic coupling between Mn^{3+} and Mn^{4+} that results from the motion of an electron between the two partially filled d shells Hund's coupling. Over the last several years a number of groups have reported broadened transitions for polycrystalline films with enhanced low field magnetoresistance[50]. The enhanced low field magnetoresistance in polycrystalline films has been attributed to either intergrain spin polarized tunneling[51], or to spin-dependent scattering of polarized electrons at the grain boundaries[52].

A thin film technology is required for practical applications of magnetoelectronic devices in microelectronic integrated circuits. For this reason a number of techniques have been used for fabrication of manganite thin films exhibiting the colossal Magnetoresistance (CMR) effect: pulsed laser deposition[53], jet vapor deposition[54], and spray pyrolysis[55] molecular beam epitaxy[56].

For most useful technologies, heat treatment temperatures below 650 °C are needed to allow the use of large area glass substrates. The spray pyrolysis is a technique that dose not require high temperatures. The results show the optical absorption coefficient as a function of wavelength for as grown and annealed $La_{0.7}Sr_{0.3}MnO_3$ films[55].

But most popular technique for growth of $La_{0.7}Sr_{0.3}MnO_3$ films is PLD[57-59]. It has been revealed the LSMO thin films deposited at low temperature are amorphous or of mixed amorphous phase and (001)-oriented crystalline phase, and those deposited at high temperature are epitaxial[60]. The LSMO film deposited at Ts<380° C is completely amorphous. The magnetic and electrical properties of samples deposited at various Ts are evaluated, and show significant dependence on Ts[60]. In our laboratory, high laser pulse energies have been used to grow $La_{0.7}Sr_{0.3}MnO_3$ films that exhibit the resistance maximum at temperatures up to 360 K and with stable smooth values up to 320 K[57]. These samples have been deposited by pulsed laser deposition onto heated polycrystalline substrates. For high laser pulse energy films, shadow and non-shadowed regions of the same substrate exhibit distinctly different textures. By utilizing both shadowed and non-shadowed deposits method together with films deposited at different pulse energies and

repetition rate the temperature of the resistance maximum can be tuned to occur at room temperature by adjusting the deposition conditions. It also has been shown that $La_{0.7}Sr_{0.3}MnO_3$ polycrystalline films, in which the grain size and intergrain coupling have restricted very small size by layering with resistive barium ferrite, exhibit the usual maximum in resistivity characteristic of polycrystalline $La_{0.7}Sr_{0.3}MnO_3$ films [59].

The properties of CMR films are known to be very sensitive to the nature of the substrate, due to strains that are imposed by the lattice mismatch between the film and the substrate. Optimized pulsed laser deposited conditions allow the fabrication of dense LSMO thin films which present an exceptional flatness with a peak-valley roughness of 1Å [61]. The temperature of the resistance maximum were different for R-plane sapphire, C-plane sapphire and Al_2O_3 substrate [57].

Although $La_{0.7}Sr_{0.3}MnO_3$ crystallizes in SG 167 with a=5.506 Å and c=13.356 Å [62], the simpler pseudocubic indexing with a≈3.9Å has been used in this work[63,64].

Chapter 2 EXPERIMENTAL METHODS

2.1 Induction

PLD system and DC magnetron sputtering are used in this work to deposit the magnetic thin film. The microstructure was studied in a high resolution Hitachi Scanning Electron Microscope model S-570 coupled with an energy dispersive X-ray spectrometer. The crystal structure and crystallite orientation were determined by x-ray diffraction measurements using $Cu_{k\alpha}$ radiation. Most of magnetoresistive measurements were measured by conventional four contacts method and parts of them were measured directly in ohms. Depend on the requirements, the deposition can be achieved at various rate and various temperature by adjusting the deposition parameters. The magnetic loops were measured by VSM. All the targets were purchased from the commercial market.

2.2 PLD System

The laser system used is Lambda Physik 305Fi excimer laser. The other parts are the system of NEOCERA PLDs, which consists of a spherical chamber assembly, a six-target carrousel flange, a substrate heater flange and control panel. The chamber is constructed using a spherical design to maximize working space and hence efficiency. It includes view ports for visual checks on the actual deposition process.

The six-target carrousel allows the user to rotate the target as well as switch the targets, without breaking vacuum. The greatest advantage is the ability to deposit multi-player thin film. By working in situ, the chance of contamination and time spent in pumping down are greatly reduced. For convenience, it was developed a control panel designed to create reproduction conditions inside the chamber. It is composed of the programmable temperature controller, heater power source, pressure gauge, flow meter, target motor switch, power distribution panel, and fine or course vent valves.

Substrates are mounted on the heater surface and then temperature can be controlled by the temperature controller. The heater enable switch is provided to disconnect the heater from the power source should any servicing or emergency situation arise.

The excimer laser is shared by two deposition chambers by changing the reflecting mirrors. One of the mirror is controlled by Encoder mike controller 18011, so during the deposition, the beam can be swept across on the target surface. Left of figure 2.1 shows the heater used in PLD, right shows the target holder.

2.3 Preparation of Materials

All the targets are from Kurt J.Lesker Company. Table 2-1 shows the list of targets used by this work.

The cycling gases are 99.99%Ar and 99.99% O_2. The substrates used are R-plane sapphire, C-plane sapphire, polished polycrystalline $Al_2O_3$and Si substrate.

2.4 Deposition of SmCo Based Permanent magnetic thin Films

The SmCo based films are synthesized in an ultra-high vacuum system (base pressure < 10^{-7} Torr) by Pulse Laser Deposition (PLD), utilizing a Lambda Physik 305Fi excimer laser, in Ar at pressures varies from 10 to 200 mTorr. Laser output energy varies from 300 to 1300 mJ. The wavelength can be either 248 nm or 193 nm. Inside the deposition chamber, it has a rotating target carousel, which can hold up to six different targets offering good advantages to deposition different materials alternatively. Argon gas is cycled during the deposition at a controllable flow rate. The flow rates can be varied by adjusting opening angle of an electric valve. The angle can be set the value between 0 - 90. Pulse rate were varied form 1 Hz to 50 Hz. Films are deposited onto heated polycrystalline Al_2O_3 corundum or Si substrates. Substrate temperature can be controlled in the range from room temperature up to 750°C. A metal strip shadow mask was used to block direct line of site transit from the laser target to substrate region of interest. So there are shadow region and non-shadow region on same film.

2.5 Deposition of nanophase dispersions of $SmCo_5$ in Al or other matrix

Films have been deposited using a wavelength of 248 nm with pulse energies from 1000 to 1250 mJ at 12-15Hz with an estimated pulse width of 15ns. Simultaneously, $Co_{0.5}Fe_{0.5}$, Si, Ti, Al or Co was deposited onto the same substrate from a 75 mm diameter DC magnetron sputtering gun. Vary the sputtering gun power then can vary the content ratio of $SmCo_5$ and matrix element. The substrates during deposition were heated to promote direct crystallization of the films upon deposition. The target arrangements were shown in Figure 2.2

In the Fig.2.2, two targets were arranged side by side. It also could be arranged concentric. The $SmCo_5$ target can be rotated during the deposition. Encoder Mike controller is attached for sweeping the reflecting mirror and can be programmable. A piece of program is written in QuickBasic, so the mirror can sweep either vertically or horizontally freely.

A narrow strip is used to block the direct sight of target so that shadowed and non-shadowed region are both obtained on same substrate. The distance between shadow strip and target or between strip and substrate can affect the sample's properties and size of shadow region.

2.6 Deposition of LaSrMnO Magnetoresistance Films

$La_{0.7}Sr_{0.3}MnO_3$ films are synthesized using same PLD equipment as mentioned above, but in Oxygen gas environment with pressures ranging from 10 to 200 mTorr. The substrate were heated by the heater up to 800°C and the samples were post heated at 600°C to 800 °C in 200 Torr Oxygen for 10 to 100 minutes. The films were deposited onto C-plane, R-plane sapphire, polycrystalline Al_2O_3 and Si substrate using a wavelength of 248 m, pulse energy of 900-1200 mJ, at pulse rates of 5-50Hz and wavelength 193 nm, pulse energy of 500-650 mJ. A narrow strip is also used so that shadowed and non-shadowed region are both obtained on same substrate.

2.7 Scanning Electron Microscopy (SEM)

The microstructure and composition were studied in a high resolution Hitachi Scanning Electron Microscope model S-570 coupled with an energy dispersive X-ray spectrometer. Thin film sample is cut small piece about 3*3 mm or 2*2 mm depend on the purpose. The sample is mounted on platform. For the thickness measurement, sample is cut freshly before the measurement and then mounted on the sample holder in vertical, use the ultra high resolution to take the photo, and then measure the thickness profile to calculate the thickness.

2.8 The Study of Crystal Structure

The crystal structure and crystallite orientation were determined by x-ray diffraction measurements using Cu $_{k\alpha}$ radiation. Automated data acquisition, and angle scanning control was achieved with a personal computer coupled to an MCA. X-ray diffraction experiments were performed on various film samples in order to investigate the crystal structure of the compound.

Precise lattice parameters were determined by using a fitting program developed in the laboratory. This program determines the weighted root mean square angular deviation between the observed and calculated Bragg angle based on a given structure and lattice parameters. Details of the x-ray diffraction can be obtained from a number of existing references[1,2,3,4].

2.9 Magnetic Measurement

The magnetic measurements were performed at room temperature using two Princeton Applied Research Vibrating Sample Magnetometers(VSM) , one equipped with 90 kOe Nb-Ti superconducting solenoid and a cryogenic system that provides stable temperature control from 4.2 K to 300 K, and the other with a low field of 20 kOe electromagnet,

shown in Figure 2.2, and a furnace that allows measurements over temperature range 300-1000 K. Automated scanning and data acquisition procedures were employed for hysterisis loop measurements, as well as for the x-ray diffraction experiments.

For the magnetic measurement, the sample holder and sample sized substrate piece has a diamagnetic contribution in the order of 10^{-6} emu/g. So, the sample holder and substrate piece, approximately of same size as various samples, were also measured at room temperature as well as at lower temperatures. The combined correction applied for both in-plane and perpendicular measurements.

The typical signal to noise ratio was about 3%. For the sample with high coercivity, it was impossible to saturate the samples fully in the both direction, in plane or perpendicular.

The thermo-magnetic measurements can be made in a field of 2-5kOe in the temperature range of 300K –1000K

Fig.2.3 is a block diagram of a vibrating sample magnetometer.

2.10 Magnetoresistive Measurements

Magnetoresistive measurements were made using a Hall probe for a field determination to eliminate any hysterisis in the magnet system from shifting the zero applied magnetic field values. The measurement set up is shown in Fig.2-4. Bridge circuit is set up for enlarging the change of MR effect. Some samples are measured directly in ohms. Some are measured in mV with a constant current source.

2.11 Heat Treatment

The heat treatment was processed either in the chamber of PLD system or the Lindberg/Blue-M Minimite laboratory tube furnace, which has maximum temperature 1100°C.

The corrosion resistances of dispersive $SmCo_5$ films were processed in the furnace with atmosphere.

2.12 DC Magnetron

DC Magnetron is used to sputter the dispersive film co-sputtered with PLD. The power can be adjusted from the power supply equipment. During the sputtering, pure Ar was used to circulate the chamber. DC magnetron use a 3" x0.125" targets. The targets can be Al, Co, Si, and Ti. etc.

Figure 2.5 is the schematic diagram of DC magnetron sputtering gun.

CHAPTER 3 SmCo BASED PERMANENT MAGNETIC FILMS

3.1 Introduction

For any magnetic system to qualify as a good permanent magnet system, a high Curie temperature, high anisotropy, high saturation magnetization as well as high remnant magnetization need to be exhibited. Transition metals, TM, such as Fe and Co, carry large magnetic moments, and high Curie temperature. Magnetism of the transition metals is due to the unfilled 3d bands and is caused by direct exchange splitting of the 3d electrons. Mean while, rare-earth elements, RE, show strong anisotropy but low ordering temperatures as their magnetization arises from the indirect exchange splitting of the largely localized 4f shell electrons. As a result, rare earth-transition metal inter-metallic compounds benefit from the high magnetic moments of the TMs and the high anisotropy of the REs, making them suitable for permanent magnet applications. SmCo based compounds satisfy the above said criteria. Among them, transition metal rich $SmCo_5$ and Sm_2Co_{17} compounds are widely used for their superior permanent magnet properties. These materials can be synthesized both in bulk and thin film form depending on their usage.

3.2 High Coercivity SmCo Based films made by 193 nm laser

SmCo based films deposited by PLD in the absence of any shadow onto heated alumina substrates exhibited a strong dependence of Sm concentration on the argon background gas pressure in the deposition chamber. Figure 3-1 shows the Sm concentration for a series of films deposited onto polished alumina substrates at 375° from $SmCo_5$ targets, and at 500°C for SmCo "2-17" targets as a function of Ar gas pressure. The targets in the latter case consisted of normal bulk type "2-17"" magnet material with a composition of Sm 13at%, Co 58 at %, Fe 20at%, Cu 7 at%, and Zr 2 at%. This result is similar as the results of $SmCo_5$ film made by RF sputtering. During RF sputtering deposition large concentration change can also be effected by using increased sputtering gas pressures and in particular admixtures of Xe as a part of the sputtering gas[1]. Changes in the sputtering gas pressure could be used to vary the film composition from 12 to 18 at% [2]. Higher pressures tend to preferentially scatter the lower mass transition metal atoms relative to the more massive Sm atoms. The net effect is that the lighter transition metal atoms are on the average scattered through larger angles and effectively removed from the deposition beam. Higher pressures in the deposition chamber tend to enrich the Sm Concentration in the films. This kind of collision processes involved in thermalizing collisions between the sputtered atoms and the sputtering gas atoms have been modeled with more and more refinements for Sm-Co system in RF sputtering. The most complete outline of the calculations was given in the thesis of H.Hedge [3].

Due to the mechanism of PLD, there are a lot of particulates during the deposition. So films made under vacuum, exhibited a large number of particulates causing such films to be unattractive for film device application.

Films of SmCo based films made without using any particulates limiting technique exhibited appreciable density of particulates. The particle density varied with gas pressure in chamber. Nonshadowed films made at 500°C and 30 mTorr Ar exhibited an average particulate density of $0.21/\mu m^2$; similar films except at 75 mTorr Ar exhibited $0.33/\mu m^2$. In order to limit the number of particulates arriving ar the substrate a stainless steel sheet metal shadow was located in the deposition plume to block the direct transport of particulates to the substrate. A higher background gas pressure of argon was then required to scatter the atoms to reach the substrate. The shadow mask strip was arranged midway between the target and substrate so that the shadow blocked a 13*50 mm substrate region. Actually there are many techniques have been explored to limit the particulates as mentioned before. But consider the deposition rate and simplicity; the simple strip may be the simplest and most applicable. In this set up, all the useful deposition behind the strip came from the scattering either with Ar atoms or target material itself. The significant result is that only atomic species in the plume can be scattered to the shadow region of the substrate. So only the region behind the shadow strip, so-called shadow region, is particulates free (no micro or sub-micro particles). This can be seen in Fig.3-2 and Fig.3-3. Fig.3-2 and Fig.3-3 are the SEM picture exhibited the difference of surface conditions. Fig.3-2 shows the non-shadowed film, which has higher

density of particulates. Fig.3-3 shows the shadowed film, which has less density of particulates. The higher coercivity film only can be obtained from shadow region.

Room temperature hysterisis loops measured in plane and perpendicular to the plane are shown in Fig.3-4 for a shadow region film deposited at 375°C and 100 mTorr Ar at a laser wavelength of 193 nm with a pulse rate of 14Hz. The laser pulse energy is 500 mJ. The PLD target was bulk $SmCo_5$. The in plane iHc was 9.7 kOe and the loop shape was characteristic of single-phase material. The perpendicular measurement shows that may some easy axes skew out the film plane, because the perpendicular loop is not closed. An x-ray diffraction pattern for the Fig.3-4 is shown in Fig 3-5. The evident $CaCu_5$ type structure (110) dominant texturing and (111) secondary $CaCu_5$ type are consistent with the relative shape of the in plane and perpendicular to the plane hysterisis loops.

Fig.3-6 shows hysterisis loops for an SmCo based film shadow deposited at a substrate temperature of 375°C in 100 mTorr Ar at a laser pulse rate of 10 Hz. The in film plane iHc was 11.3 kOe. The film surface was mirror like. The smooth mirror like surface was consistent with a small average grain size.

3.3 Fully In Plane Aligned SmCo Based Films by 248 nm Laser

As mentioned before, the PLD system can apply several different wavelengths. Simply change the laser operating gas from ArF to KrCl; the system will operate at the wavelength 248nm. The maximum output energy will be as high as 1300mJ. Using the same set up as before. A narrow strip also was used to block direct deposition. So at same sample will have both shadow region and non-shadow region.

Fig.3-7 shows room temperature hysterisis loops for SmCo film shadow deposited from bulk $SmCo_5$ targets by high pulse energy PLD using λ=248 nm at a pulse energy of 1200 mJ with repetition rate 14 Hz. The deposit was directly crystallized onto alumina substrates at 375°C in 100 mTorr Argon. In plane hysterisis loops for measurement fields up to ± 20kOe and ± 90kOe are both shown in this figure. This film was about 1 μm thick. The deposition rate is about 0.5 Å/s. For such films the low field measurements yield only minor loops that are generally offset because the films exhibit some remnant moment as removed from the PLD system. For this film the high field measurements indicated an in plane intrinsic coercive force of 22.5 kOe. For this film measurements made perpendicular to the film plane, as shown in Fig.3-7, indicated only skewed lines with no detectable coercivity or perpendicular remanence.

In most sample deposition here, films have been simultaneously deposited onto Alumina and Silicon substrate. Very little difference was observed in the film magnetic properties for these different substrate materials. Fig.3-8 and Fig.3-9 are the films

deposited at same time but on different substrates, one is on alumina , the other is on silicon substrate. Each film has the coercivity about 15 kOe. Actually the substrate may have effect on the growth of films, especially thin film and epitaxial film[1]. In this case, relative thick film, different substrate may not significantly change the film's magnetic properties.

Film compositions were determined using electron excited x-ray analysis in a scanning electron microscope SEM. The film composition measurements were calibrated against known bulk composition standards. The film in Fig.3-7 contained 20-22 at.% Sm. This is corresponded to the Fig.3-1 that the background gas pressure will vary the composition of films.

As discussed previous section, high coercivity film have only been observed for shadow deposited films. Fig.3-10 shows SEM micrographs for the film of Fig.3-7 in (left) and out of (right) the shadow region. Visually both regions were mirror-like, but the SEM examination shows the film structure to be very different. The shadow region exhibits a very fine grain structure of <0.2 μm that is not clearly discernible. In the nonshadow region only, polishing marks on the underlying substrate were replicated. The nonshadow deposit shows a mixed deposit consisting of fine and coarse grain sizes. The density of particulates is higher than the 193 nm laser deposition.

Both shadow and nonshadow regions of the same substrate showed similar x-ray diffraction patterns with $CaCu_5$ type (110) and (200) reflections dominant. Films made at

high laser pulse energies did not give any indication of crystallites with c axes skewed out of the film plane. The shadow region of such films exhibit high coercivities of >20kOe, and closed perpendicular to the film plane hysterisis loops. Fig. 3-11 shows an x-ray diffractometer trace of nonshadow region of same deposited sample as Fig.3-7. Judging from the x-ray alone there was the expectation that the nonshadow deposit should exhibit reasonable magnetic properties. But this was not the case. Figure3-12 shows the typical non-shadow region hysterisis loop. The observed nonshadow region hysterisis loops were composite loops indicative of noncoupled fine and coarse grain regions as seen in the nonshadow region SEM micrograph. The observed nonshadow hysterisis loops were constricted near the origin. It should be noted that shadowed regions of the same substrate exhibited high coercivities and single-phase type hysterisis loops. Thus contamination may not cause the loop constriction for the nonshadow regions.

Since the target is heated during deposition and no post heat treatment involved, the SmCo based material is directly crystallizing onto the heated substrate. The film with higher coercivity showed x-ray diffraction patterns with $CaCu_5$ type (110) and (200) reflections dominant. An interesting question here is whether the grain is single domain grains or multigrain domain.

For single domain grains hard magnetic thing film, in the ideal case the grains act independently and a sample can be much easy to magnetize in those directions corresponding to a preferential alignment of the easy axes of the grains. The increase in magnetization parallel to an applied field in this case is by rotation of the magnetization

within the grain. As an initially applied magnetic field is reduced, the magnetization of the grains tends to relax by rotation to the direction of the easy axes of magnetization of the grains. $SmCo_5$ with ordered $CaCu_5$ structure have hexagonal lattice constants with a~5Å and c~4 Å. Hexagonal crystal systems exhibit uniaxial structures. A bulk sample, which consists of a random distribution of crystallites in three dimension is then expected to exhibit a remanent to saturation magnetization ration of 0.50. For a film consisting of single domain uniaxial crystallites, the expected remanent magnetization is expected to be $2/\pi$=0.637. From SEM, the average size of grain is observed less 200 nm. Table 1-2 shows the typical single domain grain size for some materials. The single domain grain size is about 1.68μm for $SmCo_5$. Since the film is only about 1μm thick, so the film must be single domain grain. But the observed remanent ratio is much higher than expected.

Table 3-1 shows the list remanent ratio of $SmCo_5$ sample. All samples are come from the shadow regions, the observed isotropic in-plane M_r/M_s >0.80 values indicated that the grains were exchange coupled. In general, remanence enhancement is attributed to intergrain exchange interactions[3.5]. Exchange interactions between neighboring grains cause the spontaneous magnetic polarization to deviate from the easy axes. As a consequence the resultant polarization parallel to the direction of the applied field is increase. In two-phase permanent magnets remanence enhancement owing to exchange interactions is much more effective.

It has been calculated by T.Schrefl using numerical micromagnetic calculations[3.6] to show that in order to achieve a significant enhancement of the remanence and to preserve

a high coercive field in isotropic nanorystalline $Fe_{14}Nd_2B$-based magnets, a mean grain size d<20 nm and a homogeneous microstructure with a very small range in grain size are required. So in our case, the non-shadow region and shadow region sample have almost same x-ray diffraction pattern, but only the shadow region sample exhibit the higher coercivities and enhanced remanence ratio. We may conclude that the coarse grains of the nonshaodw deposits were too large to exchange couple so that narrow hysterisis loops were observed.

3.4 Variation of Properties with Laser Pulse Rate.

Fig.3-13 shows the room temperature iHc versus the laser pulse rate for films made with λ=193nm with pulse energies of 500-650 mJ, and for films made with λ=248 nm with pulse energies of 1000-1200 mJ. At lower temperatures the coercivities increased, as expected, as indicated by the values measured at 140 K. It was necessary to use the higher laser pulse energies to achieve the higher coercivity values. The laser pulse energy was more crucial than any difference in laser interaction due to the difference in laser wavelength. This was shown by the fact that the region of maximum coercivity was the same as a function of pulse rate for the two wavelengths. Figure 3-14 shows the five hysterisis loops with different repetition rate.

Fig.3-13 also shows that higher or lower laser pulse repetition rate cannot lead to higher coercivities. The reason for this is that higher laser pulse rates did not allow sufficient site relaxation between pulses, while lower pulse rates lead to film contamination because of the longer time between deposition pulses. An operative deposition condition is that $(T/R)^{1/2}$=const.*d, where T is the absolute substrate temperature with the surface atom speed proportional to $T^{1/2}$, d is the site relaxation distance, and 1/R is the time between laser pulses for the pulse rate R.

Normally the laser wavelength λ comes into play mainly in the effectiveness of the absorption of the laser power into the target. The different wavelength can cause the different target surface condition and eject different size particulates. When wavelength

changed from 196 nm to 248 nm, the energy per pulse is more than doubled. One of the positive effects is the energy of per particle also increased. So at the same repetition rate, the sample made with higher deposition energy may more easy to site relax to grow in long stacking texture (200) and (110). X-ray diffraction patterns for SmCo sample made by 248 nm and by 193 nm wavelengths are shown in Fig.3-15. The sample made by 193 nm wavelengths, which associated with lower energy show that (111) is comparable with (110) structure. For the sample made by 248 nm wavelengths show the dominated (200) and (110) structure.

The overall deposition rate per second for PLD is comparable to sputtering. But consider that the pulse deposition is made at very short pulse duration time, about 15 ns per pulse, the pulse deposition rate per second following a pulse is much higher than the average rate. Most deposition in PLD occurs immediately after a pulse, so in a very short time may a complete layer of atoms are deposited onto the film. Therefore, oxidation and growth relaxation may play much more important role in PLD than in sputtering. The result of this is that higher repetition rates may stop the relaxation and lower repetition rates that allow more oxidation time may control the main process. It is why the higher coercivity films only obtained at very specific repetition rates.

3.5 Variation of Properties with Pressure and Temperature.

Texture film growth requires that the energy and momentum of the deposited atoms be controlled to avoid disrupting the growth of a particular texture mode. In deposition this is accomplished by using sufficiently high sputtering-gas pressures so that the deposited atoms undergo collisions before reaching the substrate position. Various methods employing inert gases or mixtures such as Ar, Ar-Kr,Ar-Xe, Kr, and Xe have been used to enhance the degree of preferential texturing that the permanent magnet films exhibit[3.2]. In the shadow PLD deposition, the situation is more complicated. First, the pressure will change the deposition rate. Compare the thickness of non-shadow and shadow region deposition, the overall thickness of non-shadow sample is 3 to 4 times of the thickness of sample in shadow regions. The higher pressure, the more uniform the shadow region film. So change of the pressure will cause the change of deposition rate. It has been report that by lowering the sputtering pressure so that longer stacking sequence of the (200) growth mode be disrupted, the shortest in plane mode, the (110) family, will became the dominant growth mode [3.1].

The estimation based on the reference [4], the gas pressure of approximately 100 mT employed in systems corresponds to approximately $1x10^{19}$ gas atoms per square centimeter per second striking the substrate and film. The arrival rate compares to typical peak arrival rates of atoms of 10^{18}-10^{19} atoms per square centimeter and typical average

film atom arrival rates of 10^{15} -10^{16} atoms per square centimeter per second. So certainly, the change the pressure will change the growth condition on substrate.

Substrate temperatures usually used during the direct crystallization of SmCo-based films are in the range from 350 to 700°C. The films are being grown in a ferromagnetic state so that the demagnetization energy can play a role in favoring the relative growth of crystallites, which result in a lower value of demagnetization energy [3.1].

Since the complicity of PLD deposition on shadow region, it is argued that the pressure and temperature are important factors of growth dynamics. Different system may has different optimized parameters.

3.6 Conclusion

Due to the splashing, mentioned earlier, a stainless steel shadow has been used to block the direct transport of particulates to the substrate. It is shown that this steel shadow strip is essential to get the higher coercivities of SmCo based magnetic thin films. SmCo based films deposited by PLD onto heated substrates exhibited a strong dependence of Sm concentration on the argon gas pressure. Changes in the sputtering gas pressure could be used to vary the film Sm composition from 12 to 24 at%. Higher pressures tend to preferentially scatter the lower mass transition metal atom components relative to more massive Sm atoms. The net effect is that the lighter transition metal atoms are on the average scattered through larger angles and effectively removed from the deposition beam. Higher pressures in the deposition chamber tend to enrich the Sm concentration of the films. Films made in vacuum exhibited a grain size of 0.17 to 0.30 μm diameter. The particulate density for non-shadowed films increased with pressure even though the number density of the larger sized particulates remained nearly constant. Non-shadowed films made at 500°C and 30 mTorr Ar exhibited an average particulate density of 0.21/μm. similarly films at 75 mTor Ar exhibited an average particulate density of 0.33/μm.

The deposit in the shadow region was particulate free. Films made at this condition gave quite good results. The highest coercivity of 22 kOe obtained for a pulse rate of 15 Hz and laser pulse energy of 1250 mJ. The hysterisis loops for the films made at laser pulse rates between 5 to 50 Hz also have been studied carefully. The coercivities of films

are a distinct function of the laser pulse repetition rate. Higher laser pulse rates did not allow sufficient site relaxation between pulses, while lower pulse rates led to film contamination because of the longer time between deposition pulses.

At optimized conditions, SmCo-based film samples consisted of fine particles with c-axes fully in-plane aligned. As mentioned before, an independent collection of such grains should exhibit a remnant to saturation ratio of $2/\pi$. The actual ratio was much greater than this and is about the order of 0.9. This is possible when the grain size is of the order of 50- 200 nm and the separation is so small enough for them to be exchange coupled.

Results also showed that the growth textures of SmCo films are strong functions of laser pulse energy and of the laser pulse repetition rate. The films show the presence of (111) in lower laser energy, while the higher energy deposition the films show the (110) and (200) but not (111), which indicates the absence of crystallites with c-axes skewed out of the film plane. Such highly in-plane oriented films all show very high coercivities >20kOe, and closed perpendicular to the film plane hysterisis loops.

CHAPTER 4 ENHANCED MAGNETIC PROPERTIES OF NANOPHASED $SmCo_5$ FILM DISPERSIONS

4.1 Introduction

It was demonstrated that SmCo based films could be directly crystallized onto moderately heated substrates by pulsed laser deposition (PLD) with room temperature coercivities of approximately 20 kOe. The crystallite c-axes were randomly aligned onto the substrate plane. A specific laser pulse rate was acquired to allow sufficient surface mobility so that high coercivities could be obtained. The deposited material is thus aggregated into grains of a sufficiently small size to exhibit high coercivities during the time between laser pulses. Shadow deposition was necessary to produce fully textured films with uniformly small grain sizes.

A key feature of PLD is that it is a pulsed technique so that material is ablated from the targets during the laser pulse duration,≈ 15ns, which is short compared to the transit time of the ejected plume to the substrate. So the deposition rate must be very high at laser pulse duration time. The majority time between pulses may almost no deposition. Then the question rose is that if it is possible use to deposit another material during the time between pulses without or almost without change the magnetic properties of $SmCo_5$ films?

In order to make an SmCo based film with simultaneously another material deposition, a 75 mm diameter sputter gun was introduced to deposit material other than $SmCo_5$. The $SmCo_5$ target either arranged coincided or side-by-side with sputtering target. As did before, a metal strip shadow mask was used to block direct line of site transit from the laser target to substrate region of interest. Simultaneously sputter either $Co_{0.5}Fe_{0.5}$, Si, Ti, Al or Co was sputter deposited onto the same substrate from sputter gun. Vary the sputtering gun power then can vary the content ratio of $SmCo_5$ and matrix element.

4.2 Enhanced Corrosion Resistance

Figure 4-1 shows schematic diagram of laser pulse and atom arrival rate time. The pulse width is about 15 ns, time between pulses at 15 Hz is 0.067 second, suppose the distance between target and substrate is 10 cm and the plume consists 100 atoms particulates plume, then the flight time will be about $6x10^{-5}$ second for average 1eV and $2x10^{-5}$ second for 10eV. So the ratio of time between pulses to flight time to substrate=$(0.067s/6x10^{-5}s)\approx 1x10^{-3}$ for 1eV, and $3x10^{-3}$ for 10 eV. So the deposit sits exposed for site relaxation and for gas efflux attack for time=(1/15Hz)-flight time=0.067s-60μs≈0.067s at 1eV. The PLD deposition rate is very high at laser pulse duration time. The majority time between pulses may almost no deposition for PLD. This is main reason that PLD and DC sputtering co-sputtering can work.

Figure 4-2 shows room temperature hysterisis loops for a film sample made by PLD with a bulk $SmCo_5$ target while simultaneously depositing Al from the magnetron sputter source. The analyzed composition was Sm 15.8at.%, Co 74.5at.%, and Al9.7 at.%. The substrates were heated during deposition to 400-430 °C to promote direct crystallization. The PLD and sputter depositions were started and terminated simultaneously to avoid producing an Al capping layer. The room temperature intrinsic coercivity, iHc, equaled 9.9 kOe for the in-plane measurement. A partial magnetization reversal trace is also shown in Fig4-2. There was no evidence for the presence of a second magnetic phase. The openness of the perpendicular to the plane hysterisis loop indicates the presence of crystallites with c axes skewed out of the film plane. This is confirmed by the x-ray trace

shown in Fig.4-3. This film was made onto an alumina oxide substrate that complicated the x-ray pattern. Elemental Al was indicated to be present by the Al (111) diffraction peak. All of the other diffraction lines present were indexed to the $SmCo_5$ structures. Most of the samples synthesized were 0.6-1.0μm thick. Other samples made onto Si substrates yielded a cleaner elemental Al signature for the Al (111) peak. Samples made with lesser and greater Al concentrations exhibited respectively greater and lower intrinsic coercivities with 15 kOe at 5 at.% Al, and 5.7 kOe at 21 at.% Al. Smooth hysterisis loops were observed.

SmCo and Co were also co-sputtered using PLD and DC sputtering gun. Fig. 4-4 and Fig. 4-5 show in-plane and perpendicular to the plane hysterisis loops for PLD $SmCo_5$ films with a different ratio of sputtered Co matrix. It was possible to produce smooth hysterisis loops indicating exchange coupled systems for films containing 84.at % Co, Fig.4-4 and for films containing 89 at.% Co (remainder Sm), Fig.4-5. The room temperature in-plane iHc values were 9.5 and 3.4, respectively. Magnetization recovery after partial demagnetization did not show any evidence of separately acting magnetic phases. Elemental Co was indicated present in x-ray diffraction trace.

Fig.4-6 illustrates the corrosion resistance of PLD $SmCo_5$ nanodispersions in an Al or Co matrix and in PLD SmCo only films. The samples with and without the Al matrix exhibited as-deposited iHc of 15 kOe. The coercivity of the nanodispersed samples in Al remained largely unchanged after heating in air for 30 min at 300° C. In contrast to this, the coercivities of the PLD $SmCo_5$ films were rapidly deteriorated by heating in air to

only 100 °C. typically thin sputtered $SmCo_5$ films are readily deteriorated by even very short time heating in air at relatively low temperatures. In contrast to the SmCo/Al dispersions, the initial coercivity of the Co sample was 10.3 vs 15 kOe for the PLD $SmCo_5$ films. Because $SmCo_5$ grains may be wrapped by Al or Co dispersion, so that the corrosion resistance significantly increased.

4.3 Enhanced Magnetic Properties of Other Dispersion

Fig.4-7 shows room temperature hysterisis loops for a film sample made by PLD deposition from a bulk $SmCo_5$ target with simultaneously depositing $Co_{0.5}Fe_{0.5}$ from the magnetron sputter source. The analyzed film composition was Sm 15.8 at%, co 71.7 at%, and Fe 12.5 at%. High coercivity $SmCo_5$ films deposited without the sputtered matrix were Sm rich at 21 at.%, so that 12.5 at.% of the Co was associated with the sputtered matrix. The alumina substrate was heated during deposition to 400-430 °C to promote direct crystallization. The room temperature intrinsic coercivity, iHc, equaled 11 kOe for the in plane measurement. There was no evidence for the presence of a second much softer magnetic phase. The narrowness of the perpendicular to the plane hysterisis loop indicates the crystallites c-axes are strongly aligned onto the film plane. This was confirmed by the x-ray diffraction, Fig.4-8, with the dominant peaks (200) and (110) of the $CaCu_5$ type structure. The films thickness was determined about 1μm. Samples made with lesser and greater $Co_{0.5}Fe_{0.5}$ concentrations exhibited respectively greater and lower intrinsic coercivities, Smooth hysterisis loops were observed.

Fig.4-9 shows an in plane hysterisis loop for an SmCo film made by PLD while simultaneously sputtering Ti. The analyzed film composition was Sm 20.1 at.%, Co 74.8 at.%, and 4.9 at.% Ti. The room temperature in plane intrinsic coercivity, Hc, was 15 kOe. An x-ray diffraction film for this Ti dispersed film is shown in Fig.4-10. The major reflection present is the (200) peak of the $SmCo_5$ phase. This is followed by the (110) $SmCo_5$ reflection.

It should be noted that such textured film growth would not be present if the deposit had been deposited amorphous and then subsequently crystallized. The substrate for this film was polycrystalline alumina. Substrate diffraction peaks are indicated by mark S in the figure.

Fig.4-11 shows an in plane hysterisis loop as measured at room temperature for $SmCo_5$ deposited by PLD while simultaneously sputtering Si. The analyzed film composition was Sm 23.6 at.%, Co 73.8 at.%, and 2.6 at.% Si. The room temperature in plane iHc was 12 kOe. It was more difficult to maintain high coercivities with higher Si concentrations than with the other metallic additives.

Fig.4-12 shows room temperature intrinsic coercivities for a series of PLD deposited $SmCo_5$ films made while simultaneously sputtering additive elements. The additive elements were Al, Co, $Co_{0.5}Fe_{0.5}$, Si, and Ti. The compositions indicated by Fe are the analyzed Fe content of the films made by sputtering $Co_{0.5}Fe_{0.5}$. For Al and Co additions, the intrinsic coercivities followed the equation, iHc=22.0 kOe-1.7*(at.%)+(6.4E-2)*(at.%)^2-(8.2E-4)*(at.%) where at.% is the added Al or Co atomic percentage. Appreciable amounts of Al and Co could be added without any drastic degradation of the coercivity. When the additive matrix was $Co_{0.5}Fe_{0.5}$ the coercivity remained relatively high, 11.0 kOe for 12.5at.% Fe or equivalently 25 at.% $Co_{0.5}Fe_{0.5}$ .additive of Ti and Si could only be added to about 10 at.% before there was a strong degradation of the coercivity.

4.4 Conclusion

The dual deposition technique of PLD deposition in conjunction with sputtering has been shown capable of making high coercivity SmCo films that retain the crystal texturing of PLD deposited phase. It has been shown that it has been possible to make strongly in plane textured magnetic properties. Because the PLD deposited phase arrives and crystallizes in a time that is short compared to a the time between laser pulses, there is little mixing of the sputtered films exhibit properties that can be enhanced by different additive elements.

Highly corrosion resistant SmCo films were synthesized by PLD $SmCo_5$ deposition while simultaneously sputtering Al and Co. For low Al concentrations, there was little affect on the coercivity following heating in air for 30 min to 300° C. The magnetic grains become isolated at higher Al concentrations.

CHAPTER 5 MAGNETORESISTANCE FILMS

5.1 Introduction

Lanthanum manganese oxides have unique magnetic and transport properties, which interesting both for fundamental studies and for practical applications in magnetoelectronic devices. A variety of applications are including magnetic sensors, magnetic memory devices, magnetic read heads, spin polarized quasiparticle injection devices, spin-dependent tunneling devices, etc.

A thin film technology is required for practical applications of magnetoelectronic devices in microelectronic integrated circuits. For this reason workers have explored a number of techniques for fabrication of magnanite thin films exhibiting the colossal magnetoresistance (CMR) effect: pulsed laser deposition[1], jet vapor deposition[2], and spray pyrolysis[3]. PLD has been proved as an efficient way to make LSMO thin films.

5.2 Polycrystalline and Laminated $La_{0.7}Sr_{0.3}MnO_3$

The properties of LSMO films are known to be very sensitive to the nature of the substrate, due to strains that imposed by the lattice mismatch between the film and the substrate. Figure 5-1 shows the resistance of strips of $La_{0.3}Sr_{0.7}MnO_3$ films that were simultaneously deposited as masked strips onto R-plane sapphire, C-plane sapphire, and polished polycrystalline alumina substrate. The films were deposited at substrate temperatures of 750°C in 120 mTor O_2, f= 30 Hz. The sample used is from shadowed-region, which is a region away from direct deposition using a strip to block part of substrate. The deposition behind shadow is all due to the scattering with background gas O_2. The films were thus relatively particulate free and highly smooth. The resistances shown in the figure are normalized to the maximum value at the resistance maximum. The temperature of the resistance maximum and strip resistance at the maximum were for R-plane sapphire 162 K and 3.58 kΩ, for C-plane sapphire 218 K and 2.41 kΩ. The resistance maximum for the films deposited onto C-plane and polycrystalline alumina occurs at a temperature of 56 and 48 K higher, respectively, than that for the R-plane substrate.

Figure5-2 shows the low field in plane magnetoresistance of these films as measured at room temperature. The resistance are shown normalized to the zero field response to illustrate the contrasting behavior of the R-plane sapphire, C-plane sapphire, and alumina substrates. The strip resistances at 293 K, respectively for R-plane sapphire, C-plane sapphire, and polycrystalline alumina were 2.01, 2.06, and 1.28 kΩ. The film deposited

onto the polycrystalline alumina substrate exhibited a resistance of only 62% of that of the c-plane sapphire substrate sample. The low field response of the inexpensive polycrystalline alumina substrate sample is comparable to that of the C-plane sapphire substrate sample. Low field magnetoresistance at room temperature, 20°C, exhibited an enhanced (1/R)(ΔR/ΔH) of –2.2% kOe for H<0.25/kOe, and an overall (1/R)*(ΔR/ΔH)=-0.24%/kOe up to 20 kOe. The low field magnetoresistance was least for the R-plane sapphire sample. Room temperature hysterisis loops for a $La_{0.7}Sr_{0.3}MnO_3$ made onto an alumina substrate are shown in Fig.5-3. The in plane coercivity was ≈40 Oe. The room temperature $4\pi Ms$ was indicating to be 3.9 kG by the joining of the perpendicular loop to the in-plane loop. The properties of these films are so different may due to strains that are imposed by the lattice mismatch between the film and the substrate[5.4].

Figure 5-4 shows the room temperature normalized magnetoresistance response for $La_{0.7}Sr_{0.3}MnO_3$ films made with and without barium ferrite laminations in a 2:1 thickness ratio. This was accomplished by making thin $La_{0.7}Sr_{0.3}MnO_3$ film layers alternated with intervening layers of barium ferrite. Barium ferrite was chosen since it exhibits a very high resistivity compared to $La_{0.7}Sr_{0.3}MnO_3$ films, and because it offers compatible film processing conditions. The effective resistivity of the laminated film was approximately twice the resistaivity for low temperature processed polycrystalline $La_{0.7}Sr_{0.3}MnO_3$ samples. These films were made under the same conditions onto polycrystalline alumina substrate. The laminated film had a total thickness of 1.4μm and from average deposition per pulse calculations, consisted of 60 layers of 16-nm-thick $La_{0.7}Sr_{0.3}MnO_3$ alternated with 59 layers of 8-nm-thick barium ferrite such that the first

and last layers were $La_{0.7}Sr_{0.3}MnO_3$. The thickness of the layers was determined by SEM measurements of average thickness per laser pulse for separate films of $La_{0.7}Sr_{0.3}MnO_3$ and barium ferrite made under the same conditions. The layered film samples were made by sequentially switching between targets with a motorized carousel. The substrate temperature in each case was 750° C in 120 mTorr O_2 followed by 45 min at 750 °C in 200 Torr O_2. The intergrain coupling was sufficient to maintain electrical conduction, but it has not been possible to directly observe distinct layers under SEM examination. The film made with brium ferrite laminatins exhibited a linear magnetoresistance of – 0.43%/kOe from 0 to ± 5kOe, while the $La_{0.7}Sr_{0.3}MnO_3$ film exhibited the usual low field enhanced Magnetoresistance. The barium ferrite layers for the deposition conditions used did not exhibit appreciable magnetic properties. Room temperature hysterisis loops for the layered film were similar to Fig.5-3 in shape exhibited a similar coercivity as for the $La_{0.7}Sr_{0.3}MnO_3$ films only. The perpendicular to the film plane loop joined the in-plane loop at 2.0 kOe indicating an effective $4\pi Ms$ for the composite structure of 2.0 kG. The barium ferrite layers as deposited are thus mainly acting as nonmagnetic resistive layered.

5.3 Variation of Properties with Laser Pulse Rate

Resistances, normalized to the maximum value, versus temperature are shown in Fig.5-5 for several high laser pulse energy PLD deposited LaSrMnO films. Trace (c) and (d) are for shadow and non-shadow regions of the same substrate respectively. The shadow region, trace (c) , exhibits the resistance maximum at a temperature of 255 K, while for the non-shadow region, trace(d), the resistance maximum was at 155 K. This film was made with a laser pulse energy of 1000 mJ, 248 nm, at 30 Hz with a substrate temperature of 750°C. In this case there was a typical difference of 100 K between the temperatures of the resistance maximum for these film regions. Films made using lower laser pulse energies of 500-600 mJ did not show such large differences in behavior between shadow and non-shadow film regions of the same substrate. Trace (b) exhibiting the broad resistance maximum at 326 K was for the shadow region of a similarly deposited film, but with laser pulse energy of 1250 mJ at 30 Hz. The film is very stable. Subsequent to removal from the deposition chamber, this sample was not heated above 385 K. Another sample, trace (a), initially exhibited the resistance maximum at 360 K. But upon heating to 406 K, the temperature of the resistance deceased to 293 K and was subsequently stable upon recycling at that value.

Fig.5-6 shows the MR measurement of the sample with T_p=326K at different temperature. The sample exhibited a small MR effect $(1/R)\Delta R/\Delta H$=-1.1%/T at 363 K.

This indicates the Curie point would be still higher. In similar samples Curie points as high as 398 K have been measured.

Figure 5-7 shows x-ray diffraction traces, Cu kα radiation, for the shadow and nonshadow region used for Figure5-6, traces (c) and (d). The shadow region of this sample made with high laser pulse energies was very strongly (110) textured. The nonshadow region was almost completely (111) textured. In a different series of films made similarly but at slightly higher deposition rates the shadow region was mixed (111) and (110) textured. This is shown in the upper trace of Fig.5-7. The fitted tetragonal lattice constants were a=3.84 and c=3.96 Å. The substrates were polished polycrystalline alumina. The (110) texture of the shadow deposition corresponds to an appreciably longer stacking distance than the (111) texture of the nonshadow deposit regions. It should be noted that the growth rate of the nonshadow regions exceeds that of the shadowed region. This is consist with more site relaxation time being required to facilitate the growth of the (110) texture mode as has been observed for sputtered films in other magnetic systems. The T_p values, maximum resistance temperature, for similarly prepared films were maximized for a laser pulse rate of 30Hz. No evidence of preferential crystallite alignment within the plane of the film was observed. The use of shadow deposited PLD allowed a uniform and small grain size to be obtained in the films. A film with T_p=292K exhibited a uniformly small grain size of 0.25μm diameter. Nonshadowed regions of that same substrate exhibiting a much lower T_p value consisted of similarly sized triangular grains indicative of the (111) texture for that texture. A film with T_p=265 K exhibited a somewhat larger less regular grain size.

If site relaxation is important, there is an expectation that the laser pulse rate will influence the film properties. Fig.5-8 shows the dependence of the temperature of the maximum resistance for two series of films made from slightly different targets. Except for the pulse rate the deposition conditions were held constant for each series and the films were made over a narrow time period. The laser pulse energy for each series was 1100-1200 mJ. Both series exhibited the highest temperature for the resistance maximum is at 30Hz.

5.4 Texture of $La_{0.7}Sr_{0.3}MnO_3$

Fig.5-9 and Fig.5-10 are the low field magnetoresistive response for two different textured films. The low field magnetoresistive response was distinctly greater when the applied magnetic field was directed in plane and parallel to the sample current than when in plane but perpendicular to sample current. Demagnetization effects reduced the response for applied field range. For these (110) textured films the easy direction of magnetizations of the crystallites were randomly aligned in the film plane and the magnetic hard axes were perpendicular to the film plane. Hysterisis loops measured in plane at different angles were the same. The coercivity peaks at 2.6-3.0 mT are as expected from magnetic hysterisis loops. The arrows on Fig.5-11 show that the response lagged the applied field. A new feature is the large degree of anisotropy in the low field MR for magnetic fields applied in plane parallel versus perpendicular to the sample current for these (110) textured polycrystalline films. At a nominal bias field of 3-10 mT the in plane parallel to I sensitivity was 3.5V/T.

Figure 5-10 shows the low field MR response for a mixed (111) and (110) textured LaSrMnO film corresponding to trace(c) in Figure 5-2 with a T_p value of 269K. The measurements were made at 293K. In this case the response for low fields applied perpendicular to the plane was appreciable because many of the crystallite easy magnetization directions were skewed out of the film plane. The overall response in terms of $\Delta R/R$ was reduced, but still exhibited an enhanced response for fields applied parallel versus perpendicular to the current direction.

Fig.5-11 shows the MR measurement of (110) textured film at different angle between magnetic field and the direction current. The MR of the textured films has been shown to be strongly anisotropic with respect to magnetic fields applied in plane parallel to the current versus perpendicular to the current.

5.5 Conclusion

There are several conclusions can be inferred. One is that high laser pulse energies have been used to grow $La_{0.7}Sr_{0.3}MnO_3$ films that exhibit the resistance maximum at temperatures up to 360 K and with stable smooth values up to 320 K. These samples have been deposited by pulsed laser deposition onto heated polycrystalline substrates. For high laser pulse energy films, shadow and non-shadowed regions of the same substrate exhibit distinctly different textures. By utilizing both shadowed and non-shadowed deposits method together with films deposited at different pulse energies and repetition rate the temperature of the resistance maximum can be tuned to occur at room temperature by adjusting the deposition conditions.

Second the actual magnetoresistance response does not peak at the temperature of the resistance maxima, but does show a more gradual response above that temperature. A well defined low field magnetoresistance is exhibited with a relatively constant intrinsic coercivity up to at least 316 K. This temperature is 26 K above the temperature of the zero field resistance maxima.

Third the properties of LSMO are sensitive to the substrate type. The inexpensive polycrystalline alumina substrate is one of the suitable substrate for growing LSMO films.

It also has been shown that $La_{0.7}Sr_{0.3}MnO_3$ polycrystalline films, in which the grain size and intergrain coupling have restricted very small size by layering with resistive barium ferrite, exhibit the usual maximum in resistivity characteristic of polycrystalline $La_{0.7}Sr_{0.3}MnO_3$ films.

CHAPTER 6 DEVICE APPLICATION OF $La_{0.7}Sr_{0.3}MnO_3$ MAGNETORESISTIVE FILM

6.1 Introduction

The transport of a spin polarized current via the double-exchange mechanism makes these materials attractive for applications in spin electronics. Thin films have been used in the fabrication of prototype devices with a special interest in LSMO because it has the lowest resistivity and the highest Curie temperature (Tc) of the ferromagnetic manganite series, while related materials with calcium LCMO and barium LBMO have higher resistivity and lower Tc[1,2].

6.2 Patterned $La_{0.7}Sr_{0.3}MnO_3$ films

To test whether the films could be patterned for device applications, the films used for Fig.5-5 traces (a) and (b) were dry etch patterned to make strips ≈ 50 microns wide by ≈ 1.5 and 2.5 mm length segments. The dry etch patterning of such films has been previously described[6.3]. The film for Fig.5-5 trace(a) after patterning exhibited a smooth resistance maximum at ≈290K which was the same value as before patterning. The patterned film obtained from the Fig.5-5(a) sample was deemed the most suitable for device applications since the resistance maximum was at nominally room temperature. This patterned film with a nominal resistance of 30 kΩ per mm length was used in a bridge circuit with comparable values to obtain the magnetoresistance data shown in Fig.5-6. Values of the bridge output for 275, 295, and 306 K are shown as a function of an in-plane applied magnetic field. In each case the bridge was adjusted slightly to give zero output at zero applied magnetic field. In plotting Fig.5-7 the magnetoresistive response for 295 and 306K have been offset by 15 and 30mV respectively to avoid overlapping the traces. At each temperature the response was a typical low field behavior exhibiting two maxima separated by twice the film intrinsic coercivity.

Plotted in Fig.6-1, left axis, are the sensitivities in volts per Tesla at an applied field of 10^{-2} T, which is at a position beyond the peak bridge response in each case. The bridge sensitivities at 10^{-2} T were 2.0, 0.80, 0.53, and 0.40 V/T at 275, 295,306,and 316 K

respectively. The peak positions, or intrinsic coercivity values, iHc, versus temperature are also plotted in Fig.6-1, right axis. The bridge circuit was powered by a 9 V battery. No temperature compensation was used for measurements in the vicinity of room temperature. It should be noted that the magnetoresistive element of the bridge was a simple selection of patterned $La_{0.7}Sr_{0.3}MnO_3$ film made onto a polycrystalline substrate.

6.3 Prototype Memory Element

A prototype memory element was tested by placing a small bias magnet parallel to and above the magnetoresistive film strip to be electrically isolated from it. Since the bias field was due to the looping field of the bias magnet, the direction of the bias field was opposite to that of the bias magnet itself. An external sweep magnetic field was then applied parallel to the strip and magnet. The geometry is shown by the inset in figure6-2,. As the external applied magnetic field was swept between plus and minus field values approaching the intrinsic coercivity of the bias magnet, the net magnetic field applied to the strip caused a highly nonlinear response for the LasrMnO strip resistance. The bias magnet was measured to exhibit an intrinsic coercivity between 61 and 62 mT. The response of such a biased LaSrMnO filmstrip as measured at 292 K is shown in Fig.6-2. In the figure the applied field has been cycled between ±59mT three times to demonstrate the stability of the results. It should be noted that the response is distinctly different from the case of a simple bias field that would simply translate the appropriate curve of Fig.6-1. by the bias field value. A distinctive feature as shown by the arrows is that the maximum for positive field values occurs while the field is being reduced from positive values. For negative field excursions the maximum bridge response occurred at zero applied field. The position of the zero applied field is marked by the vertical line in Fig.6-2. Field excursions to 58 mT parallel versus antipallel to the strip length produced zero applied field voltage levels separated by 13.2 mV in this case. The initial magnetization direction of the bias magnet establishes which part of the trace represents the low and high voltage levels at H=0.

Stable and repeatable voltage level differences at zero applied fields were obtained by using trailing pulse logic. In this mode of operation, the bias magnet was reset by a leading pulse exceeding the coercivity of the bias magnet, +100 mT here, which was followed by either a positive or negative applied field pulse of 60mT. Representative pulse train values and the resulting memory state values are shown in Fig.6-3. The value of the memory voltage following the coupled pulse pairs differed by 18 mV in the specified geometry. The memory state voltage was either high or low depending upon whether the trailing pulse had been +60 or –60mT.

The magnetoresistance of the patterned (110) textured films has been shown to be strongly an isotropic with respect to magnet fields applied in plane parallel to the current versus perpendicular to the current, and to be immune to perpendicular fields in the low field region. Since the patterned LaSrMnO strip used in this bridge exhibited a broad resistance maximum as a function of temperature at 292 K, temperature compensation was not needed for room temperature operation. The introduction of a small interacting bias magnetic, and in principle a film magnet, oriented parallel to the strip resulted in a memory structure with separate zero field voltage levels depending upon whether the last applied field state had been parallel or antiparallel. Stable repeatable memory states have been obtained by using trailing pulse logic in which the bias magnet state is reset by the leading pulse. The zero applied field memory states of LaSrMnO biased filmstrip were nonvolatile and persisted in the absence of any current flow. Consequently current would

only need to be present during memory state poling. Thus low duty cycle operation would be anticipated.

6.4 Conclusion

LaSrMnO films exhibiting room temperature T_p values were patterned into thin strips by dry etch methods to yield appreciable low field MR for stable room temperature operation.

A stable memory element was constructed by placing a small interacting bias magnet strip parallel to and slightly above the film strip. Two appreciably different voltage states were observed for the zero applied field values following positive versus negative applied magnetic field excursions.

Table1.1 Excimer Laser Operating Wavelengths

Exciemer	Wavelength(nm)
F_2	157
ArF	193
KrCl	222
KrF	248
XeCl	308
XeF	351

Table 1-2 Magnetic properties of domains and domain walls for samarium-cobalt and neodymium-iron-boron

	Domain wall surface energy (mJ/m^2)	Domain wall width (nm)	Single-domain particle Diameter (μm)
$Nd_2Fe_{14}B$	30	5.2	0.26
$SmCo_5$	85	5.1	1.6
Sm_2Co_{17}	43	10.0	0.66

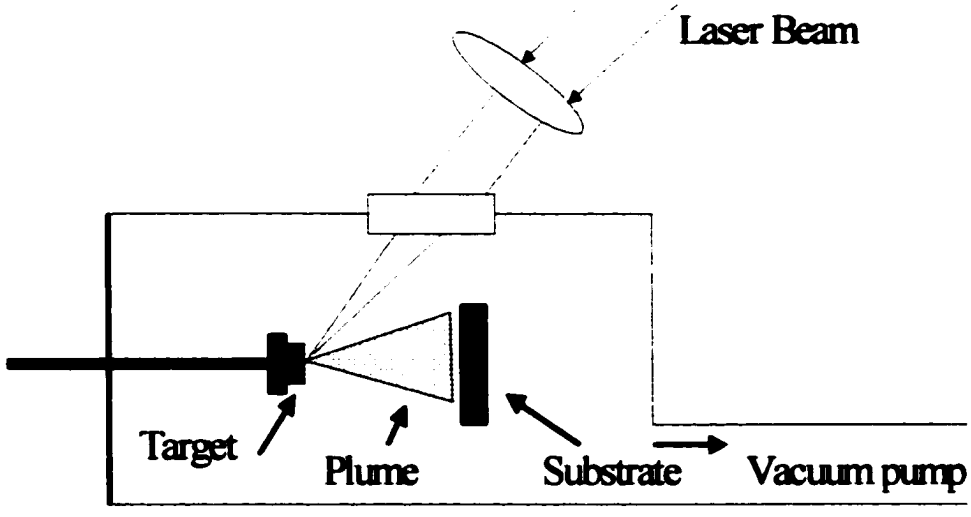

Figure 1.1 Schematic diagram of a pulsed laser deposition apparatus

Table 2.1 List of targets used in this work

Target	Purity	Dimension
Fe	99.9%	1.00" DIAx0.125"
Ti	99.7%	1.00" DIAx0.125"
Si	99.999%	1.00" DIAx0.125"
Si	99.999%	3.00" DIAx0.125"
Co	99.95%	1.00" DIAx0.125"
Co	99.95%	3.00" DIAx0.125"
SmCo		1.00" DIAx0.25"
Al	99.7%	3.00" DIAx0.125"
LaSrMnO		1.00" DIAx0.125"

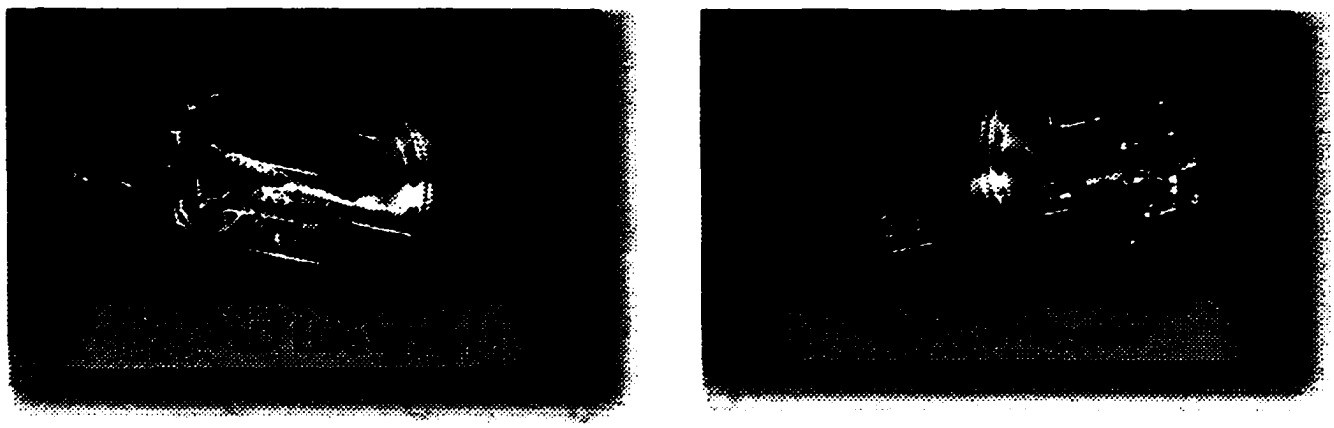

Figure 2.1 Heater and Carrousel of PLD system

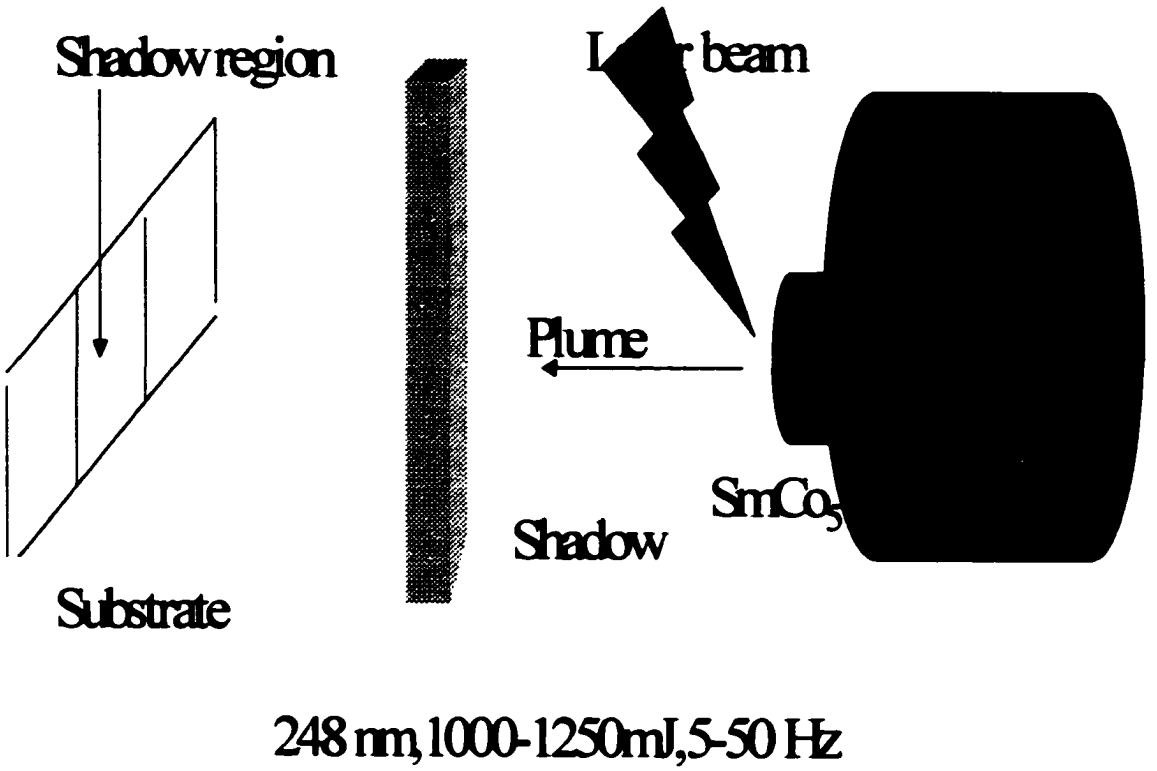

Fig.2.2 An arrangement of targets, shadow strip and substrate.

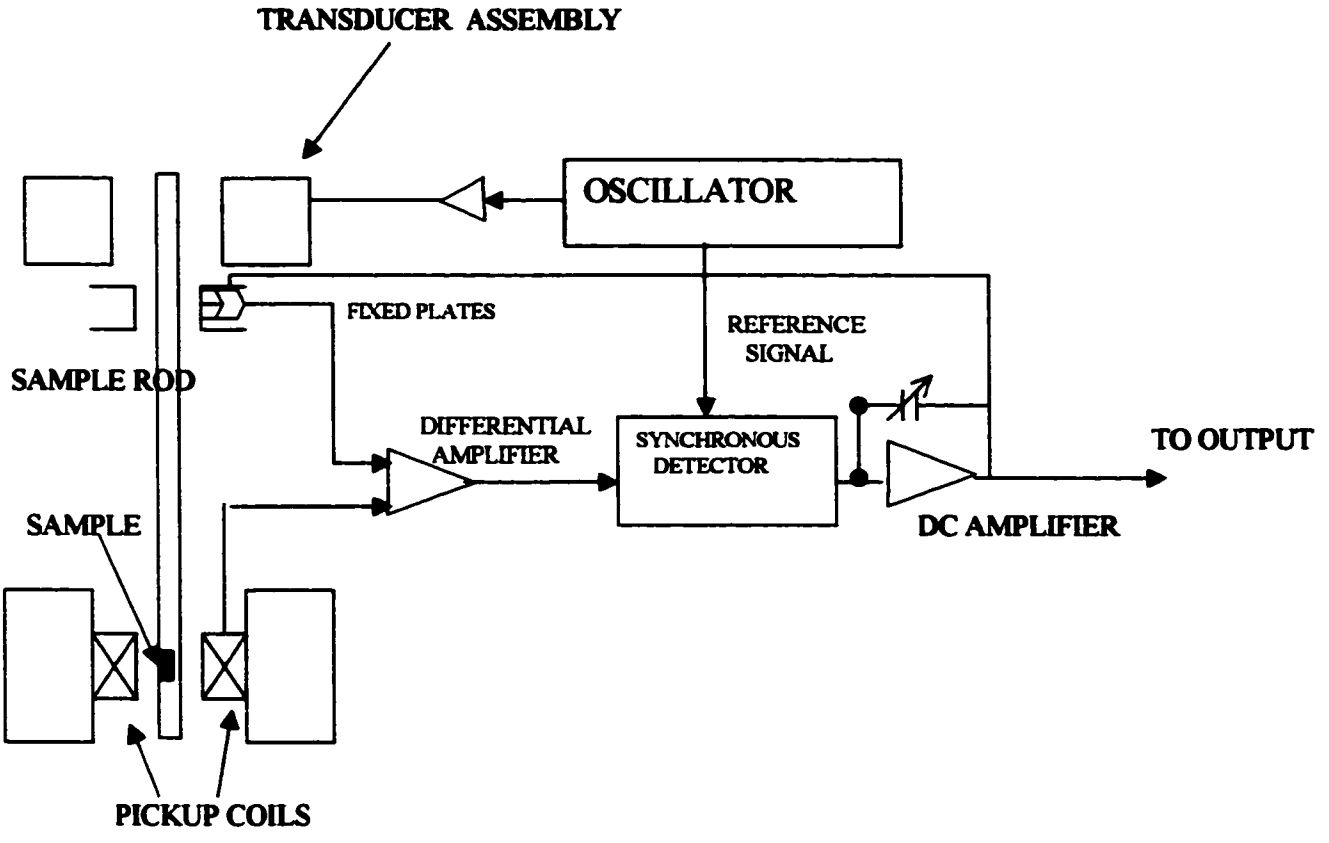

Fig.2.3 Block diagram of a vibrating sample magnetometer

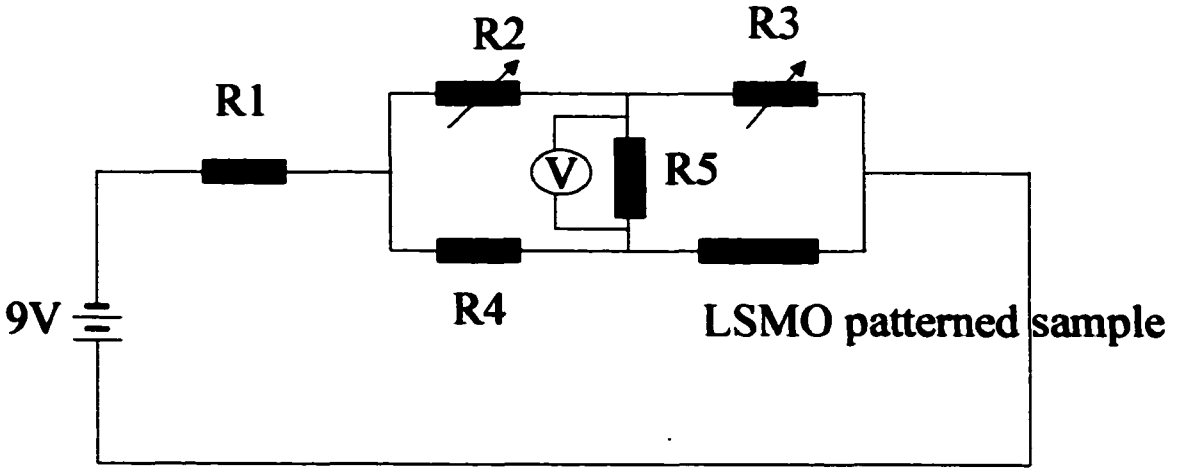

Fig.2-4. Bridge circuit used for measuring the MR effect of patterned LSMO sample.

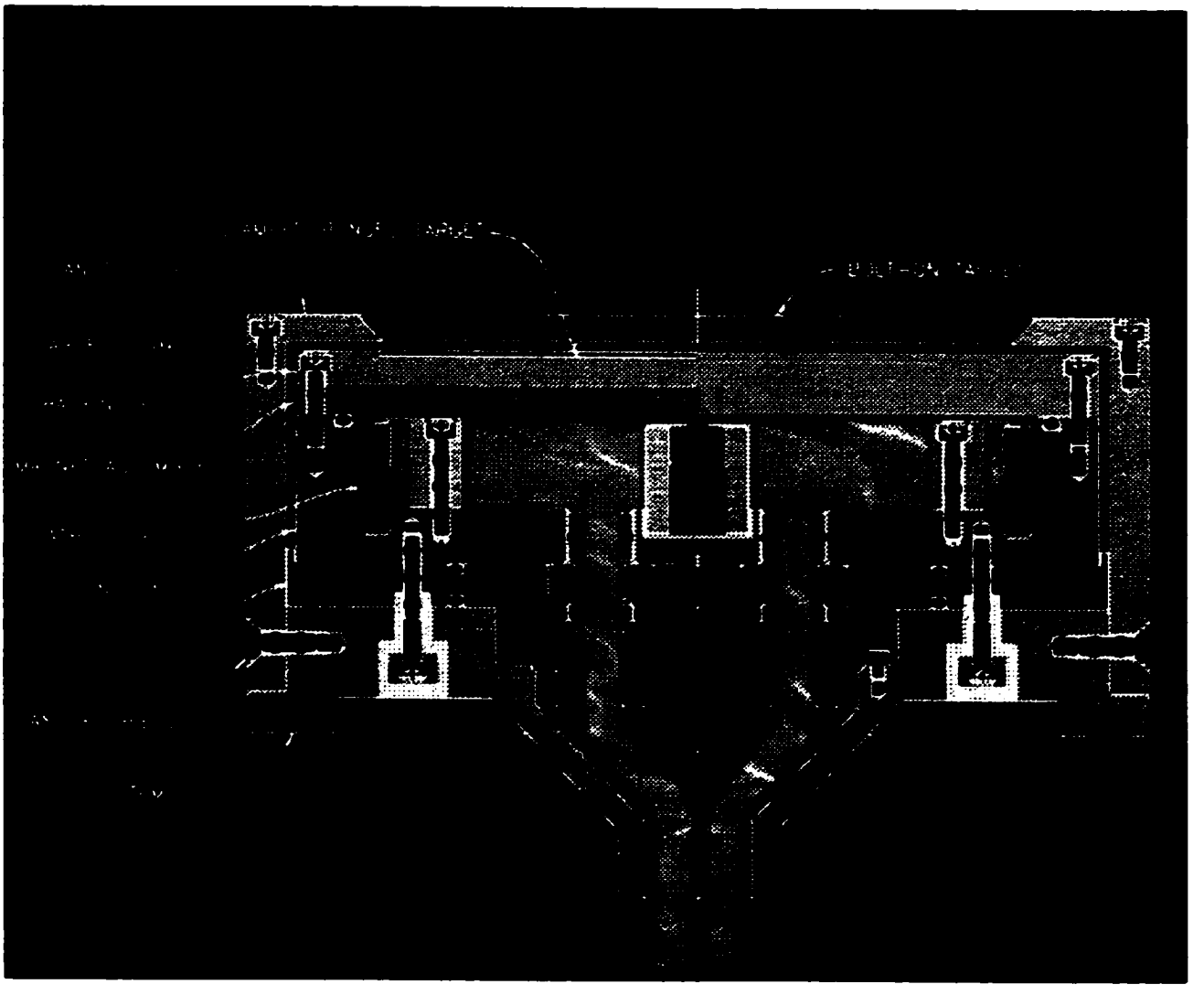

Figure 2.5 Schematic diagram of DC magnetron sputtering gun

Table 3-1 The Mr/Ms ratio of $SmCo_5$ films deposited by PLD

High Laser Pulse Energy SmCo Shadow Deposition				
SAMPLE TEMP.	**(Mr/Ms) IN-PLANE**	**PULSE RATE**	**iHc**	
C28S1(AL_2O_3)	**0.96**	**12Hz**	**18.9kOe**	**295K**
CS28S2(SILICON)	**0.85**	**12Hz**	**18.9kOe**	**295K**
C28S2(AL_2O_3)	**0.91**	**12Hz**	**18.9kOe**	**295K**
C29S1(AL_2O_3)	**0.85**	**15Hz**	**17.7kOe**	**295K**
C29S2(AL_2O_3)	**0.85**	**15Hz**	**17.3kOe**	**295K**
C30S2(AL_2O_3)	**0.75**	**10Hz**	**18.5kOe**	**295K**
CS28S2(SILICON)	**0.83**	**12Hz**	**24.2kOe**	**140K**
C28S2(AL_2O_3)	**0.87**	**12Hz**	**24.2kOe**	**140K**

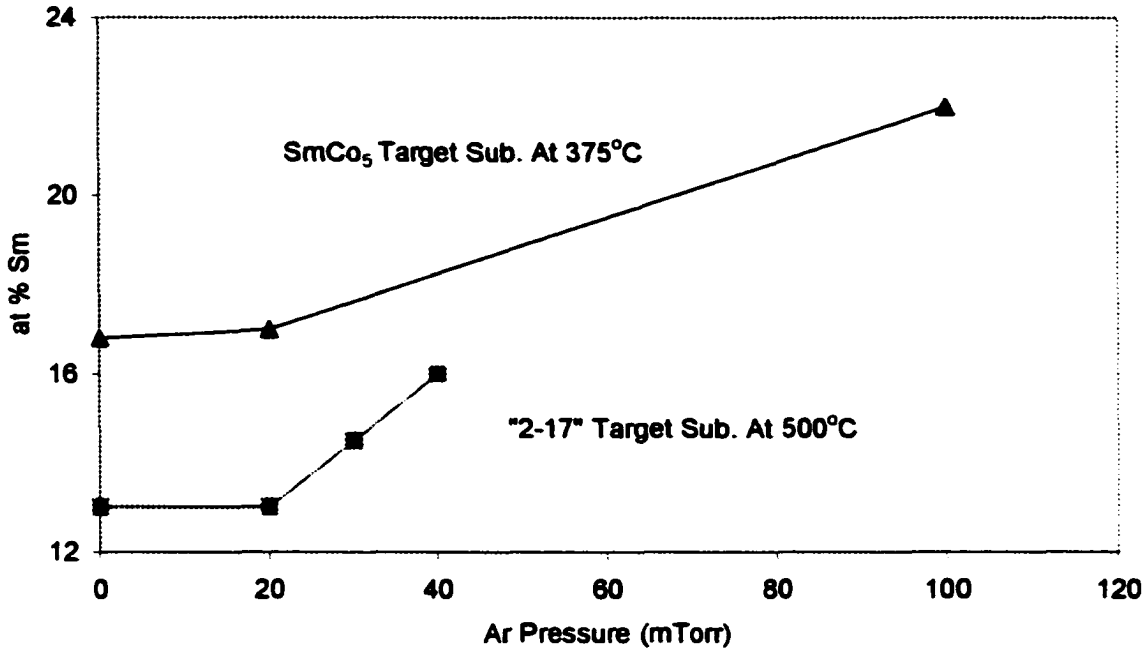

Fig.3-1. The Sm at. % for a series of PLD films made on to 375°C substrates from bulk $SmCo_5$ targets, and films made onto 500°C substrates from bulk SmCo "2-17" targets, for different Ar pressures during the deposition is shown.

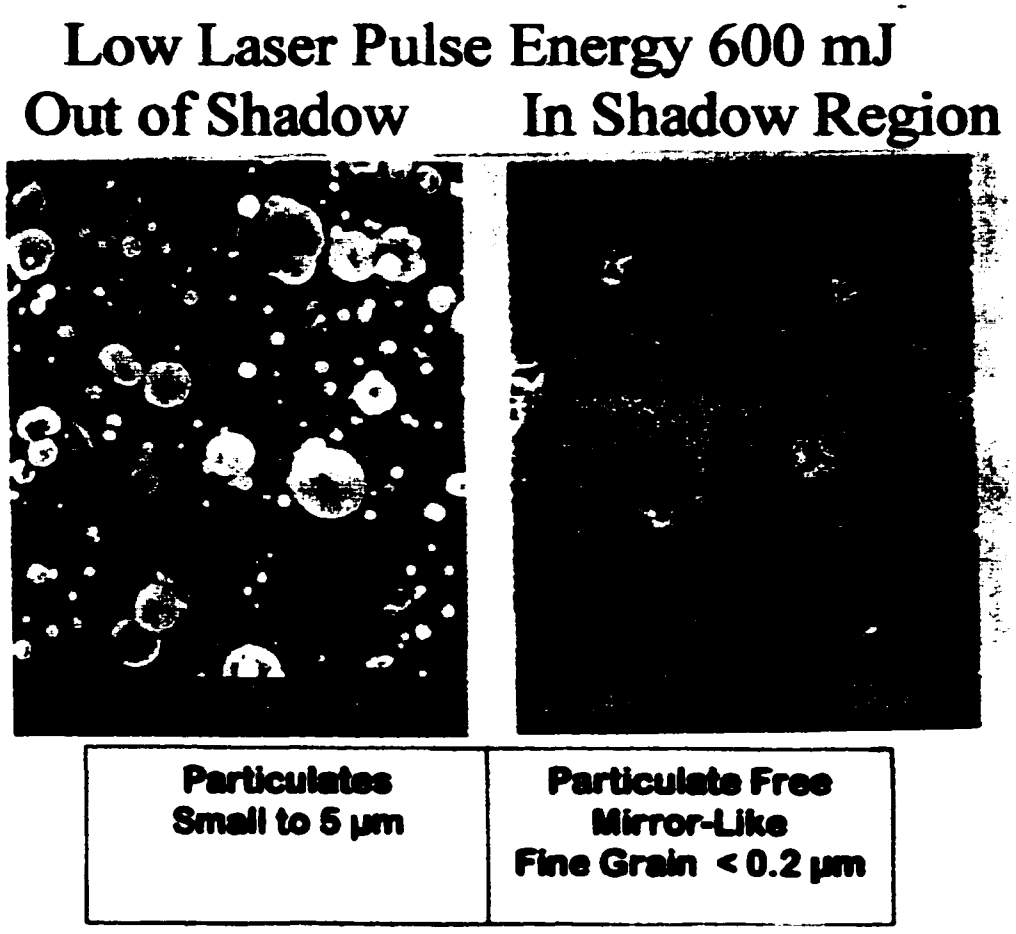

Fig.3-2 (right) and Fig.3-3 (left)

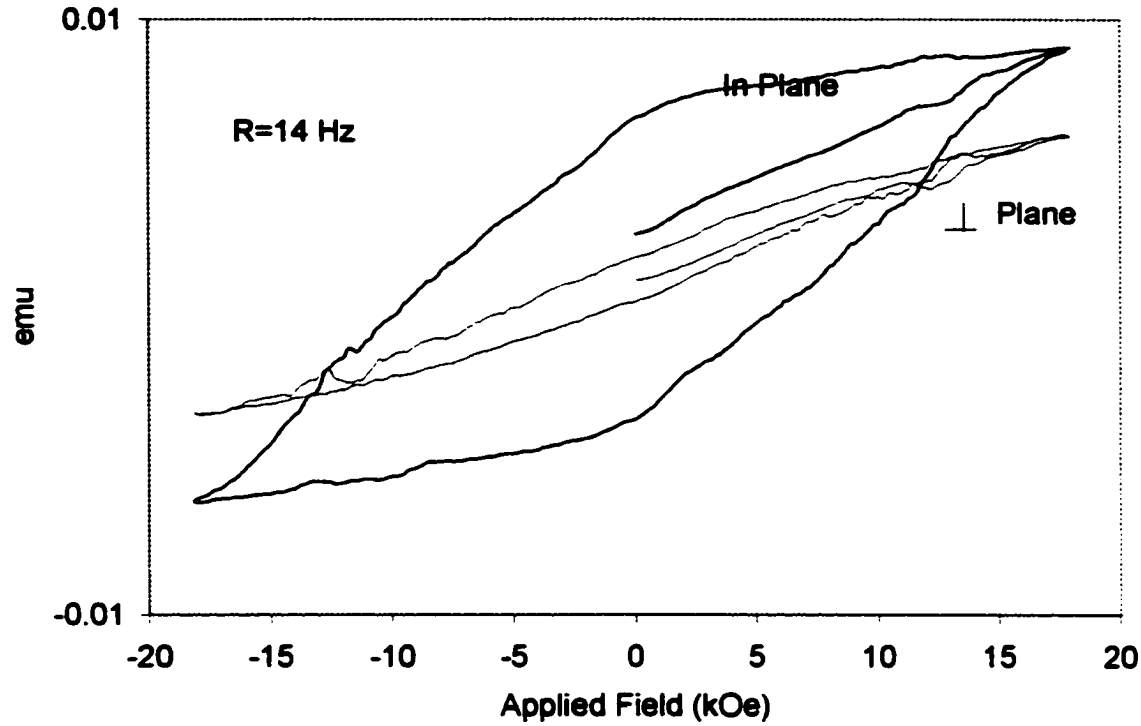

Fig.3-4. Room temperature hysterisis loops for a shadow deposited PLD film made from $SmCo_5$ target at 375°C onto alumina substrate, pressure 100 mTorr Ar, pulse rate 14 Hz are shown. The intrinsic Coercivity is 9.7 kOe.

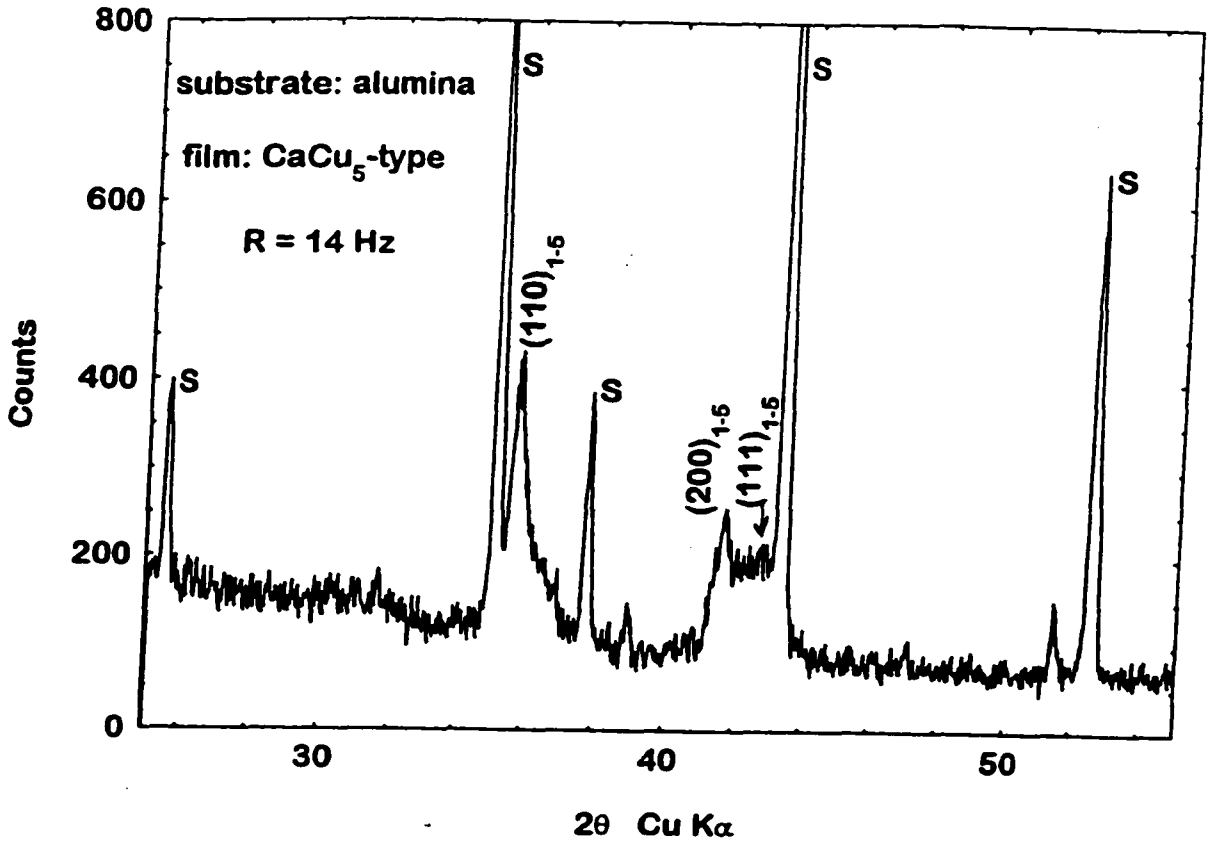

Fig.3-5. An x-ray diffraction trace for the film of Fig.3-4 is shown which indicates (110) dominant and (111) secondary texturing. X-ray indexed as $CaCu_5$-type structure film. The substrate lines form the polycrystalline Al_2O_3 are indicated by s in the figure.

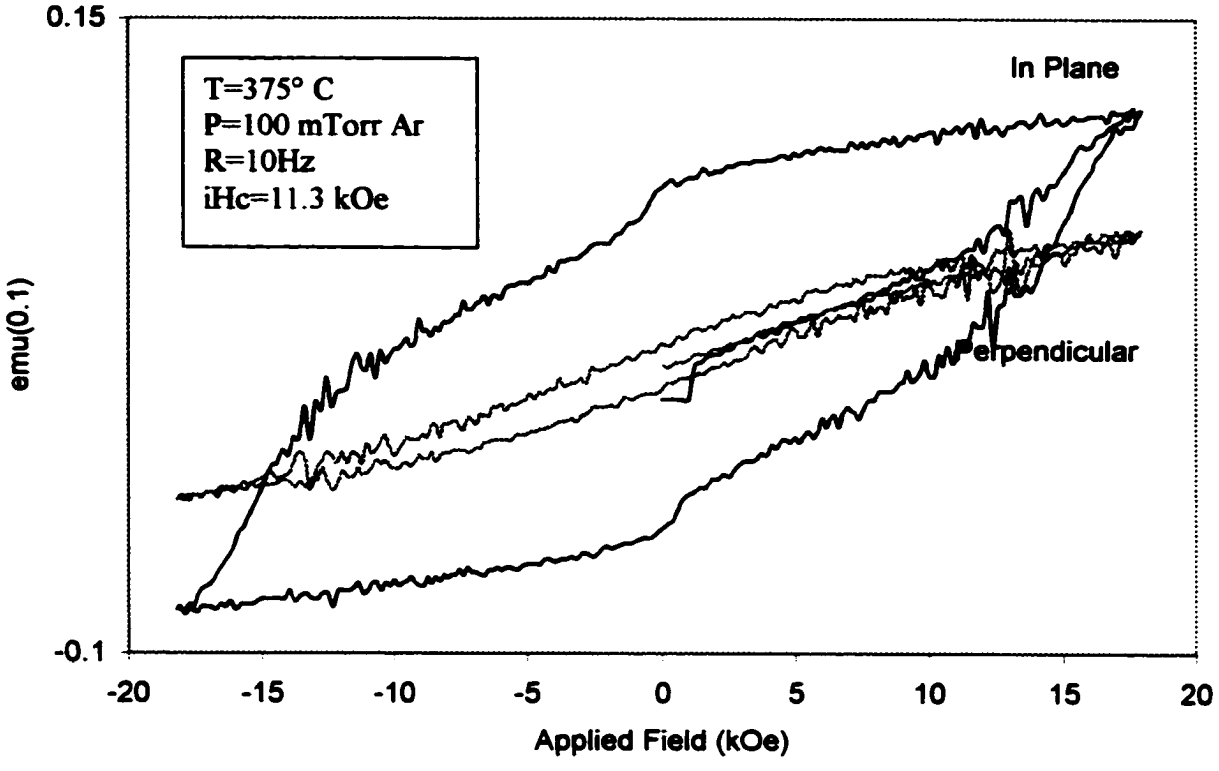

Fig.3-6 Room temperature hysterisis loops are shown for a PLD film deposited from bulk $SmCo_5$ target at 375°c, pressure 100 mTorr Ar, shadowed deposition. The laser settings were 193 nm, 600 mJ pulses, 10 ns pulse width, and 10 Hz.

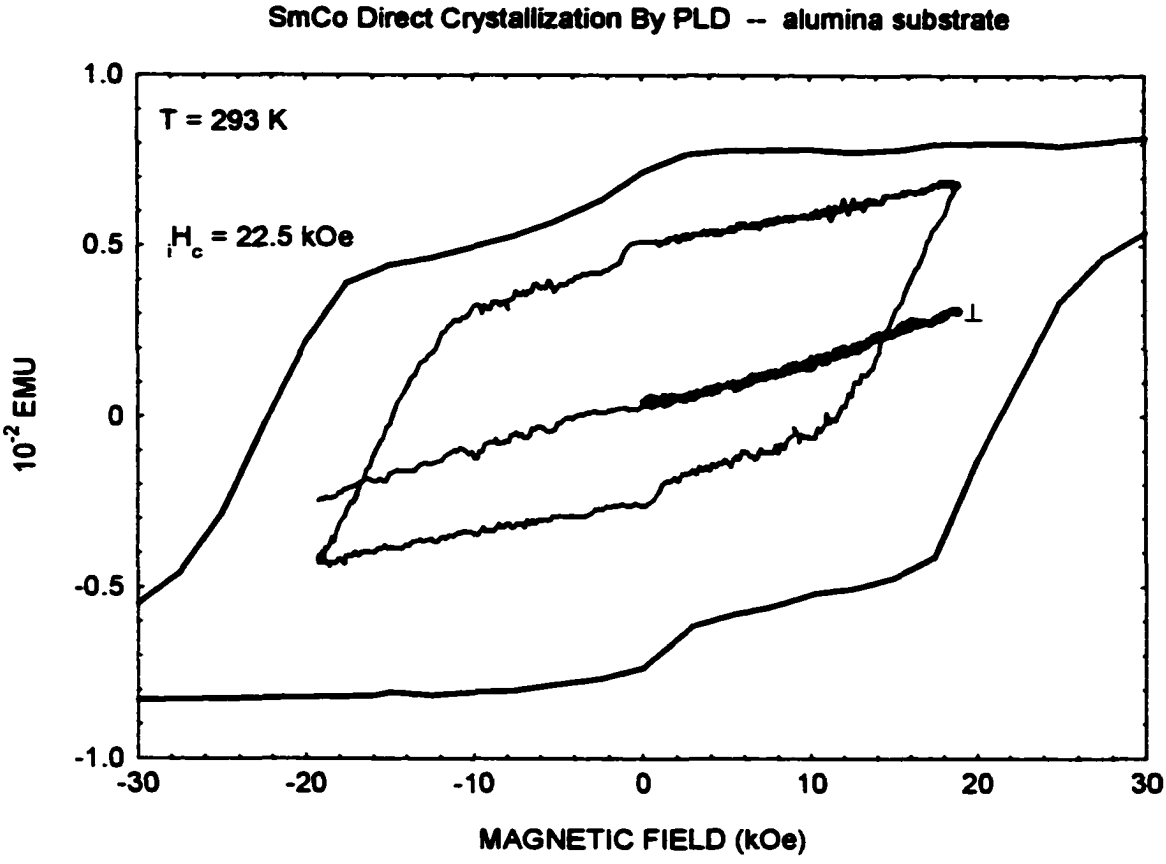

Fig.3-7 Hysteresis loops as measured at 293 K are shown for a SmCo shadow deposited film deposited with a pulse energy of 1200mJ with a repetition rate of 14 Hz. In plane loops for magnetizing fields of ± 20 and ±90 kOe are shown. The perpendicular to the plane loop is closed. This film was PLD deeposited firm a $SmCo_5$ target on to 375°C alumina substrate at a pressure of 100 mTorr Ar.

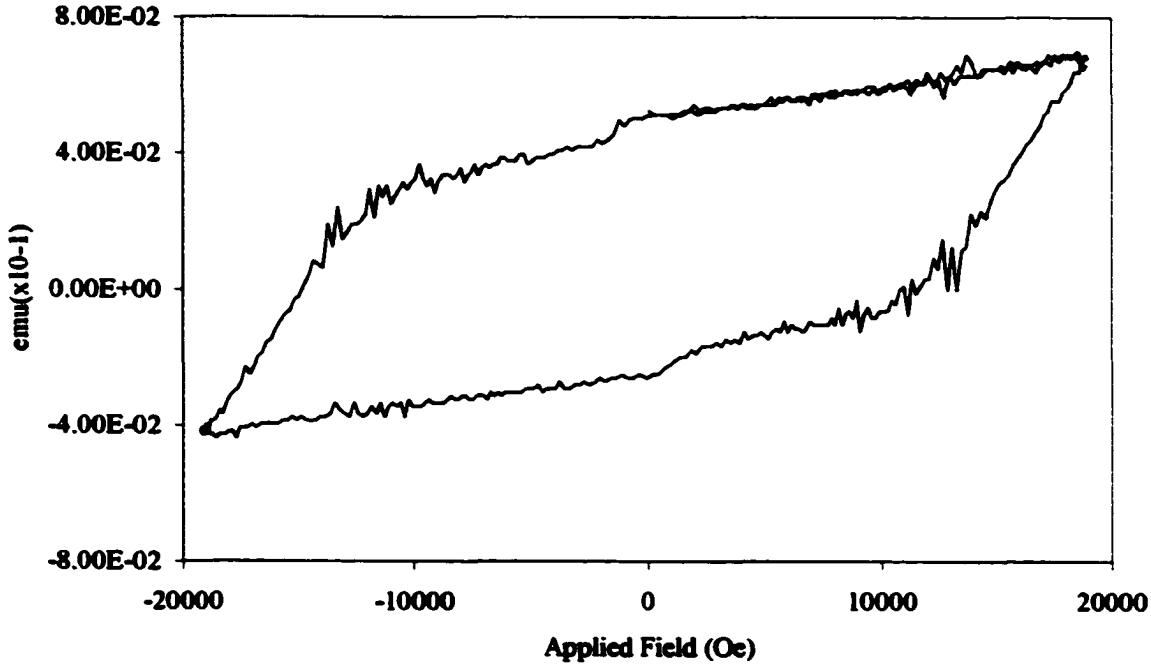

Fig.3-8.$SmCo_5$ film deposited on Al_2O_3 substrate. The coercivity is 15 kOe. The deposition condition is f=14Hz, T=375°C, 248 nm laser wavelength.

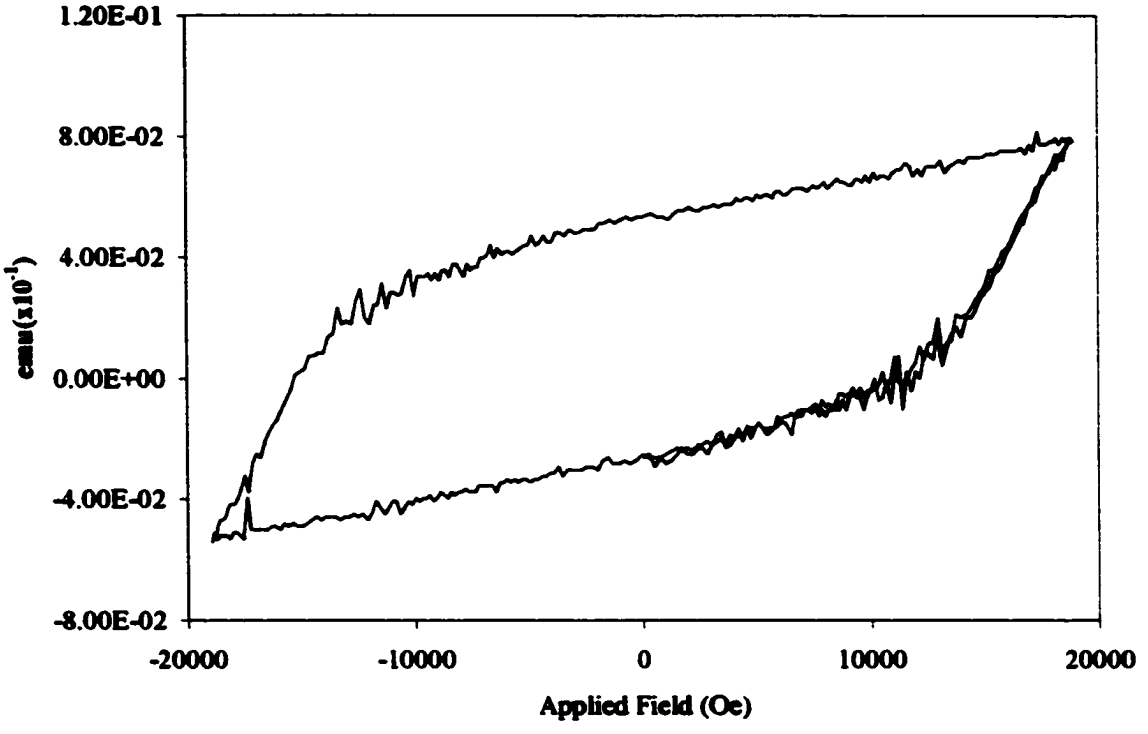

Fig.3-9.$SmCo_5$ film deposited on Si substrate. The coercivity is 15 kOe. The deposition condition is f=14 Hz, T=375 °C, 248 nm laser wavelength.

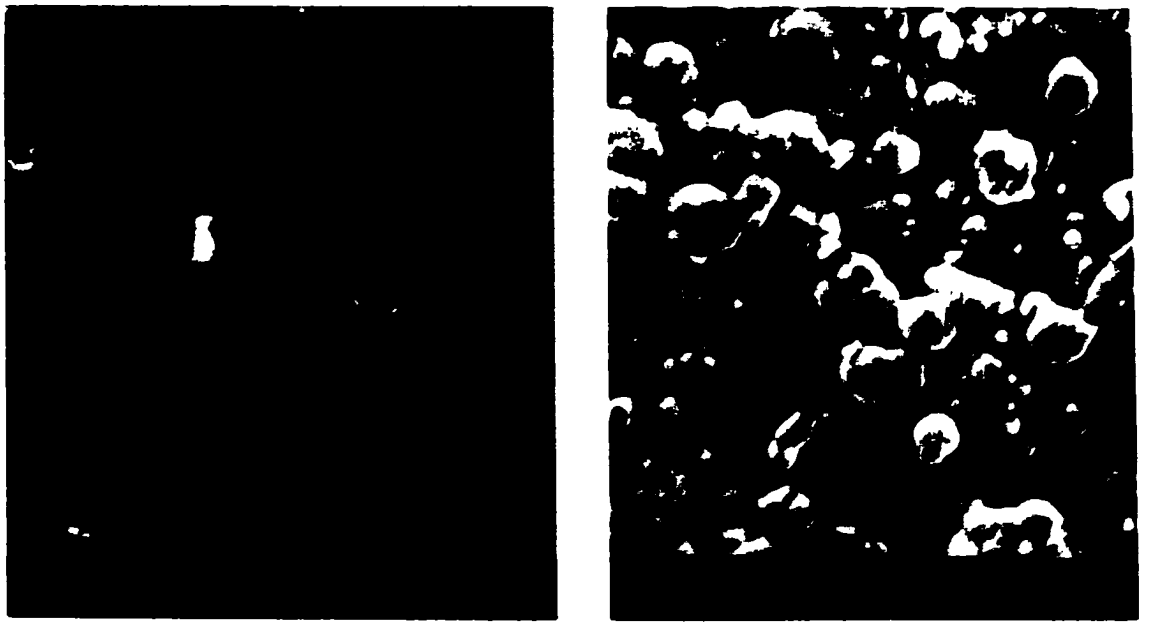

Fig.3-10. SEM micrographs are shown for shadow deposit (left) and non-shadow deposit (right) regions for a $CaCu_5$-type structure film deposited with 1200 mJ and a pulse rate of 16 Hz.

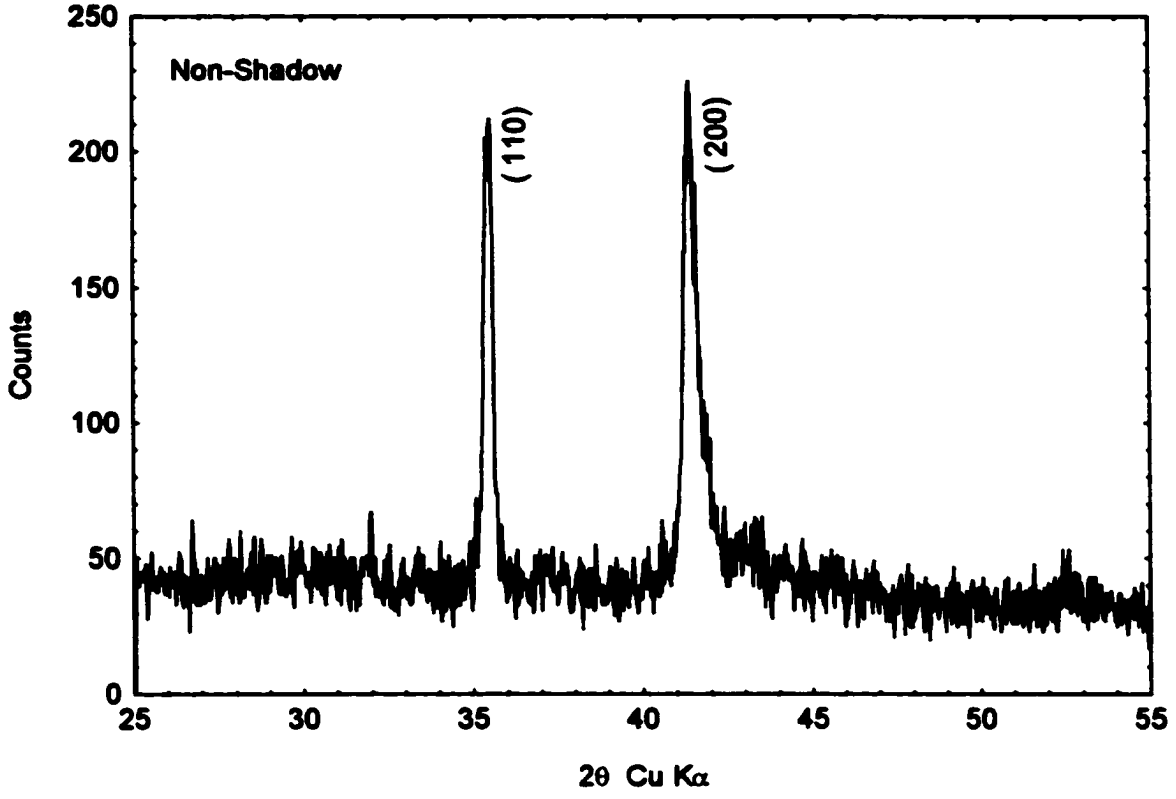

Fig.3-11. An x-ray diffraction trace for the nonshaodw region of the film of Fig.3-7. is shown which indicates (110) and (111) texturing. X-ray indexed as $CaCu_5$ structure film.

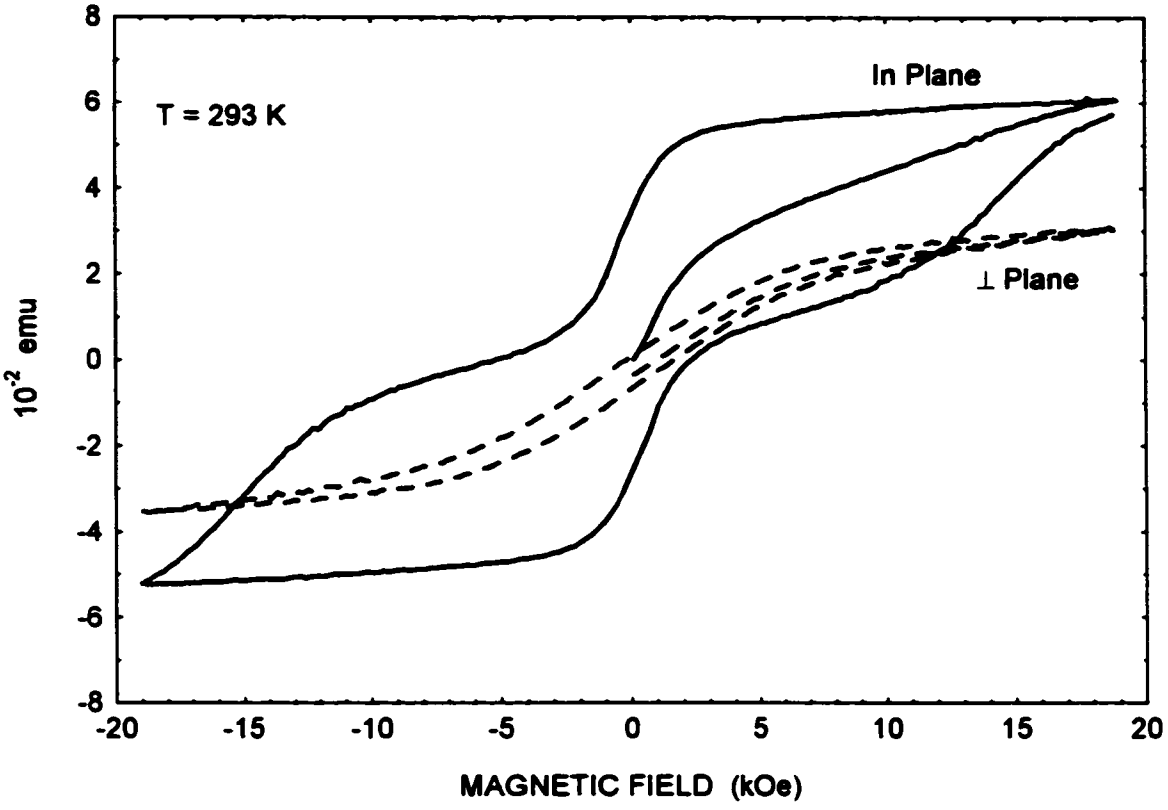

Fig.3-12 Room temperature hysterisis loops are shown for the non-shadow region film.

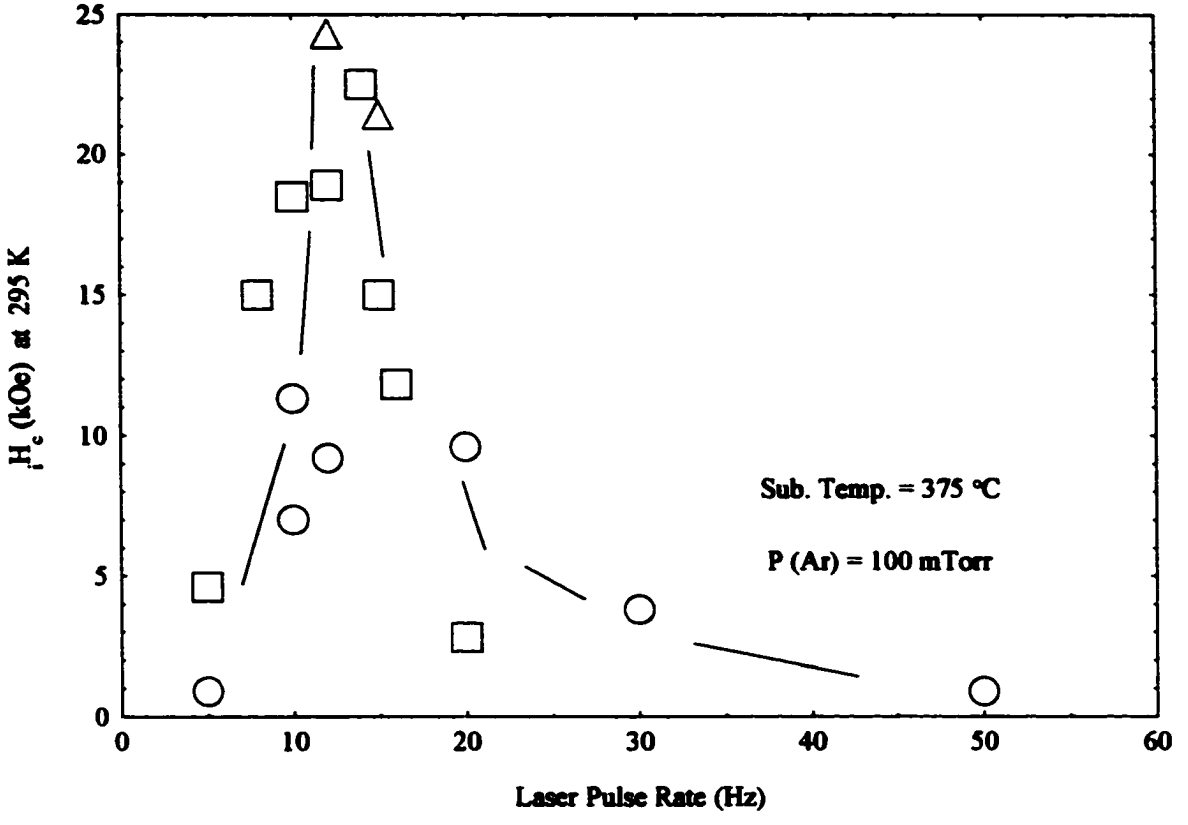

Fig.3-13. The intrinsic coercivity is shown for a series of SmCo films shadow deposited by PLD onto alumina substrates held at 375°c in 100 mTorr Ar. All points were measured at 295 K except for thosed indicated by Δ, which were measured 140 K. the points indicated by O were deposited with λ=193 nm with pulse energies of 500-650 mJ. The points indicate by □ were deposited with λ=248 nm with pulse energies of 1000-1250 mJ.

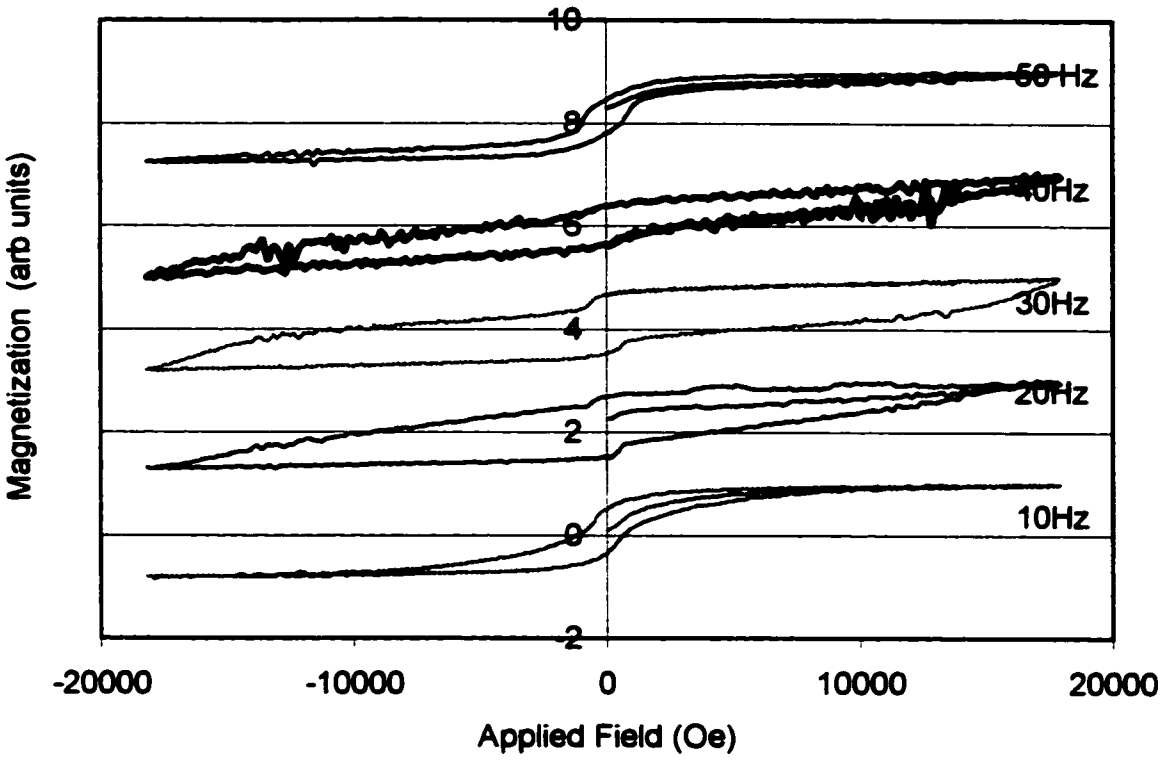

Fig.3-14. Five hysterisis loops with different repetition rate.

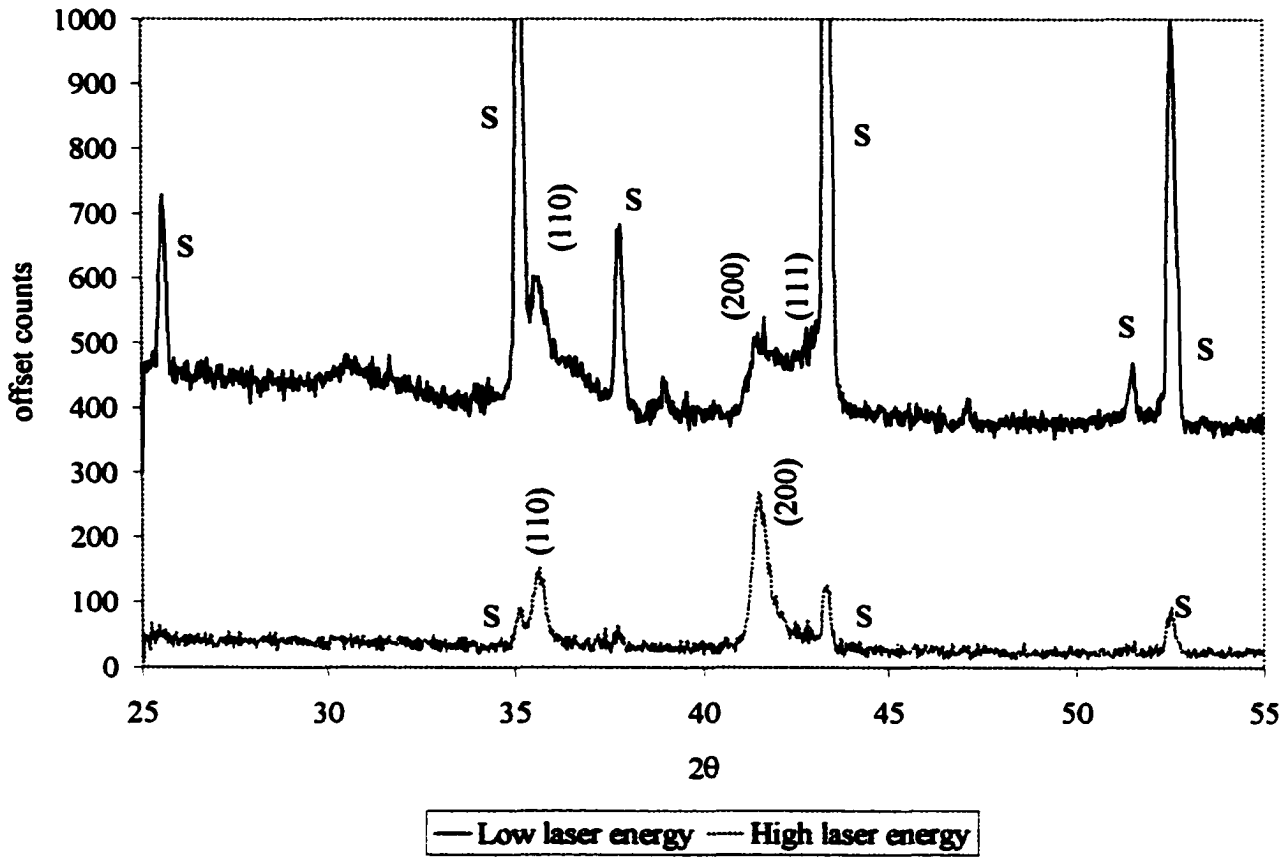

Fig.3-15.Two x-ray diffraction traces, Cu Kα, for the film made by 193 nm laser wavelength, 500 mJ maximum laser energy (top one) and by 248 nm laser wavelength, 1300 mJ maximum laser energy (bottom one). The lower energy shows that (111) is comparable to (110) and (200). The higher energy one shows the dominant (110) and (200) structure.

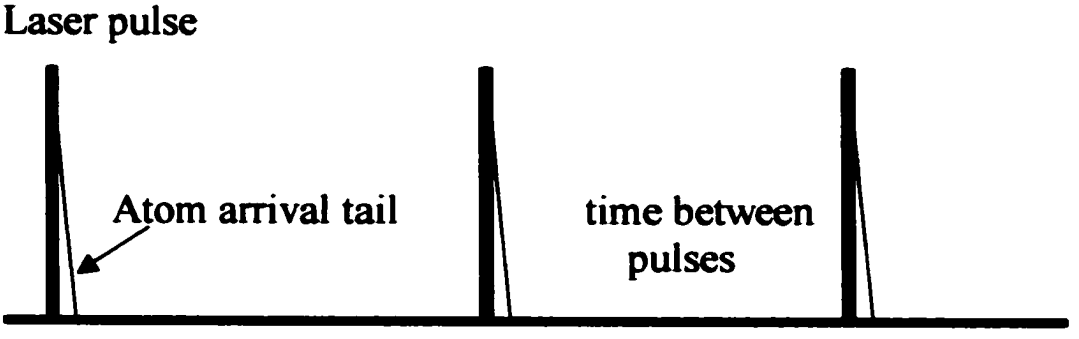

Fig.4-1 Schematic diagram of laser pulse and atom arrival time.

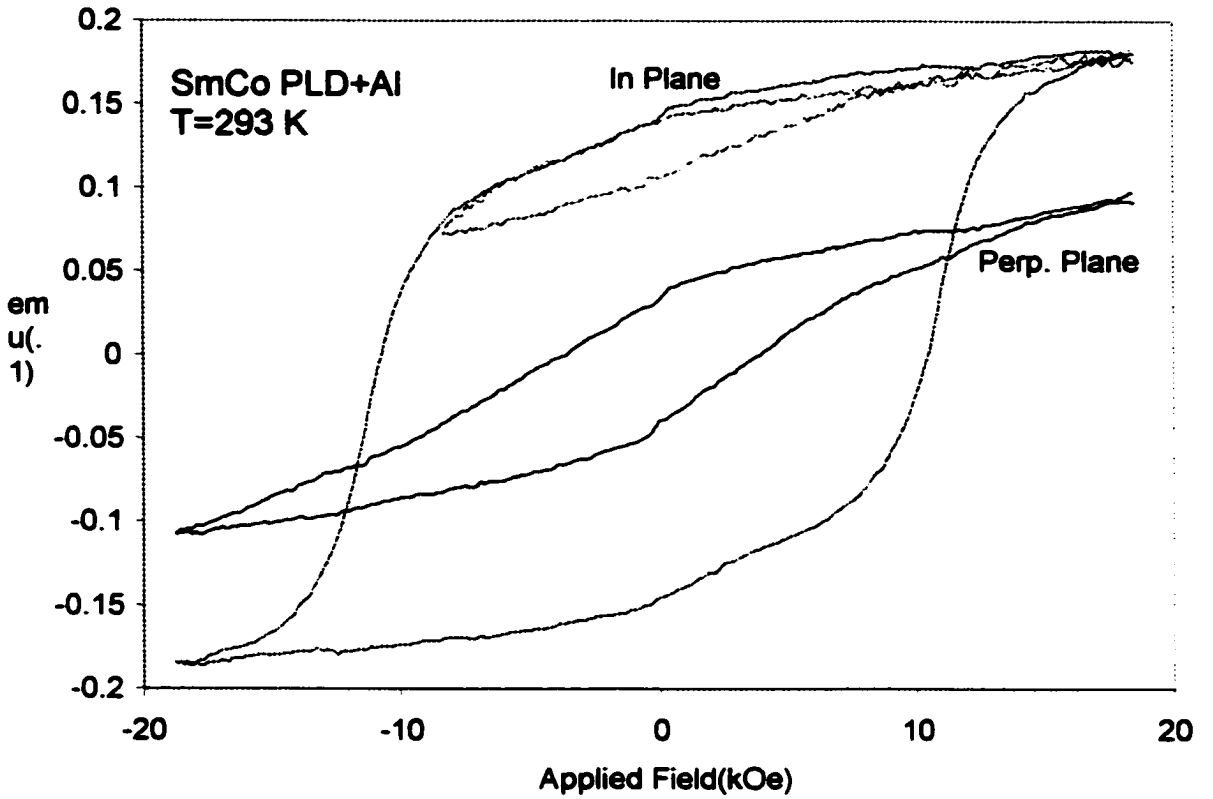

Fig.4-2 Room temperature hysterisis loops are shown for a PLD $SmCo_5$ plus Al sputter film containing Sm 15.8 at.%, Co 74.5 at.%, and Al 9.7 at.%. The intrinsic coercivity was 9.9 kOe.

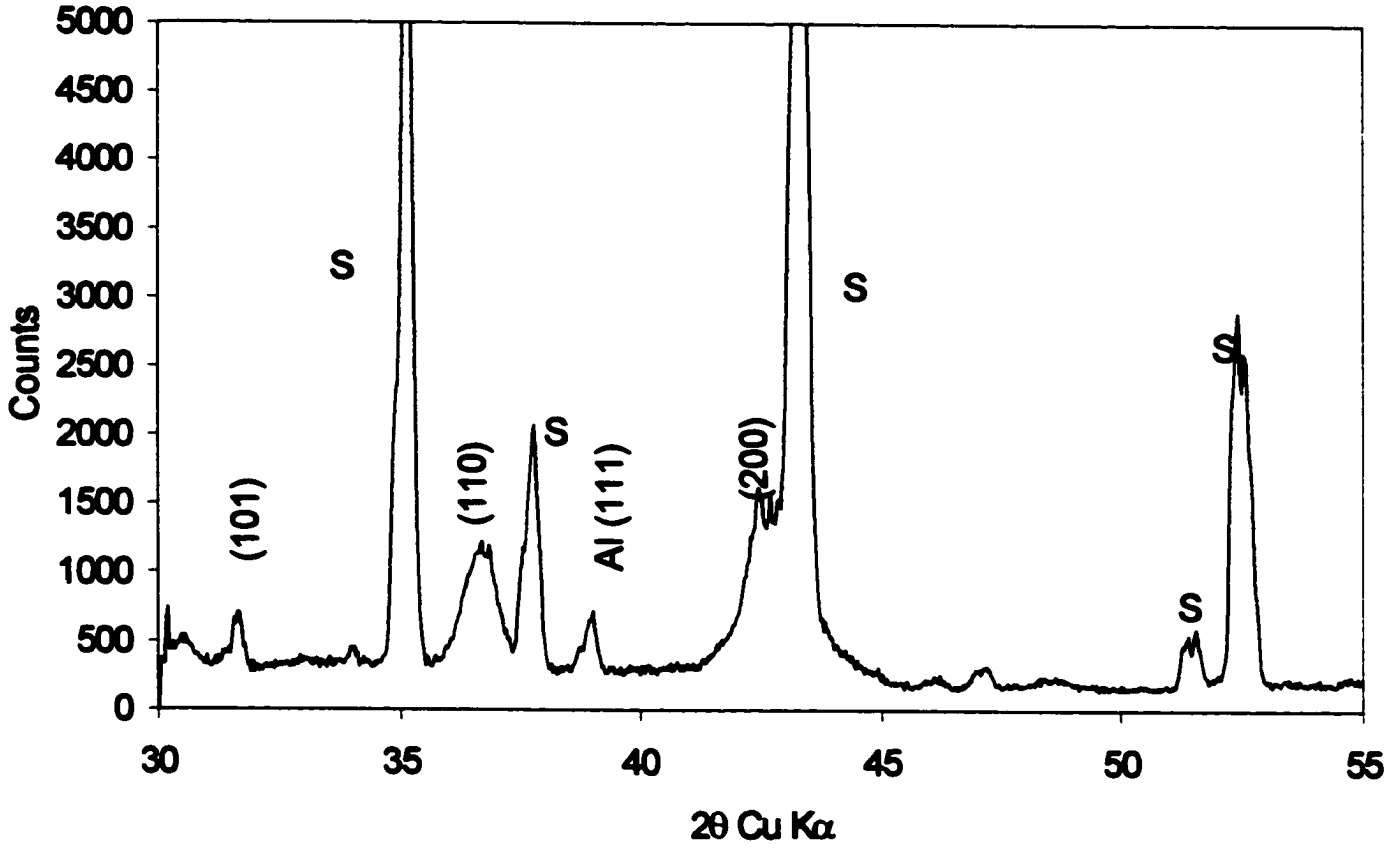

Fig.4-3. X-ray diffractometer trace, Cu Kα radiation is shown for the sample of Fig4-2. Substrate lines were denoted by S.

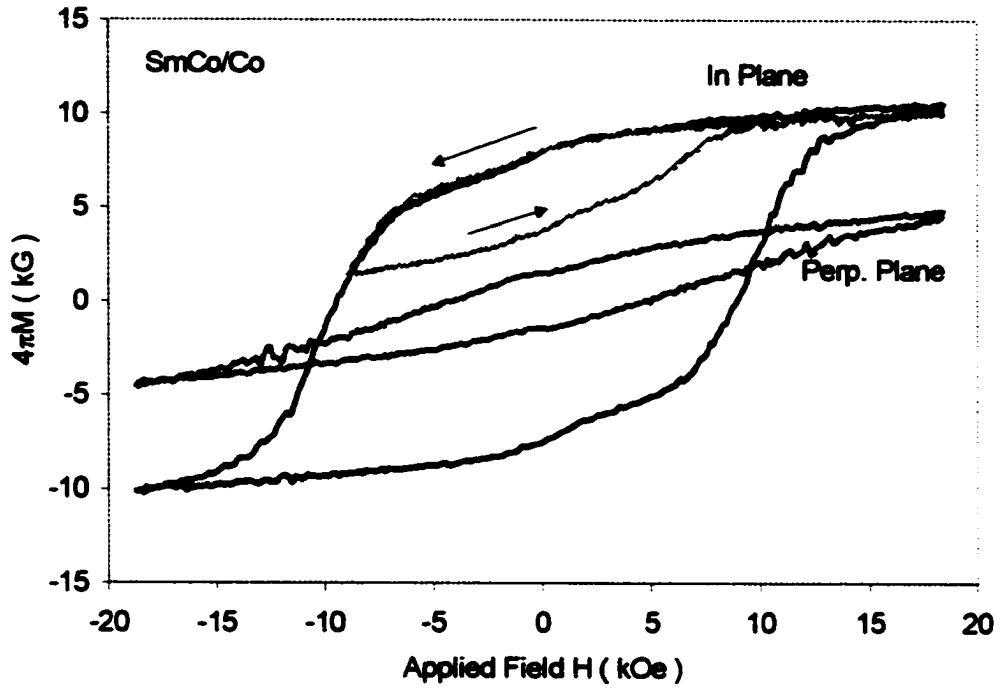

Fig.4-4 Room temperature hysterisis loops are shown for a high coercivity PLD $SmCo_5$ sample plus simultaneous Co sputter deposition. The RT in-plane coercivity was 9.5 kOe.

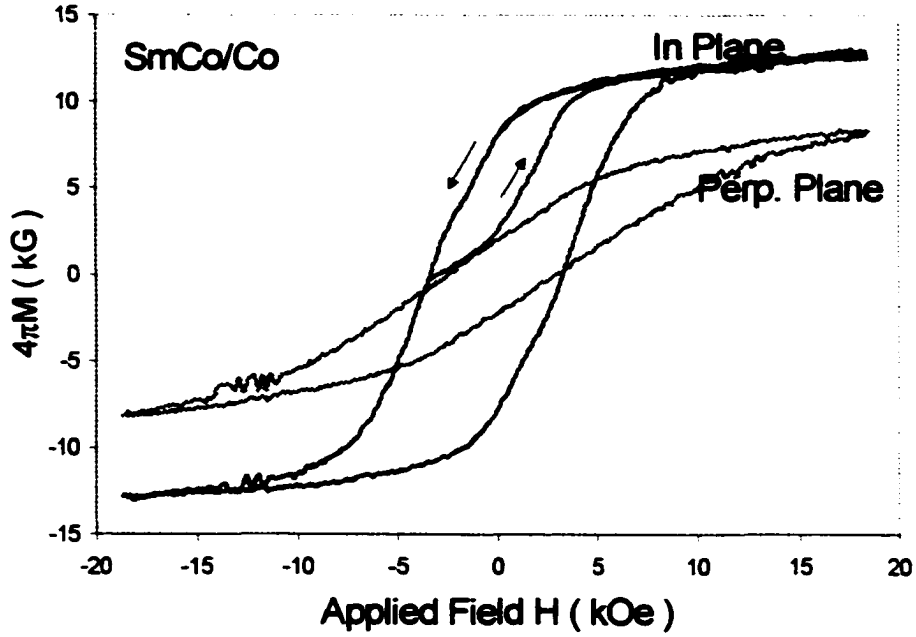

Fig.4-5. Room temperature hysterisis loops are shown for a lower coercivity PLD $SmCo_5$ sample plus simultaneous Co sputter deposition. The RT in-plane intrinsic coercivity was 3.4 kOe.

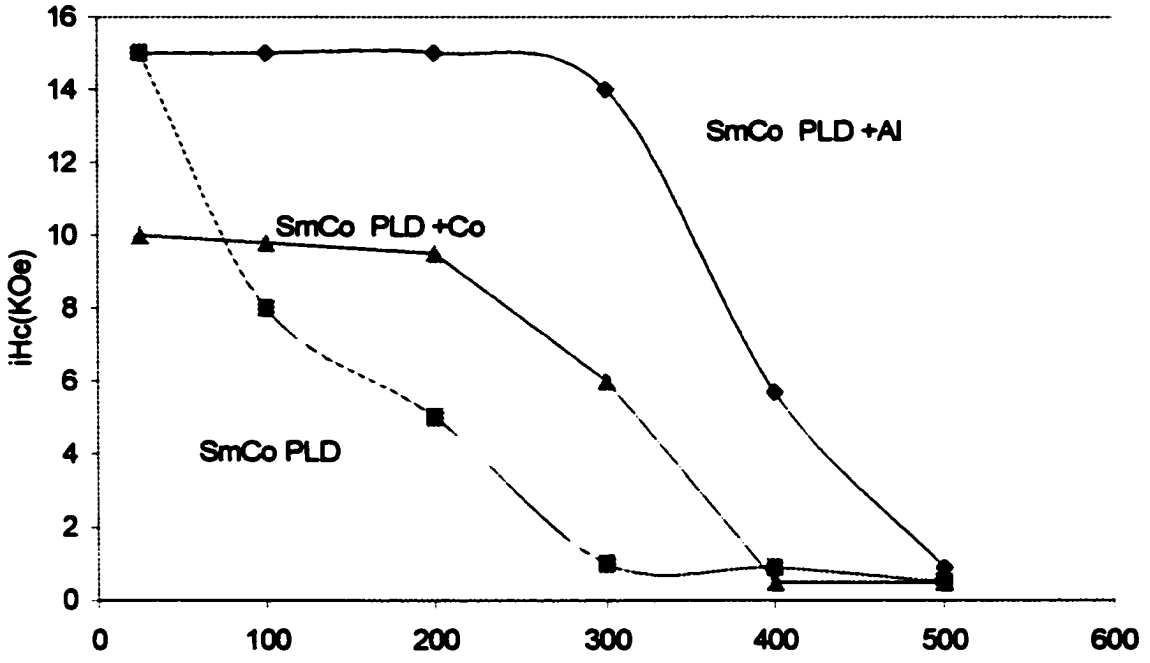

Fig.4-6. Intrinsic coercivities measured at room temperature following heating for 30 min in air at various temperatures are shown for PLD SmCo plus Al films, diamonds, PLD SmCo plus Co, crosses, and PLD $SmCo_5$ only films, circles.

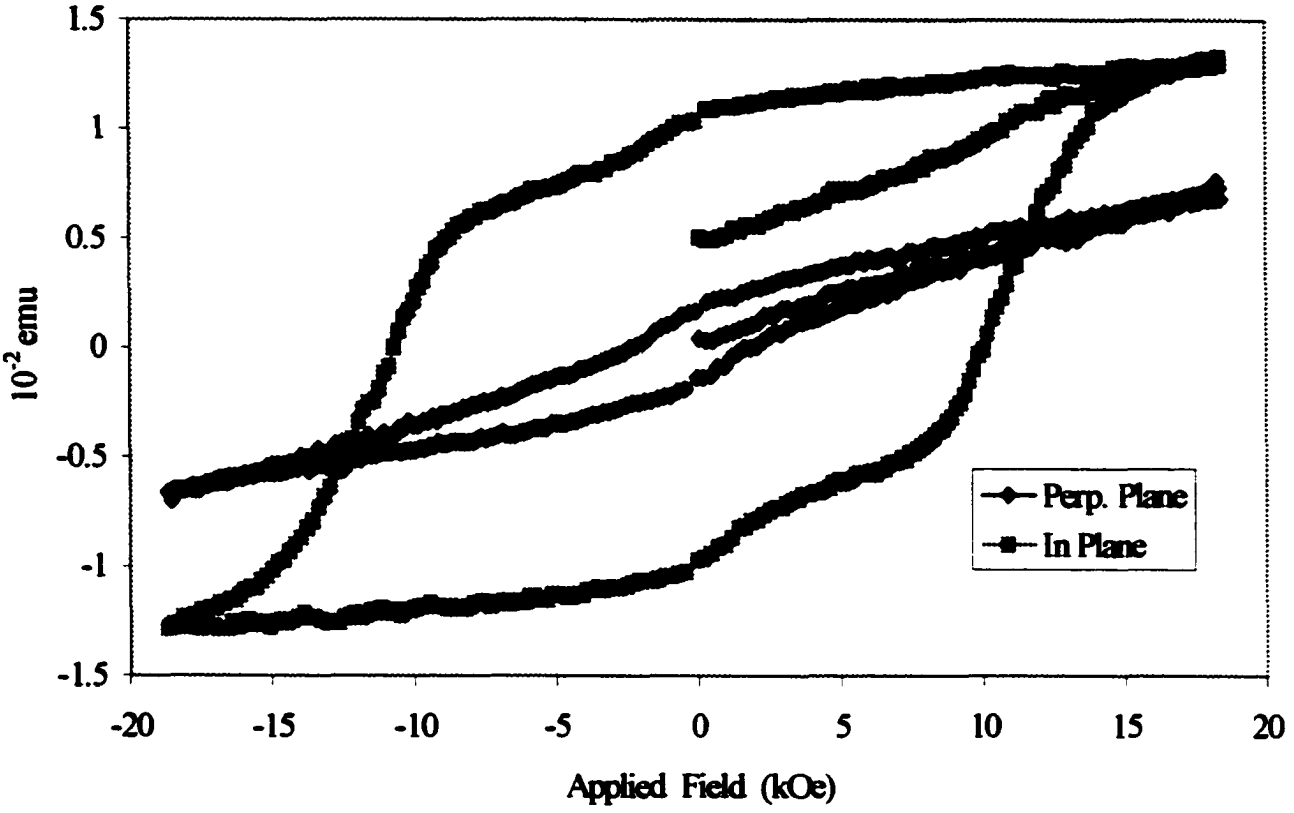

Fig.4-7 In plane and perpendicular to the plane hysterisis loops as measured at room temperature are shown for a PLD deposited $SmCo_5$ film while simultaneously sputtering $Co_{0.5}Fe_{0.5}$. The substrate was alumina.

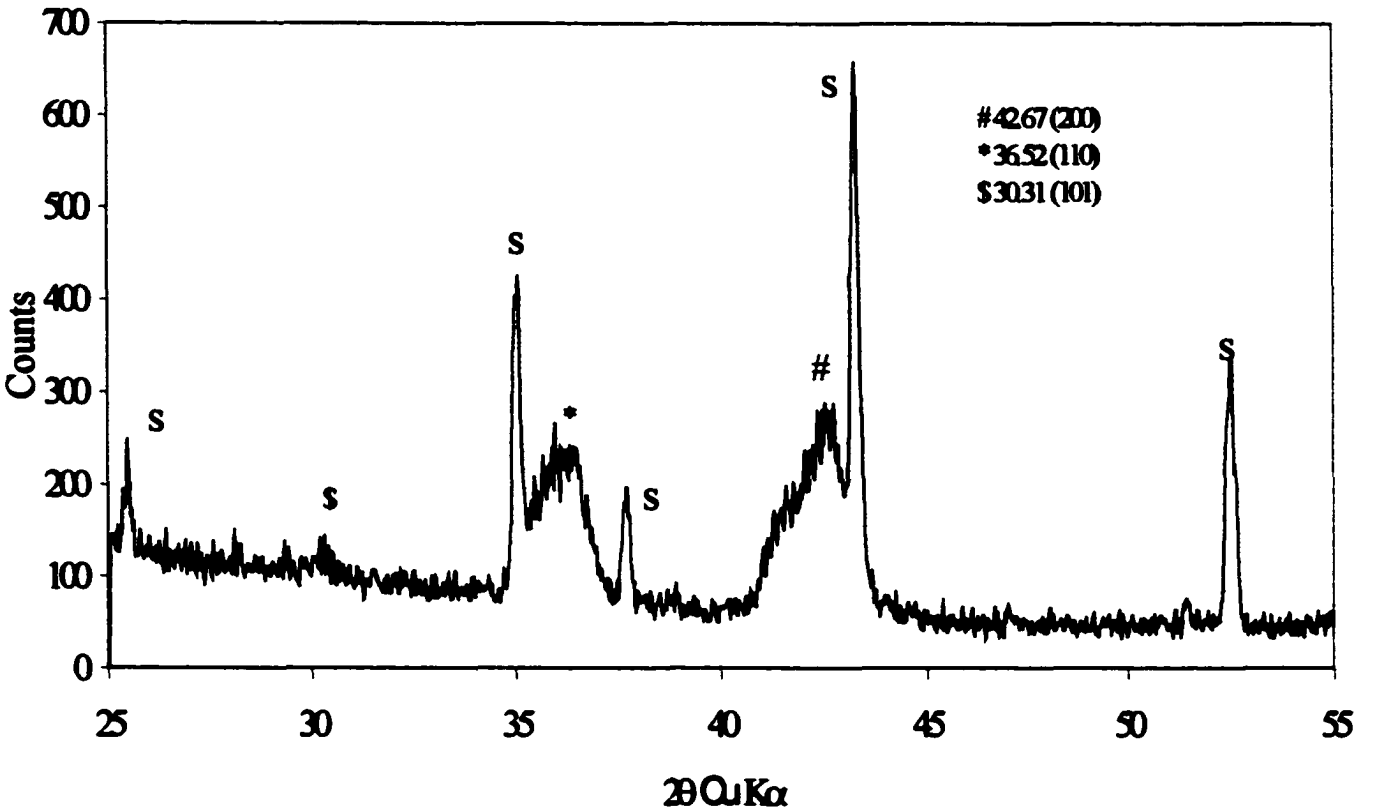

Fig.4-8 An x-ray diffraction trace, Cu kα radiation, for the film of fig.4-7 is shown. The positions of Alumina substrate reflections are denoted by S. The positions of the (101), (110) and (200) $CaCu_5$-type structure reflection are indicated.

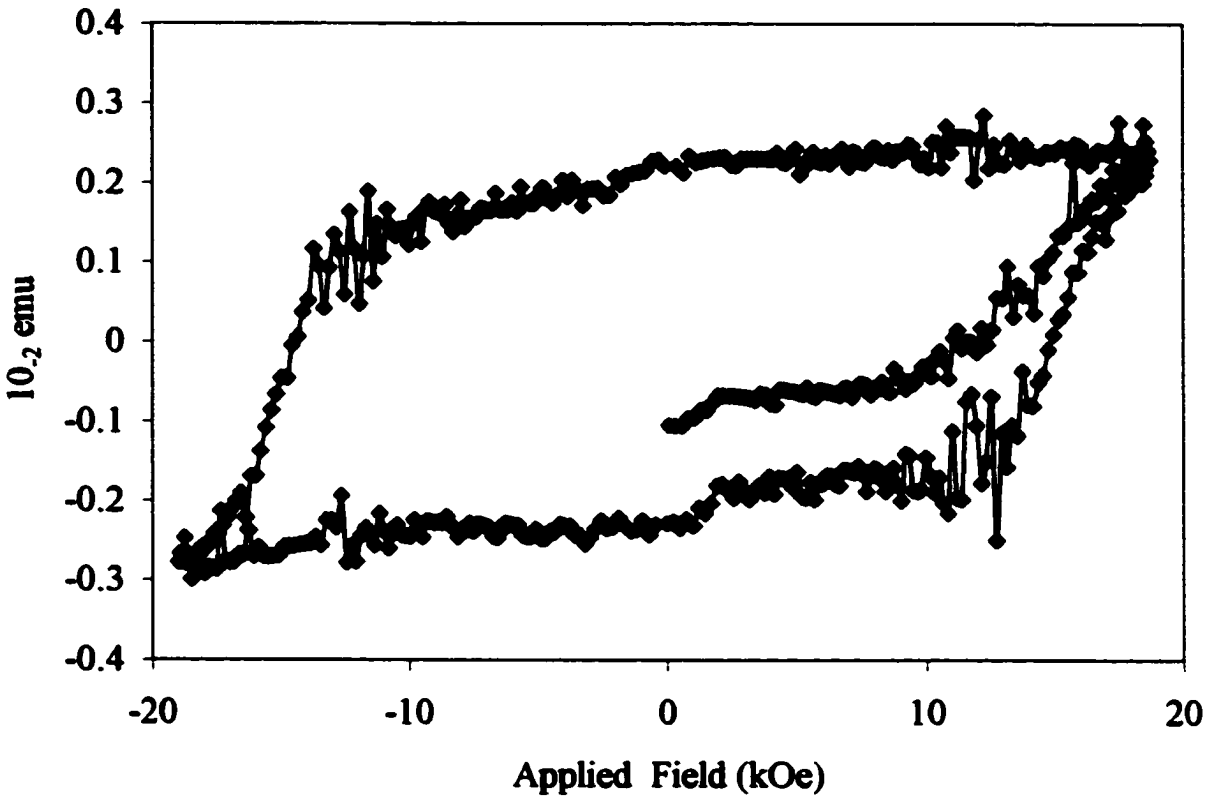

Fig.4-9. An in plane hysteresis loop measured at room temperature is shown for a film with Sm 20.1 at%, Co 74.8 at%, and 4.9 at.% Ti. The in plane intrinsic coercivity was 15 kOe.

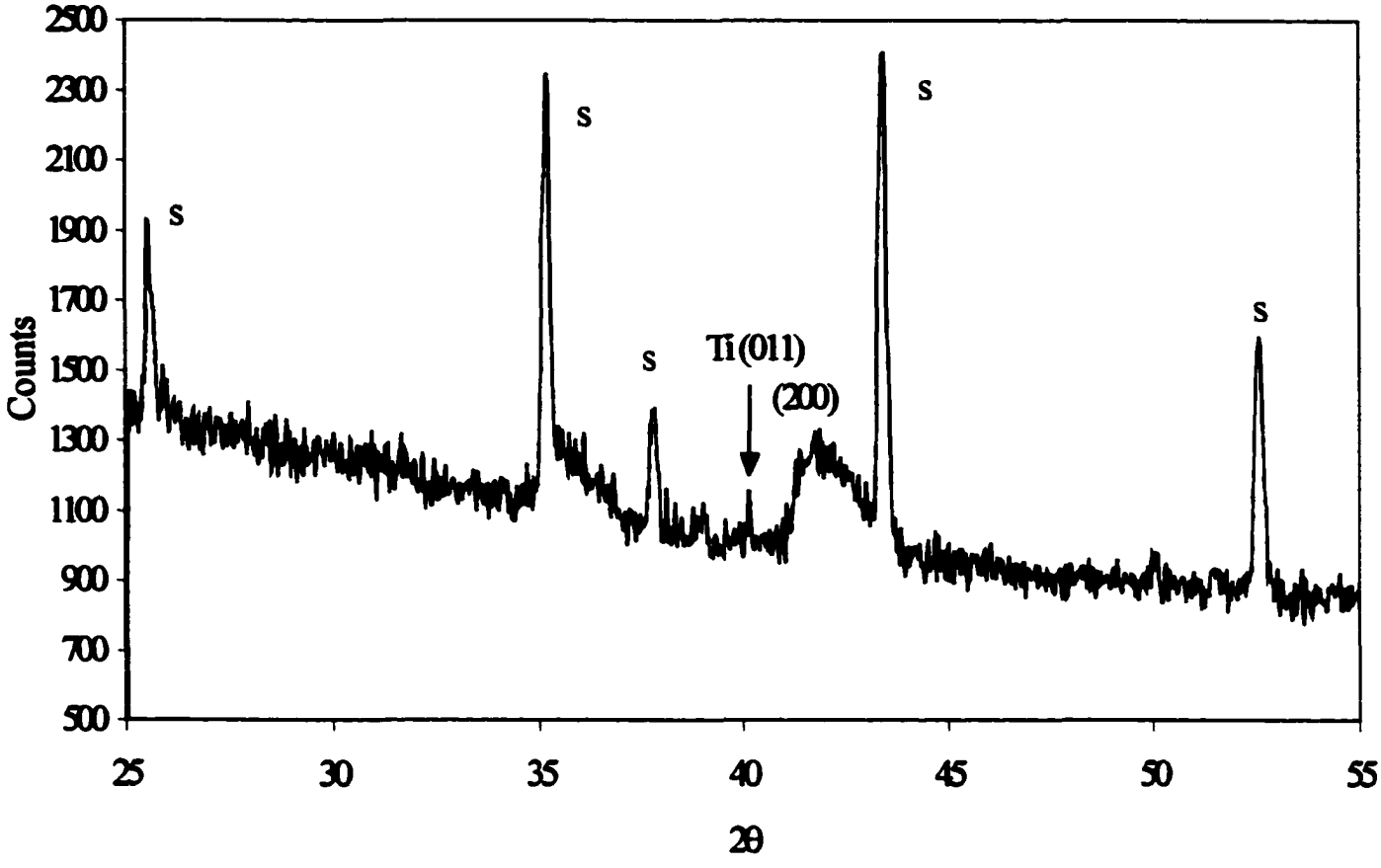

Fig.4-10. A x-ray diffraction trace, Cu Kα radiation, for the film of SmCo+Ti film of fig.4-9. The alumina substrate lines are indicated by S. The expected positions of the $CaCu_5$-type (110), (200), and (111) diffraction lines are indicated. The (111) diffraction peak is absent. The Ti (011) reflection position is also indicated.

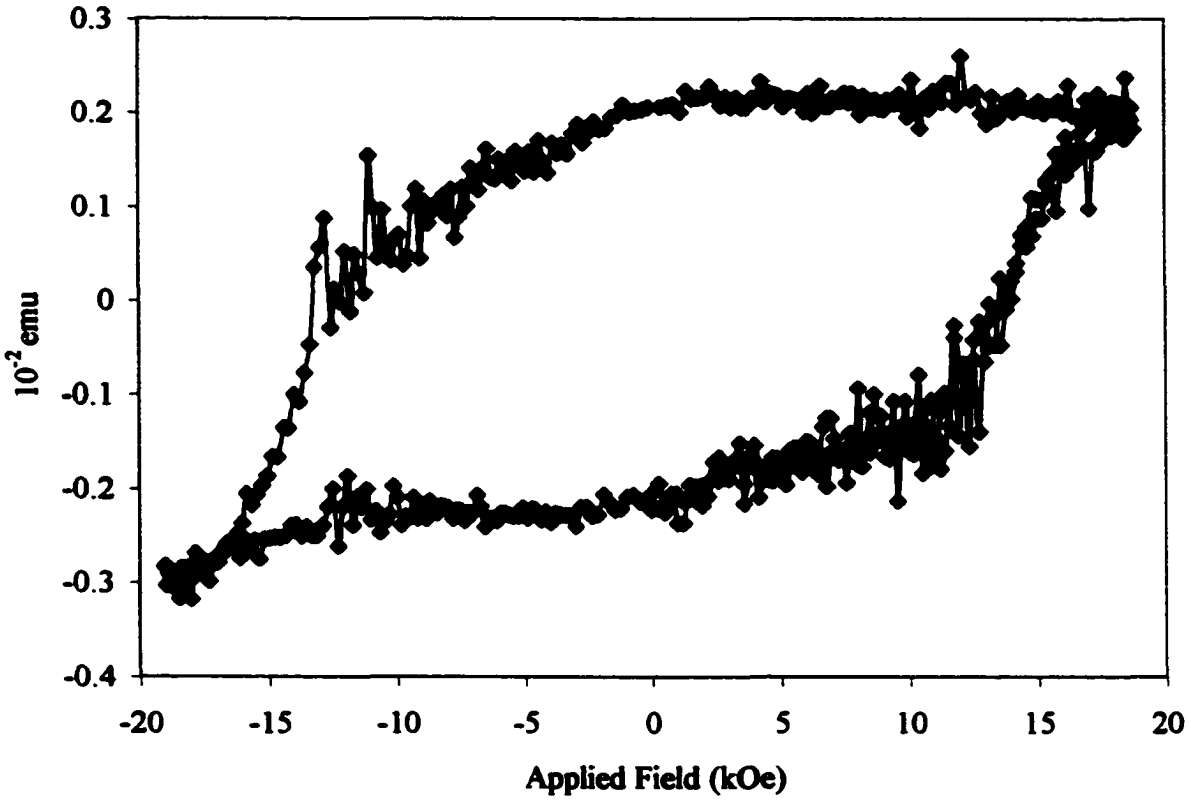

Fig.4-11. The in plane hysteresis loop for a $SmCo_5$ film with Si, Sm 23.6 at.%, Co 73.8at. %, Si 2.6 at.% .

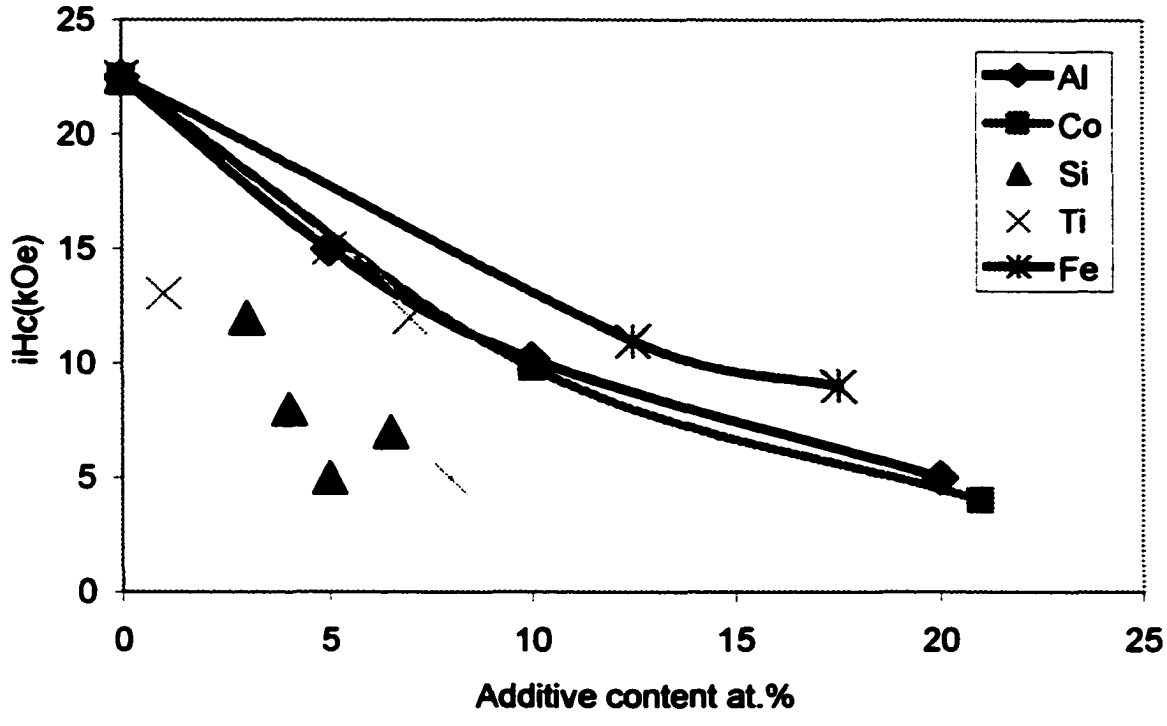

Fig.4-12 Room temperature intrinsic coercivities, $_iH_c$, versus sputtered atom matrix addition are shown for element additions of Al, Co, Si, Ti, and $Co_{0.5}Fe_{0.5}$. For the CoFe series, the absissa is the film Fe at.%.

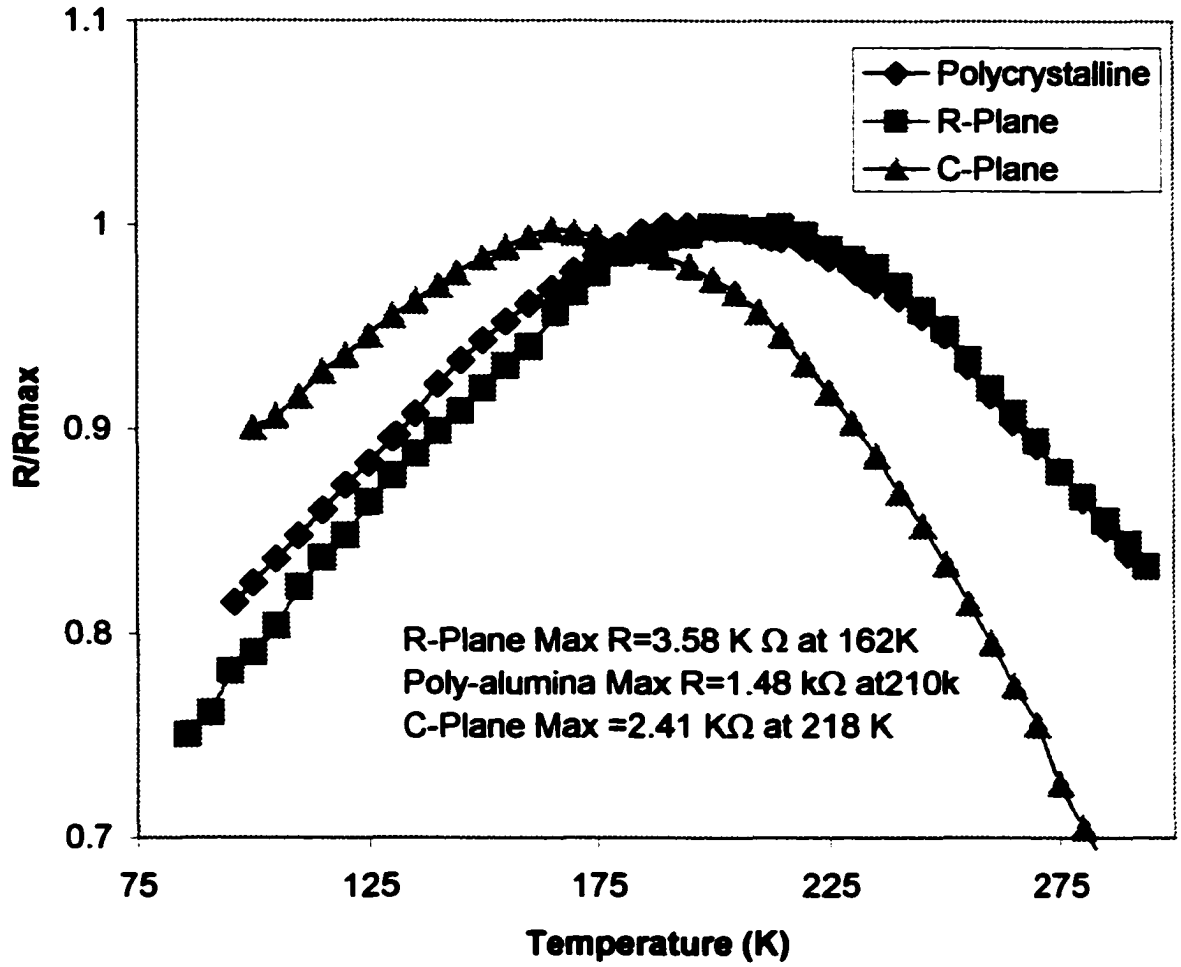

Fig.5-1 The normalized resistances measured in zero field for a set of La0.7Sr0.3MnO3 films simultaneously made onto R-plane sapphire, C-plane sapphire, and polycrystalline alumina substrates are shown as a function of temperature.

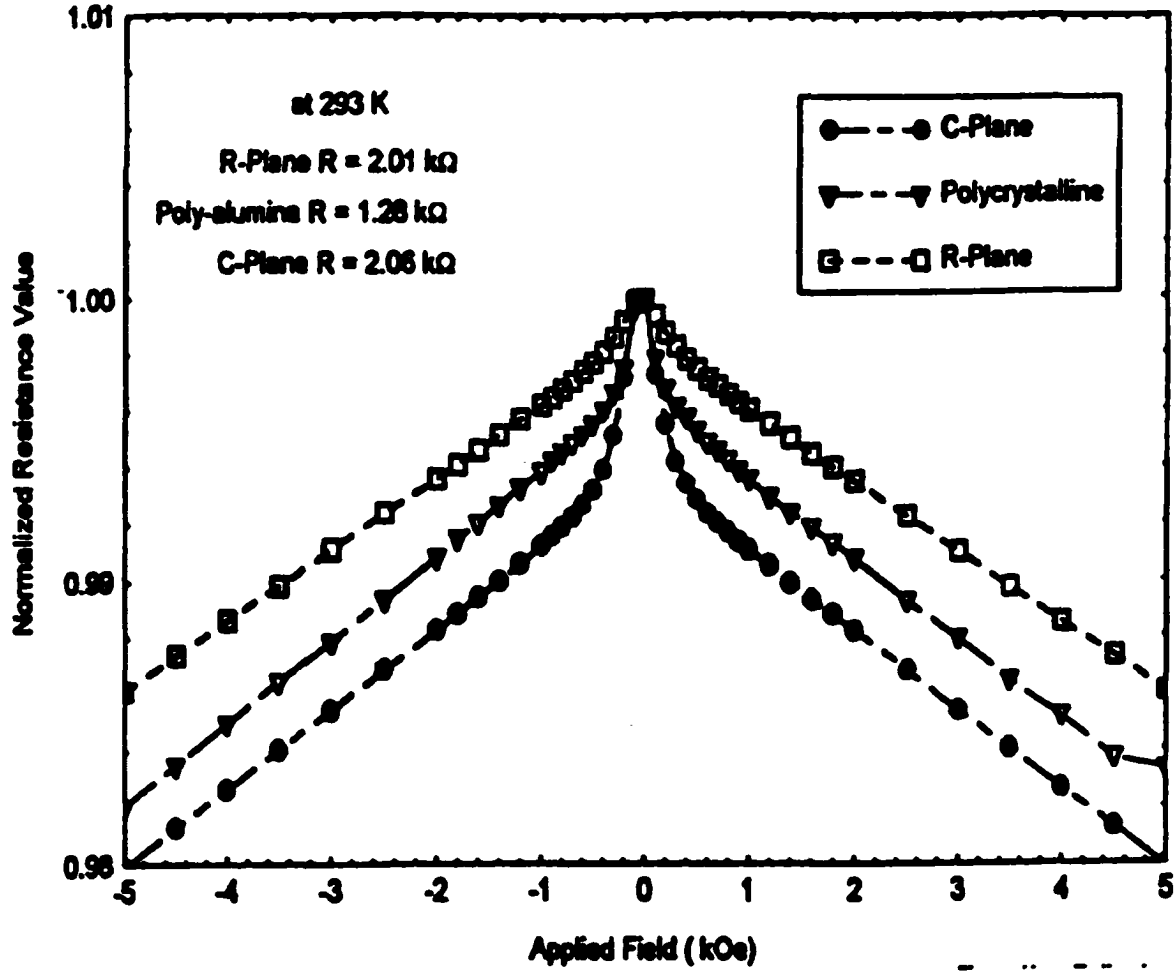

Fig.5-2 The normalized resistances measured at 293 K are shown as a function of applied magnetic field for the same set of substrates as shown in Fig.5-1.

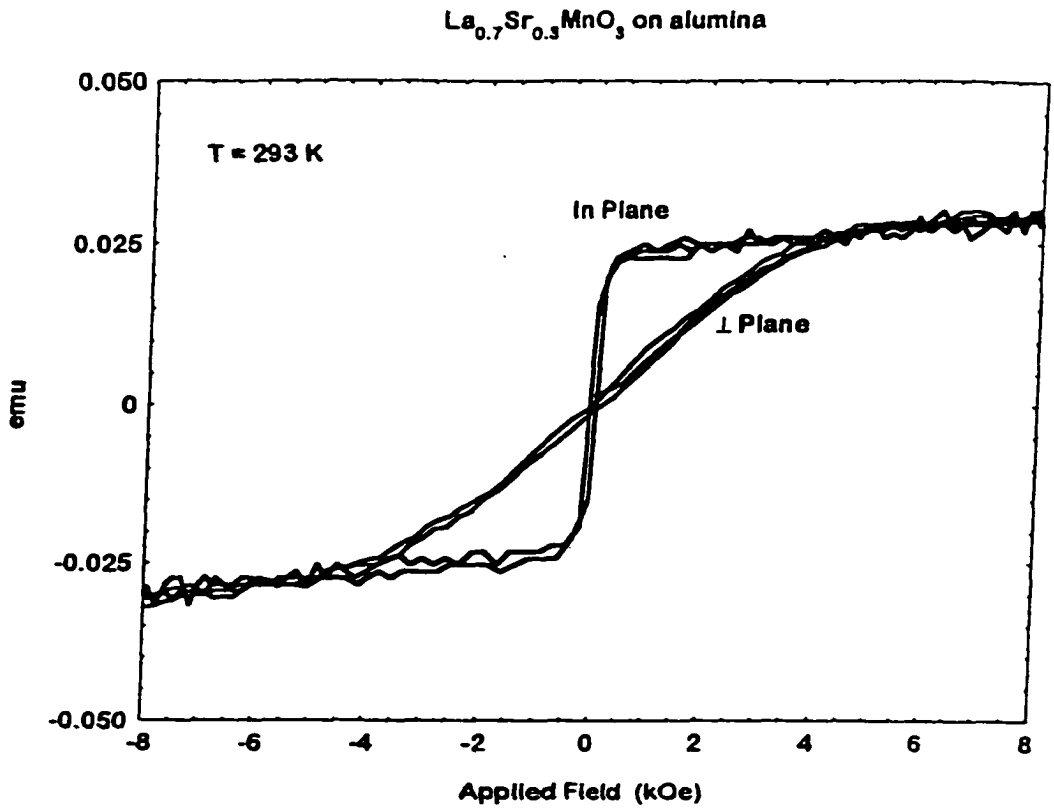

Fig.5-3. Room temperature hysteresis loops are shown for a polycrystalline $La_{0.7}Sr_{0.3}MnO_3$ film deposited onto an alumina substrate.

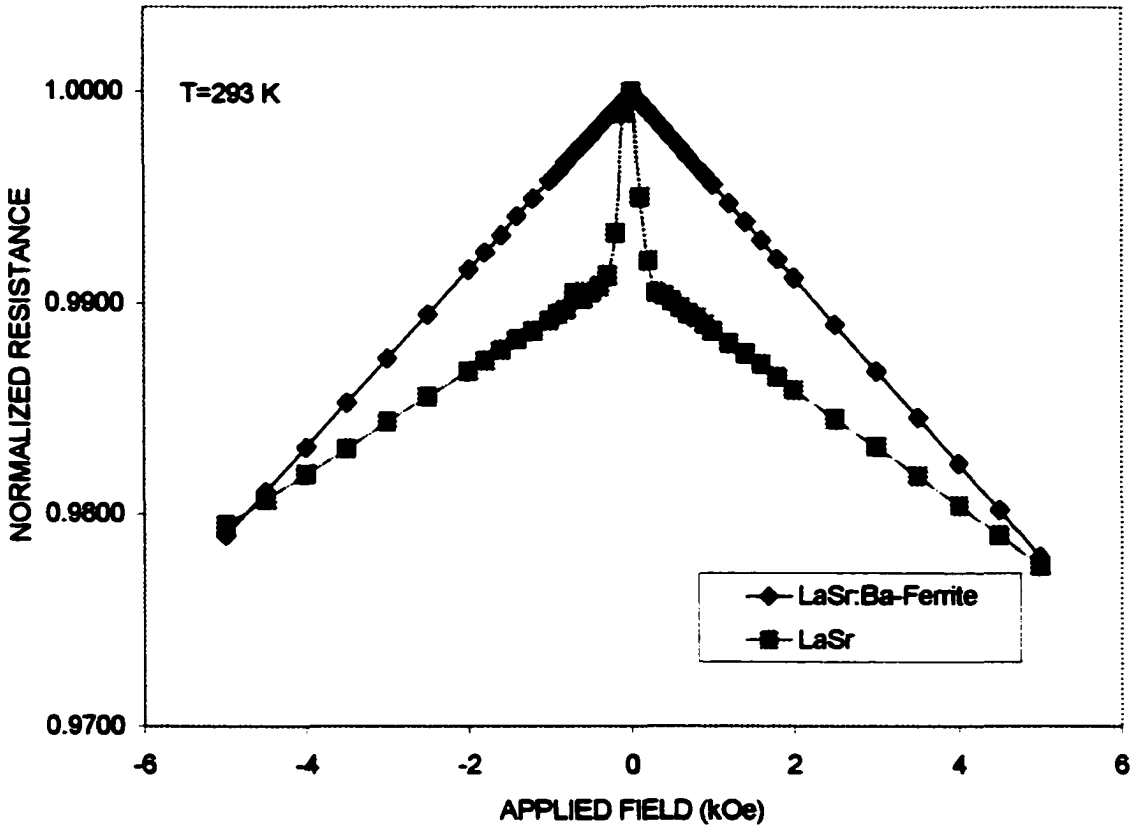

Fig.5-4. Normalized resistances as measured at 293 K for $La_{0.3}Sr_{0.7}MnO_3$ films made with and without barium ferrite laminations, 2:1 thickness ratio, are shown.

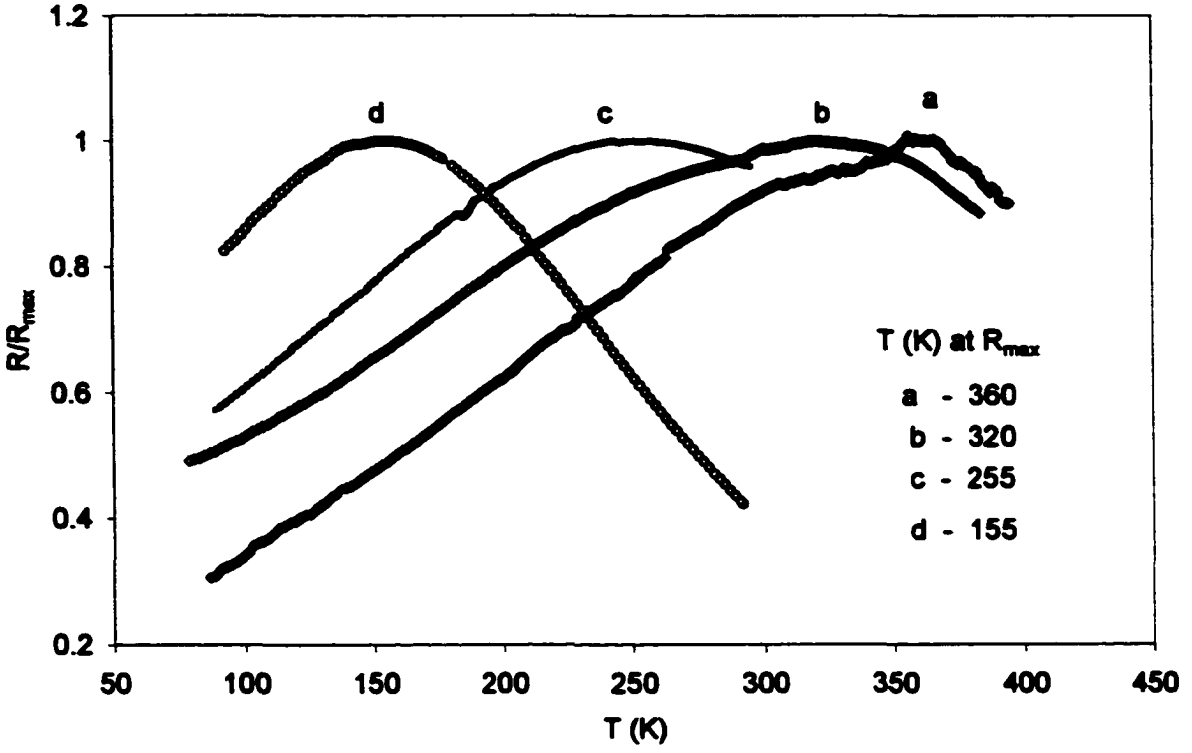

Fig.5-5. This figure indicates the range of R vs T variation for high laser pulse energy LaSrMnO PLD deposited films. Traces (a), (b), and (c) are for shadow deposited films at high laser pulse energies. Trace (d) was for the non-shadow deposited region of the same substrate as trace (c). The temperatures corresponding to the maximum resistance for each trace are indicated.

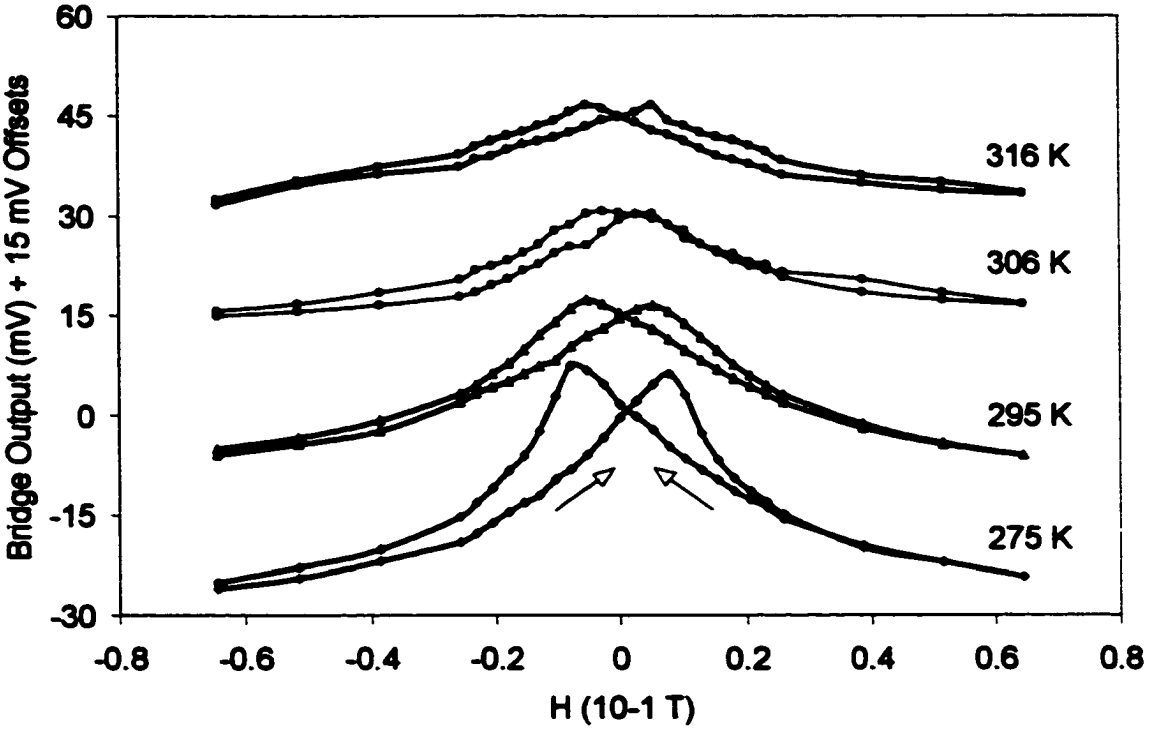

Fig.5-6. Bridge output versus in-plane applied magnetic field as measured at 275 K, 295 K, 306 K, and 316 K. The traces for 295 K, 306 K, and 316 K have been successively displaced by 15 mV to separate the traces. The arrows indicate the cycle path for all curves.

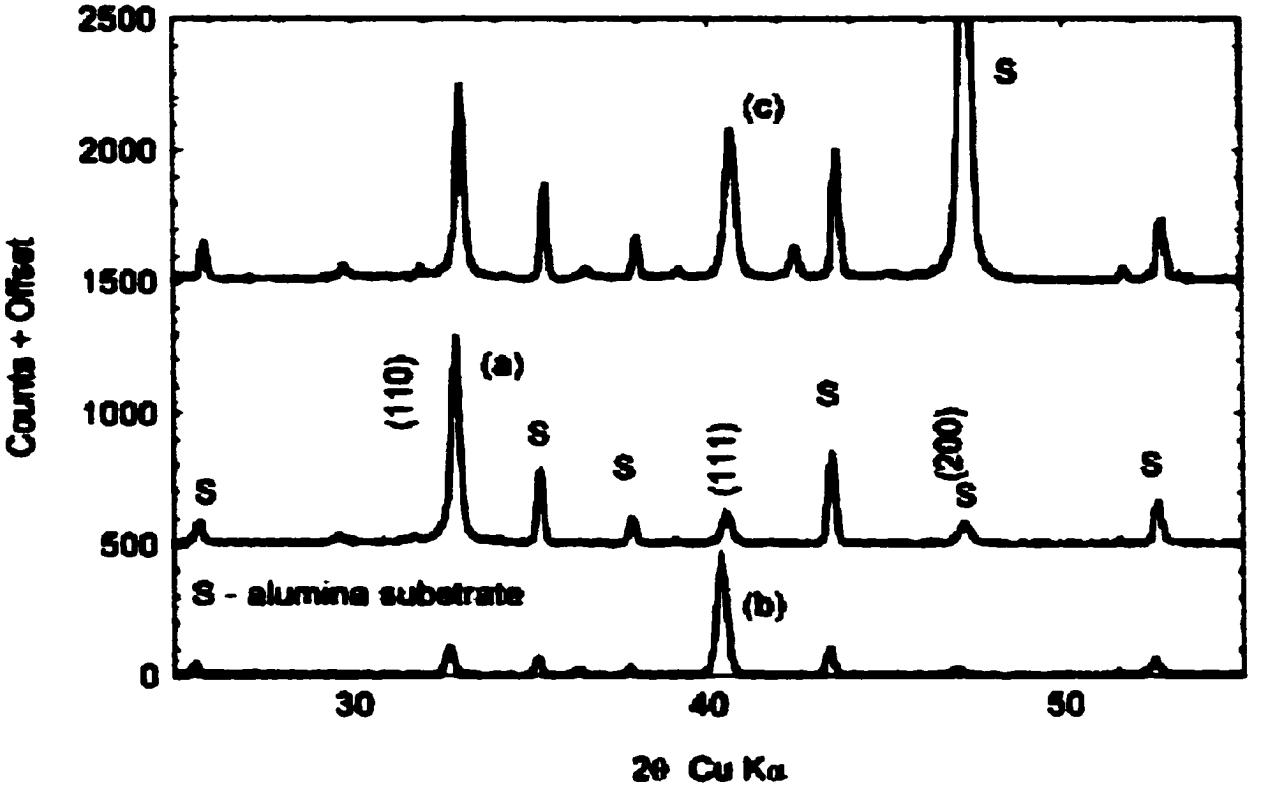

Fig.5-7 X-ray diffraction traces are shown for the shadow, trace (a), and nonshadow regions, trace (b), corresponding to traces (c) and (d), respectively, of Fig.5-5. The shadow region trace has been displaced by 500 counts to separate the traces. Trace (c) is for the shadow region of a (110) and (111) mixed texture high pulse shadow deposited textured film. Trace (c) has been offset by 1500 counts. Peaks due to the polycrystalline alumina substrate are denoted by S.

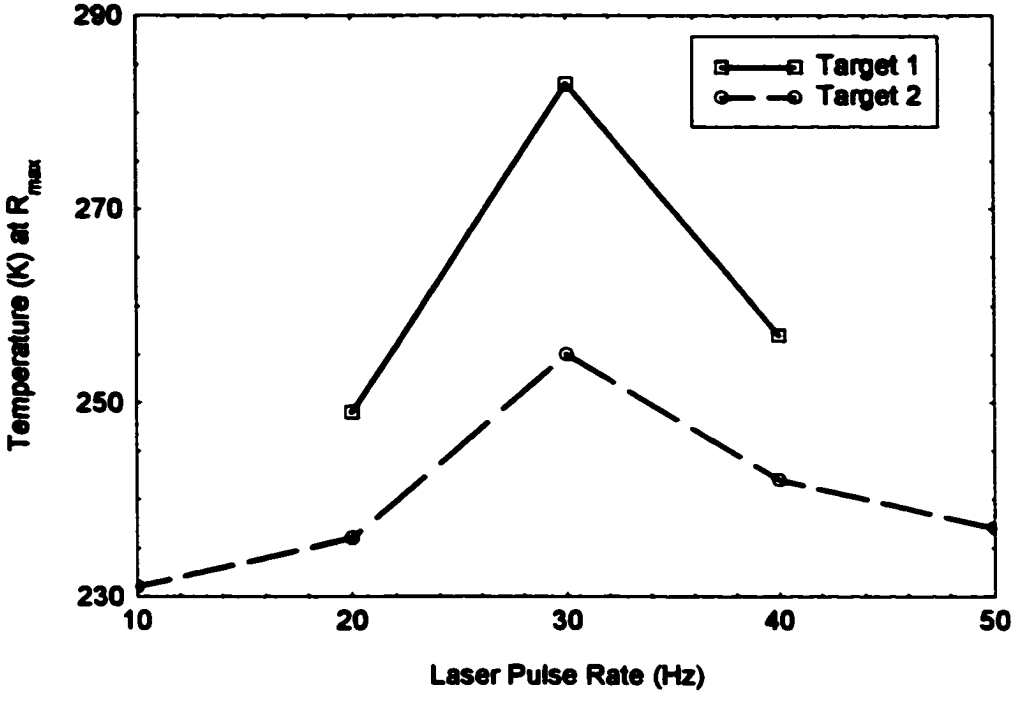

Fig.5-8. Temperature at resistance maximum versus laser pulse rate for two slightly different $La_{0.7}Sr_{0.3}MnO_3$ targets.

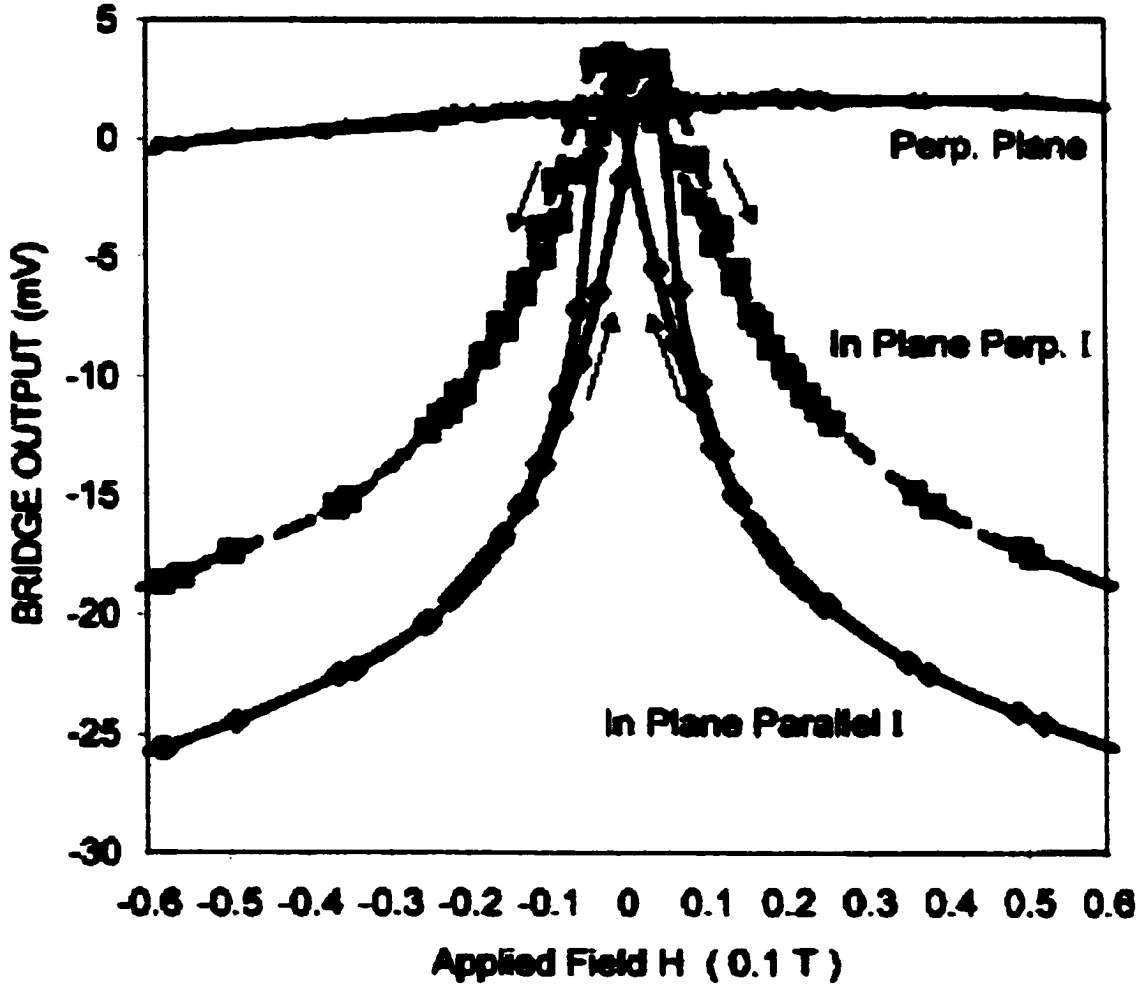

Fig.5-9. The low field MR vs applied magnetic fields applied in plane, parallel and perpendicular to current, and perpendicular to plane as at measured 294 K are shown. The curves were hysteretic with the peaks lagging the applied field values. A bridge output of 100 mV corresponds to a resistance change $\Delta R/R \approx 2.2\%$.

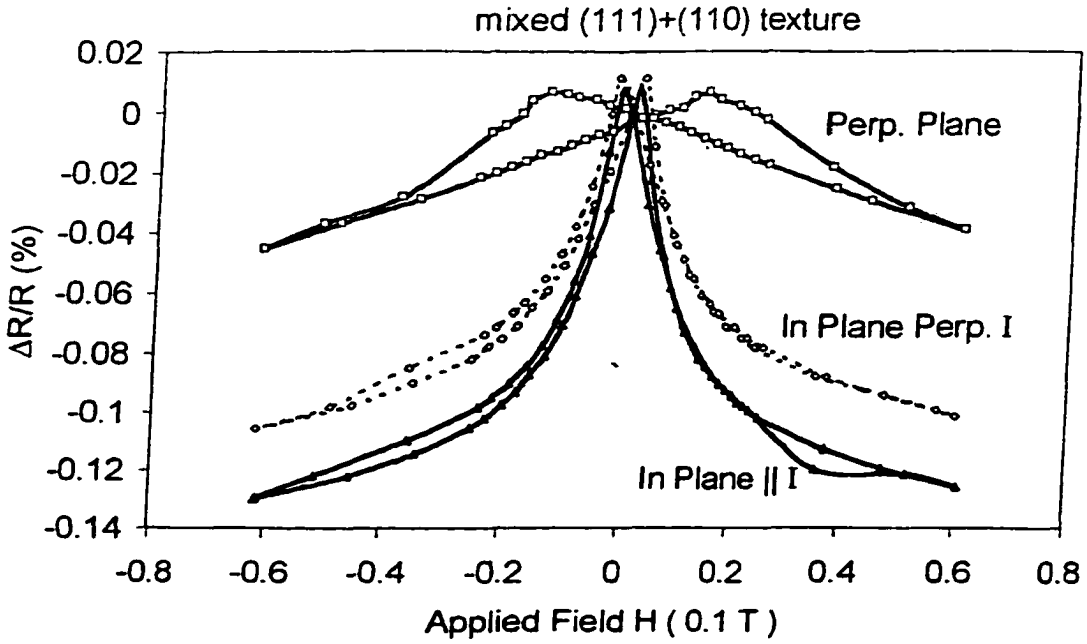

Fig.5-10. The low field MR anisotropy for a mixed (111)+(110) textured film is shown versus applied magnetic fields applied in plane, parallel and perpendicular to current, and perpendicular to plane as at measured at 293K.

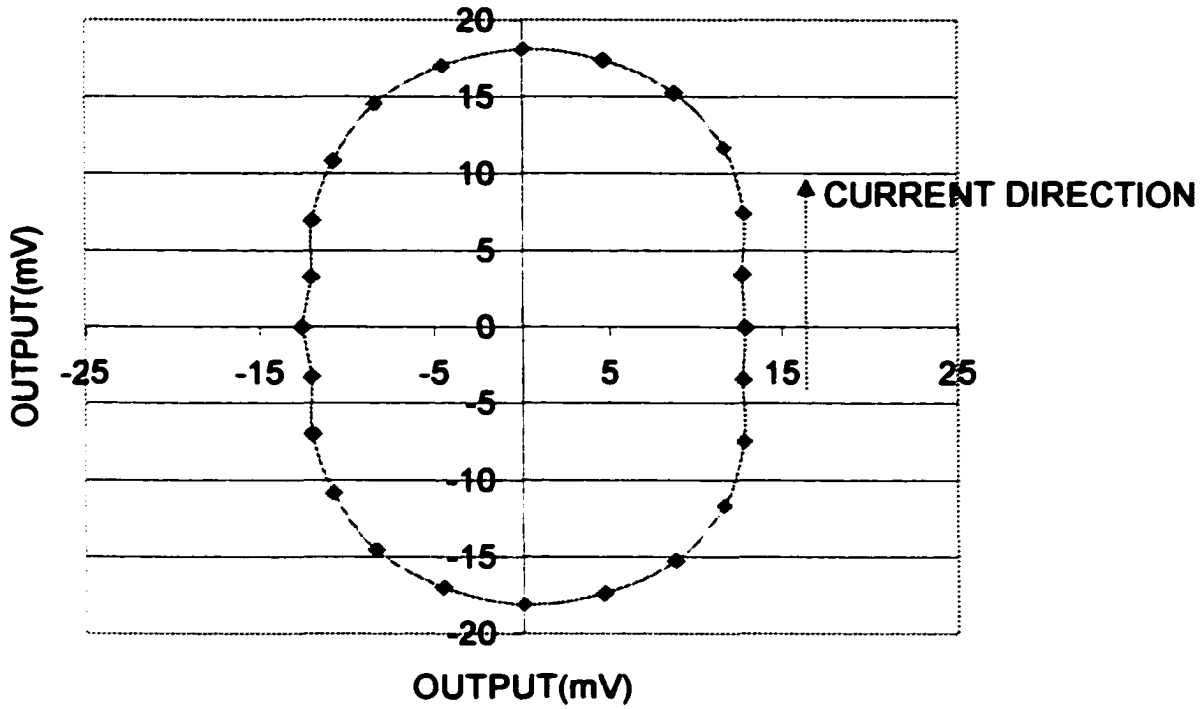

Fig.5-11. The MR bridge output at various different relative angle between magnetic field and current direction.

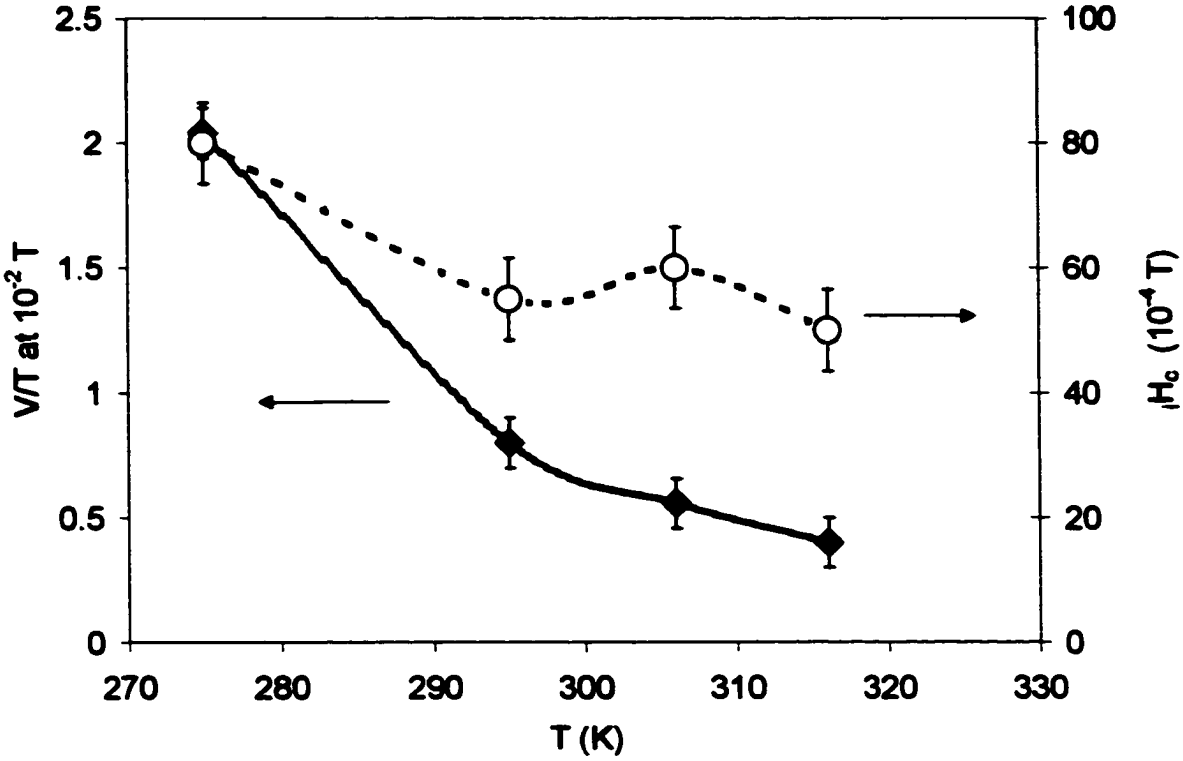

Fig. 6-1. The slope of the bridge output at 10^{-2} T is shown as measured from the bridge output. (left axis) The film coercivity versus temperature is shown as deduced from the bridge output. (right axis)

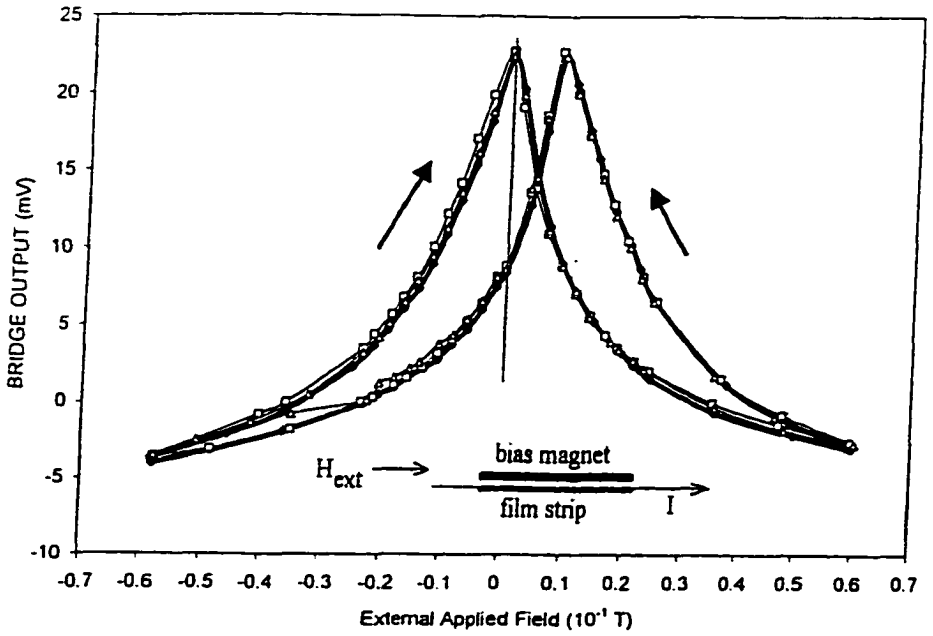

Fig.6-2. The bridge output, cycled three times, vs applied magnetic field for a LaSrMnO patterned film strip biased by a small bias magnet parallel to the strip is shown. The inset shows that the film strip current, bias magnet, and external field are all aligned parallel to each other. The vertical line is located at the H=0 position.

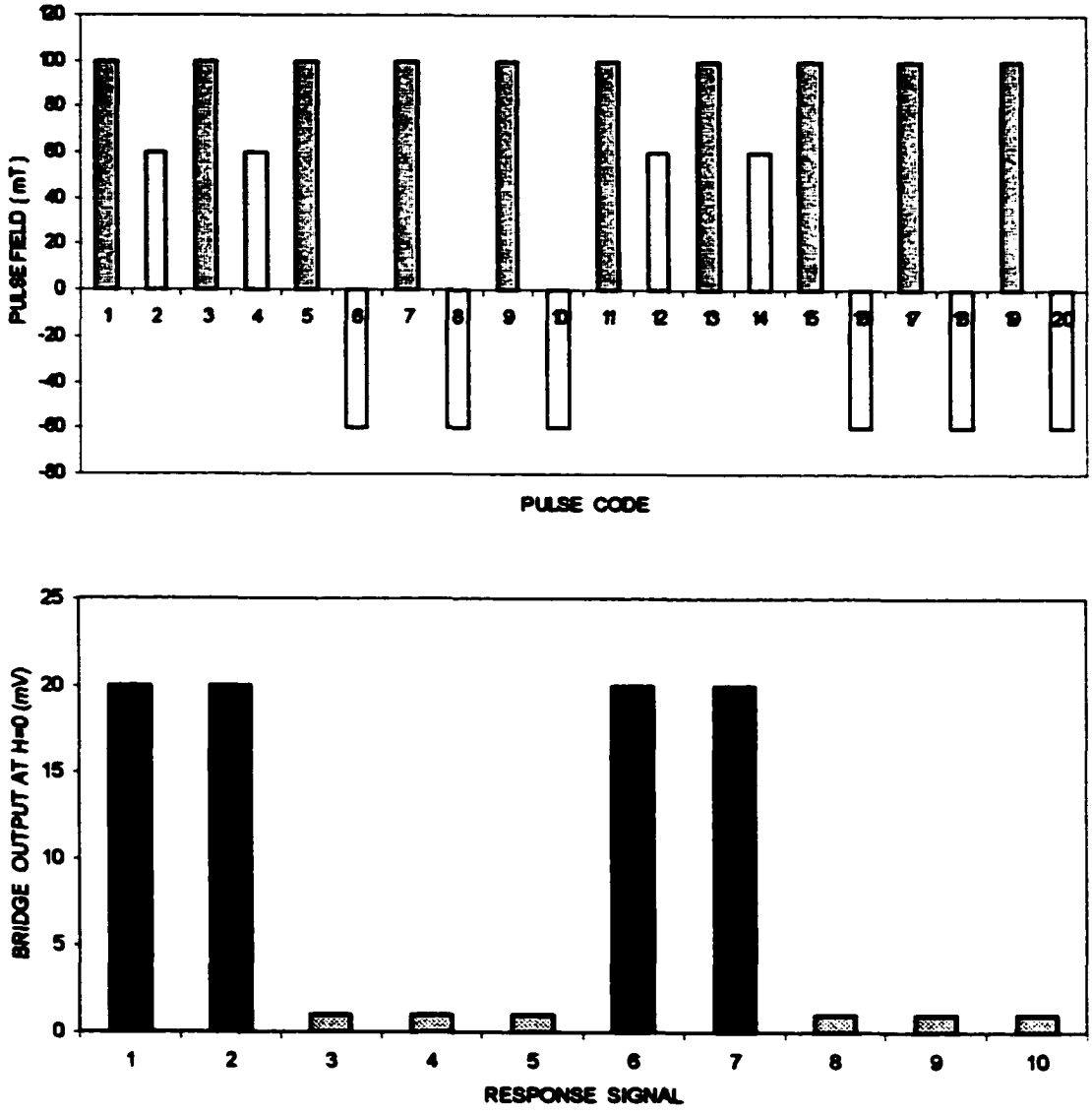

Fig.6-3. The upper graph shows the pulse train of applied field values used to produce the zero applied field voltage state values of the lower panel. The zero applied field voltage levels differed by 18 mV.

REFERENCES:

Chapter 1

1. F.J.Cadieu R.Rani, X.R.Qian, and Li Chen. *J.Appl.Phys.* **83**:6247(1998).

2. F.J.Cadieu, R.Rani, T.Theodoropoulos, and Li Chen. *J.Appl.Phys.* **85**:5895(1999).

3. F.J.Cadieu, R.Rani, X.R.Qian, and Li Chen, W.Mendoza and S.A.Shaheen, *J.Appl. Phys.* **83**:7195(1998).

4. F.J.Cadieu, Li Chen, Biao Li, and T.Theodoropoulos *J.Appl. Phys.* **87**:6770 (1999).

5. F.J .Cadieu, in Magnetic Materials, Processes, and Devices IV. L.T.Romankiw and D.A.Herman, Jr., Editors, PV 95-18, p.319-335, The Electrochemical Society Proceeding Series , Pennington, NJ(1996).

6. R.Rani , F.J.Cadieu ,X.R.Qian , W.A.Mendoza, and S.A.Shaheen, *J. Appl. Phys.* **81**(8) (1997).

7. Douglas B, Chrisey and Graham K.Hubler *Pulsed Laser Deposition of Thin films* . John Wiley & Sons, Inc(1994).

8. H.Lemke, C.Echer, and G.Thomas, *IEEE Trans. On Magn.* **32**, 404(1996).

9. Pulsed Laser Deposition System, Operator's manual, Neocera, Inc(1995).

10. Lubben, D., S.A.Barnett, K.Suzuki, S.Gorbatkin, and J.E.Greene, *J. Vac.Sci.Technol.* B3, 968(1985).

11. Kennedy, R.J., *Thin Solid Films* 214, 223(1992).

12. Greer, J.A., *J.Vac.Sci. Technol.* A10(4),1821-1826(1992).

13. Foltyn, S.R., R.E.Muenchausen, R.C.Dye, et al., *Appl.Phys.Lett.***59** (11), 1374-1376(1991).

14 . F.J.Cadieu, Li Chen and Biao Li, "Enhanced magnetic properties of $SmCo_5$ film dispersions" *IEEE Trans. On Magnetics*, MMM-INTERMAG, January 2001.

15. Li Chen, Biao Li, C.F.Cadieu, T.Theodoropoulos, and F.J.Cadieu "Nanophase dispersed SmCo films with high remanence and corrosion resistance" *Journal of Applied Physics*, vol. 87, No. 9, May 2000.

16. Lewis, B., and J.C.Anderson , *Nucleation and Growth of Thin Films*, Academic Press, New York(1978).

17. David Jiles, *Introduction to magnetism and magnetic materials*. St Edmundsbury press Ltd(1991).

18. J.P.Liu, Y.Liu, C.P.Luo, Z.S.Shan, and D.J.Sellmyer Magnetic hardening in FePt nanostructured films. *J.Appl.Phys.* **81**:5644 (1997).

19. J.P.Liu, Y.Liu, C.P.Luo, and D.J.Sellmyer High energy products in rapidly annealed nanoscale Fe/Pt multilayers. *Appl.Phys.Lett.* **72**:483 (1998).

20. F.J.Cadieu, T.D.Cheung, and L.wickramasekara Magnetic properties of Sm- Ti-Fe and Sm-Co based films, *J.Appl.Phys.* **57**:4161 (1986).

21. F.J.Cadieu, T.D.Cheung, L.wickramasekara, and Kamprath. N, High iHc perpendicular anisotropy Nd-Fe-B sputtered films. *IEEE Trans. Magnetics* **MAG-22**: 752(1986).

22. F.J.Cadieu, T.D.Cheung, and L.wickramasekara, Magnetic properties of sputtered Nd-Fe-B films *J.Magn.Magn.Mater.* **54-57**: 1641(1986).

23. F.J.Cadieu, H.Hedge, A.Navarathna, R.Rani, and K.Chen High energy product TM_{12} Sm-Fe-T and Sm-Fe permanent magnets synthesized as oriented sputtered films. *Appl.Phys.Lett.* **59**:875 (1991).

24. R.Rani, H.Hedge, A.Navarathna, and F.J.Cadieu, High coercivity $Sm_2Fe_{17}N_x$ and related phases in sputtered film samples. *J.Appl.Phys.* **73**:6242(1997).

25. D.N.Lambeth, E.M.T.Velu, G.H.Bellesis, L.L.Lee, ahd D.E.Laughlin, *J.Appl.Phys* 79, 4496(1996).

26. Levy, M., Osgood, R.M., Jr., Heghe H., Cadieu, F.J., Wolfe,R. and Fratello, V.J.(1996). Integrated optical isolators with sputter-deposited thin-film magnets. *IEEE Photonics Technology Letters* **8**:903 (1996).

27. H.Hedge, S.U.Jen, K.Chen and F.J.Cadieu, Film Sm-Co permanent magnets for the biasing of thin permalloy strips. *J.Appl.Phys.* **73**:5926(1993).

28. Derek Craik, *Magnetism- principles and application* . John Wiley & Sons Inc(1995).

29. F.J.Cadieu, H.Hedge, E.Schloemann, and H.J.Van Hook, In-plane magnetized YIG substrates self biased by SmCo based sputtered film coatings. *J.Appl.Phys.* **76**:6059(1994).

30. K.Chen, H.Hedge, and F.J.Cadieu, Induced anisotropy in amorphous Sm-Co sputtered films. *Appl.Phys.Lett.* **61**:1861(1992).

31. K.Chen, H.Hedge, S.U.Jen and F.J.Cadieu, Different types of anisotropy in amorphous SmCo films. *J.Appl.Phys.* **73**:5923(1993).

32. M.Yu, Y.Liu, S.H.Liou, and D.J.Sellmyer Nanostructured NdFeB films processed by rapid thermal annealing. *J.Appl.Phys* 83: 6611(1998).

33. E.E.Fullerton, C.H.Sowers, J.P.Pearson, S.D.Bader, X.Z.Wu, and D.Lederman, A general approach to the epitaxial growth of rare-earth-transition-metal films, *Appl.Phys.Lett* **69**:2438(1997).

34. E.E.Fullerton, J.S.Jiang, C.H.Sowers, J.P.Pearson, S.D.Bader, High coercivity, epitaxial sm-Co films with uniaxial in-plane anisotropy. *Appl.Phys.Lett* **71**:1579(1998).

35. R.E.C.Farrow, D.Weller, R.F.Marks, M.F.Toney, A.Cebollada, and G.R.Harp, Control of the axis of chemical ordering and magnetic anisotropy in epitaxial FePt films. *J.Appl.Phys* **79**:5967(1996).

36. K.Kumar, J. Appl. Phys., 63, R13, (1988).

37. F.J.Cadieu, "Permanent Magnet Thin Films," in Physics of Thin Films (Academic, San Diego),Vol.16.(1991).

38. D.Wang, S.H.Liou, P.He,D.J.Sellmyer, G.C.Hadjipanayis, and Y.Zhang, J.Magn.Magn.Mater. 124,62(1993).

39. I.Panagiotopoulos, D.Wang, D.Niarchos, and D.J.Sellmyer, *Appl.Phys.Lett.***62**, 3528(1993).

40. F.J.Cadieu, H.Hedge, A.Navarathna, R.Rani, and K.Chen, *Appl.Phys.Lett.* **59**, 875(1991).

41. K H J Buschow, Rep.Prog.Phys.**54** 1123-1213. printed in the UK(1991).

42. F.J.Cadieu, J.Vac.Sci. and Tech. A,6, 1668(1988)

43. F.J.Cadieu, "Permanent Magnet Thin Films," in Physics of Thin Films (Academic, San Diego),Vol.16.(1991)

44. F.J.Cadieu, T.D.Cheung, S.H.Aly, L.wickramasekara, and R.G.Pirich, *J.Appl.Phys.***53**,8338(1982).

45. F.J.Cadieu, H.Hedge, K.Chen Enhanced crystal texture control for Sm-Co based films sputtered in Ar-Xe gas mixtures. *Thin Solid Films.* **193/194**:857.(1990).

46. Warren E.Pickett and Jagadeesh S.Moodera *Physics Today* May of 2001.

47. S.Jin et al. *Science* 264,413 (1994)

48. Y.Tokura, A.Urushihara, Y.Moritomo, T.Arima, A.Asamitsu, G.Kido, and N.Fukawa, *J.Phys.Soc.Jpn.* 63,393(1994)

49. Y.Moritomo, A.Asamitsu and Y.Tokura *Phys.Rev.* **B** 51, 16491(1995)

50. A. Gupta et al. *Phys.Rev.* **B** 54, R15629(1996)

51. H.Y.Hwang,S.W.cheong,N.P.Ong,and B.Batlogg, Phys.rev.Lett.77,2041(1996)

52. X.W.Li,A.Gupta,Gang Xiao,and G.Q.Gomg,Appl.Phys.Lett.71,1124(1997)

53. A.Goupta, G.Q.Gong, G.Xiao, P.R.Duncomber, P.Lecoeur, P.Trouilloud, Y.Y.Wang, V.P.Dravid, and J.Z.Sun, *Phys.Rev.B54*, 15629(1996)

54. J.Q.Wang, R.C.Barker, G.J.Cui, T.Tamagawa, and B.L.Halperin, *Appl.Phys.Lett.*71,3418(1997)

55. S.A.Studenikin, Nickolay Golego,and Michael Cocivera, *J.Appl.Phys.* **88**,6652(2000)

56. J.O'Donnell, M..Onellion, M.S.Rzchowski, J.N.Eckstein, and I.Bozovic, *Phys.Rev.B* 55,5873(1997).

57. F.J.Cadieu, Li Chen, Biao Li, and T.Theodoropoulos "Enhanced room temperature magnetoresistance response in textured $La_{0.7}Sr_{0.3}MnO_3$ strips made by pulsed laser deposition" Journal of Applied Physics, vol. 87, No. 9, May 2000.

58. F.J.Cadieu, Li Chen, Biao Li, and T.Theodoropoulos " Room Temperature $La_{0.7}Sr_{0.3}MnO_3$ Magnetoresistive Prototype Memory Element". *Appl.Phys.Lett* **75**,3369(1999).

59. F.J.Cadieu, R.Rani, X.R.Qian, Li Chen, W.Mendoza and S.A.Shaheen, "Polycrystalline and Laminated $La_{0.7}Sr_{0.3}MnO_3$ Films Made By Pulsed Laser Deposition." Jan.1998, *J.Appl. Phys.* 83, 7195(1998).

60. J.-M.Liu *et al. J.Appl.Phys.*88,2791(2000)

61. A.M.Haghiri-Gosnet, et al, J.Appl.Phys. 88,4257(2001).

62. P.G.Radaelli, G.Iannone, M.Marezio, H.Y.Hwang, S.-W..Cheong, J.D.Jorgensen, and D.N.Argyrious, *Phys.Rev.* **B** 56, 8265(1997)

63. Y.Suzuki and H.Y.Hwang, *J.Appl.Phys.* **85**,4797(1999)

64. T.Walter *et al.*, *Appl.Phys.Lett.* **74**, 2218(1999)

Chapter 2

1. B.D.Cullity, *Elements of X-ray Diffraction*, 2nd , Addision-wesley.(1978).

2. W.B.Pearson, *The Crystal Chemistry of the Lattice Spacing and Physic of Metals and Alloys*, Wiley Interscience, New York, 1972.

3. L.S.Birks, *X-ray Spectrochemical Analysis*, Interscience Publisher, New York.(1969).

4. P.Villars and L.C.Calvert, *HandBook of Crystallographic Data for Intermetallic Phases* Volume 1-4 Materials Park, OH ASM International(1991).

Chapter 3

1. F.J.Cadieu, "Permanent Magnet Thin Films," in Physics of Thin Films (Academic, San Diego),Vol.16(1991).

2. F.J.Cadieu, in Magnetic Materials, Precesses, and Devices IV, edited by L.T.Romankiw and D.A.Herman, Jr., Proc. Electrochen. Soc.(Electrochemical Society, Penningto, NJ), paper PV 95-18, pp.319-335(1996).

3. H.Hegde, Ph.D. Thesis, City University of New York(1990).

4. Douglas B, Chrisey and Graham K.Hubler *Pulsed Laser Deposition of Thin films* . John Wiley & Sons, Inc.(1994).

5. G.B.Clemente, J.E.Keem, and J.P.Bradley, JAP. 64, 5299(1988).

6. T.Schrefl,J.Fidler, H.kronmuller, Physical Review B, Vol 49 No.9, 6100 (1994).

Chapter 5

1. A.Goupta, G.Q.Gong, G.Xiao, P.R.Duncomber, P.Lecoeur, P.Trouilloud, Y.Y.Wang, V.P.Dravid, and J.Z.Sun, Phys.Rev.B54, 15629(1996).

2. J.Q.Wang, R.C.Barker, G.J.Cui, T.Tamagawa, and B.L.Halperin, *Appl.Phys.Lett.***71**,3418(1997).

3. S.A.Studenikin, Nickolay Golego,and Michael Cocivera, *J.Appl.Phys.***88**,6652(2000).

4. A.M.Haghire-Gosnet, J.wolfman, B.Mercey, Ch.Simon P.Lecoeur, M.Korzenski, and M.Hervieu, R.Desfeux, G.Baldinozzi, *J.Appl.Phys.* **88**,4257(2000).

Chapter 6

1. J.Fonhtcuberta, V.Laukhin, and X.Obradors, *Appl.Phys.Lett.* **72:**2607(1992).

2. A.Urushibara, Y.Morimoto. T.Arima, A.Asamitsu, G.Kido, and Y.Tokura, Phys.Rev.B51,14103(1995).

3. J.J.Wang, J.R.Childress, and S.J.Peraton *et al.* Journal of Electronchemical Society, Vol.145, No.7(1998).